

1       **Environmental signal in the evolutionary diversification of bird skeletons**

2                   Guillermo Navalón<sup>1,2,3\*</sup>, Alexander Bjarnason<sup>2</sup>, Elizabeth Griffiths<sup>2</sup>, Roger B. J. Benson<sup>2\*</sup>

- 3
- 4       1. Department of Earth Sciences, University of Cambridge, Cambridge, UK.  
5       2. Department of Earth Sciences, University of Oxford, Oxford, UK.  
6       3. Unidad de Paleontología, Departamento de Biología, Universidad Autónoma de Madrid, Madrid, Spain.

7       \*Corresponding authors: [gn315@cam.ac.uk](mailto:gn315@cam.ac.uk); [roger.benson@earth.ox.ac.uk](mailto:roger.benson@earth.ox.ac.uk).

8

9

10

11

12

13

14

15       **Abstract**

16       Characterising how variation in the tempo and mode of evolution has structured the phenotypic diversity  
17       of extant species is a central goal of macroevolution<sup>1-3</sup>. However, studies are typically limited to a handful  
18       of traits<sup>4-6</sup>, providing incomplete information. We analyse morphological diversification in living birds, an  
19       ecologically diverse group<sup>7</sup>, documenting structural scales from ‘pan-skeletal’ proportions down to the  
20       localised 3D shape changes of individual bones. We find substantial variation in evolutionary modes among  
21       avian subgroups and among skeletal parts, indicating widespread mosaicism, and possible differences in  
22       the structure of the macroevolutionary landscape across Earth’s major environments. Water-linked  
23       groups, especially Aequorlornithes (waterbirds) have repeatedly explored a large portion of their total  
24       morphospace, emphasizing variation in body proportions and in the shape of bones close to the body core,  
25       which are functionally related to the mechanics of locomotion<sup>8</sup>. In contrast, landbirds (Inopinaves) evolved  
26       distinct, group-specific body forms early in the aftermath of the K-Pg and subsequently emphasised local  
27       shape variation, especially in the head and distal limb bones, which interact more directly with the  
28       environment. Passerines, which comprise more than half of all bird species, show a conservative  
29       evolutionary dynamic that resulted in low disparity across all skeletal parts. Evidence for early  
30       establishment of the morphospace of living birds is clear for some skeletal parts, including beaks and the  
31       combined skeletal morphology. However, we find little evidence for early partitioning of that morphospace,  
32       contrary to more specific predictions of ‘niche-filling’ models<sup>1,9</sup>. Nevertheless, early divergence among  
33       broad environmental types may have caused an early divergence of evolutionary modes, suggesting an  
34       important role for environmental divergence in structuring the radiation of crown-group birds.

35

36

37

38

39

40

41

## 42 Introduction

43 Organisms show a spectacular phenotypic disparity, and this disparity is distributed unevenly among lineages and  
44 environments. Macroevolutionary research has long sought to understand how this evolved, and the processes that  
45 cause some groups to attain far greater disparity than others<sup>1,2</sup>. Individuals, comprising many anatomical parts,  
46 are the subject of natural selection. However, even the most comprehensive macroevolutionary studies have used  
47 data from only limited parts of the organism, especially the head (e.g., <sup>4-6</sup>), leaving important questions  
48 unanswered. For example, do different structures exhibit distinct evolutionary trajectories (i.e., mosaic evolution)?  
49 To what extent do evolving lineages express differing amounts and kinds of phenotypic variation (i.e.,  
50 evolutionary versatility)? And to what extent are patterns of morphological evolution shaped by interactions  
51 among species, versus environmental factors? Environmental and among-species drivers are conceptually unified  
52 under the widespread ‘niche filling’ narrative, in which environment controls the availability of ecological niches,  
53 and interactions among species drive partitioning of those niches, with direct effects on morphological evolution  
54 <sup>1,9-11</sup>. This hypothesis predicts early establishment of a broad phenotypic space during evolutionary radiations into  
55 novel adaptive zones (e.g. <sup>12</sup>), as well as early partitioning of that space into subgroup-specific subspaces (e.g. <sup>13</sup>).

56 Birds are ecologically diverse and speciose, with prominent ecological roles in practically all Earth’s surface  
57 environments<sup>7</sup>, providing an informative study system for these questions. As vertebrates, they are structurally  
58 complex, and major hypotheses propose a highly modular pattern of bird evolution<sup>14-16</sup>. Molecular phylogenetics,  
59 including genome-scale analyses, provide an increasingly clear understanding of avian relationships and  
60 divergence times<sup>17,18</sup>. The latest common ancestor of all extant bird species was likely a ground-dwelling  
61 species<sup>19,20</sup> and lived in the Late Cretaceous (83-66 million years ago), and extant bird diversity is suggested, at  
62 least in part, to have resulted from an ecological radiation following the Cretaceous-Paleogene (K-Pg) mass  
63 extinction event 66 million years ago (MYA) (e.g., <sup>21,22</sup>). This radiation was characterised by early partitioning of  
64 lineages among major environments, giving rise to speciose water- and land-based groups, as also seen during  
65 earlier divergences (e.g., arboreal enantiornithines vs. water-linked ornithuromorphs in the Mesozoic<sup>23</sup>). This  
66 divergence along environmental lines is embodied most strikingly by the major extant sister clades  
67 Aequorlithornithes (waterbirds), and Inopinaves (landbirds), the latter of which includes the hyper-diverse  
68 Passeriformes (passerines)<sup>17</sup>. Some of these groups have conserved their climatic niches since the early Cenozoic  
69 suggesting early partitioning of environmental space was central to the crown avian diversification<sup>24</sup>.

70 In addition to early partitioning of environmental space, many hypotheses of bird diversification also assume a  
71 pattern of early partitioning of morphological diversity after the K-Pg (e.g., <sup>16,25-27</sup>), perhaps similar to the post-K-  
72 Pg radiation of crown placental mammals<sup>1,28,29</sup>. However, strong evidence for these patterns remains elusive and  
73 mostly comes from characterisations of variation for single anatomical structures, with especially intensive study  
74 of the head<sup>5,30-32</sup> and beak<sup>4,33-35</sup> morphology, yielding mixed results<sup>4-6,30</sup>.

75 Here, we take an anatomically integrated approach to avian macroevolution, examining different aspects of  
76 morphological variation across the skeleton of birds, asking how they have varied through time and among groups  
77 with different ecologies. The vertebrate skeleton is a structural scaffold for most biological systems, with  
78 demonstrated links to ecology and well-understood functional significance<sup>8</sup>. We quantified skeletal variation in  
79 the 3D shape and size of 13 skeletal elements in 228 species spanning the entire phylogeny of extant birds. This  
80 dataset provides information spanning from the Late Cretaceous origin of the bird crown-group up to the present,  
81 including the deep divergences between major avian subgroups.

82 We analyse multiple hierarchical levels of skeletal structure: 1) The relative sizes of elements drawn from across  
83 the skeleton, combined to reflect body proportions; 2) The unified relative sizes and shapes (=‘form’) of skeletal  
84 elements, combined to reflect overall skeletal form; 3) The shapes of individual skeletal elements (size-  
85 normalised); and 4) Local shape variation of elements, both individually and when combined together into regions  
86 or the whole skeleton (proportions-normalised; see Methods). This allows us to analyse the relative contributions  
87 of variation at different structural scales, offering insights beyond the scope of previous studies. For example,  
88 local shape variation can be swamped by proportional shape variation in conventional analyses. Nevertheless, it  
89 has potentially high functional importance, encompassing changes in joint surface morphologies and processes



for muscle attachment, which we analytically separate from proportional variation such as elongation, widening or deepening (see Methods).

## Results and Discussion

We assess variation in morphological diversity (disparity) among structural scales, anatomical regions and groups, evaluating hypotheses about the evolutionary mode by which that disparity was acquired through time. Our analyses differentiate between two separate predictions of the niche filling model of morphological diversification, by comparison to diffusive, multivariate Brownian motion models to establish statistical significance: (1) The hypothesis of ‘early establishment’ of a large portion of the morphospace of extant lineages; and (2) The hypothesis of ‘early partitioning’ of that morphospace, in which subgroups divide morphospace into group-specific subspaces that restrict subsequent evolution (see Methods; Extended Data Figures 1 & 2 methods summary and also<sup>11</sup>). Throughout our analyses, we find great variation in the mode of morphological evolution among elements and regions of the skeleton (Figs.1-4). This confirms the widespread occurrence of mosaic evolution in birds, and we suggest that it most likely is ubiquitous among anatomically complex organisms, necessitating a more detailed dissection of the patterns shown by different anatomical regions.

We find that birds established a wide morphospace of overall skeletal form during their early evolution (Fig. 1), driven primarily by divergence of the head and forelimb morphology (Fig. S15). This pattern is also evident for some individual elements, including the skull and mandible (Fig. S16), as well as the local shape variation of the sternum and tarsometatarsus, and overall shape (but not local shape) of the humerus, radius and ulna (Fig. S16). Other elements, especially of the hindlimb and pectoral girdle, show no evidence of this (Fig. S15). Our finding of early establishment of bird beak morphospace directly replicates most of the pattern from Cooney et al.<sup>4</sup> using a much larger dataset (2,000 species), when we exactly replicate their approach (Fig. 1b). This shows that our dataset, in spite of its smaller size, has sufficient power to test hypotheses of early morphological evolution among birds, which is the focus of our analysis and interpretations. Our finding of early establishment of the morphospace of overall skeletal form, the head, forelimb, and various individual elements of birds is consistent with fossil evidence that some groups established their distinctive morphologies by the early Cenozoic (e.g., penguins, rollers, mousebirds, frigatebirds<sup>36</sup>). It also complements palaeontological evidence that many animal groups established a large portion of their total disparity during their early history<sup>12,37</sup>.

In spite of the early establishment of many aspects of bird morphospace, we find little evidence for strong early partitioning of that morphospace (Figs. 2, 3 and Extended Data Figures 3-10). We quantify this using a version of the Morphological Disparity Index modified to accommodate high dimensional data (MDI<sup>11</sup>; Extended Data Figures 1 & 2). Negative MDI values indicate a pattern of early partitioning, whereby subclades explore smaller morphospaces than expected given the disparity of the full clade. This would indicate that whole-clade morphospace was divided into group-specific subspaces early on (Extended Figure 2; <sup>11</sup>), as predicted by the niche-filling hypothesis<sup>1,9</sup>. However, we instead find mostly positive MDI values, indicating that subclade disparities are generally higher than expected given the disparity of the full clade, indicating that constraints on morphological evolution at the level of all birds are similar to those of its subgroups (Extended Figure 2). This result suggests only weak partitioning of avian skeletal space, allowing at least some groups to engage in repeated re-exploration of morphospace throughout much of avian evolution (Figs 2-3; Neornithes), especially among waterbirds (see below). This pattern is evident both for the combined form of skeletal regions and for the individual shapes of many bones, both across birds and in most subgroups (Fig 3 and Extended Data Figure 3).

Various bird groups partitioned surface environments following the K-Pg mass extinction. The most speciose of these are the sister clades landbirds (Inopinaves/ Telluraves + Opisthocomiformes), largely radiating into terrestrial/arboreal niches, and waterbirds (Aequorlornithes/ Ardeae + Charadriiformes + Mirandornithes) largely diverging in marine/coastal/estuarine environments (with rare reversions; Fig. S35). We have shown that this environmental divergence did not produce the expected early partitioning of morphospace. Nevertheless, we do find strong evidence that this split gave rise to stark differences in overall disparity (Figs. 2, 4), and in the evolutionary mode by which this disparity was obtained (Fig. 3 and Extended Data Figures 3-10). Landbirds and their subgroups, especially passerines (Passeriformes), exhibit low overall disparity, with few exceptions (e.g., high disparity of skeletal form in toucans + barbets; Figs. 2, 4). Unlike other groups, landbirds also show early

partitioning of overall skeletal form (significantly negative MDI), although this is not evident for body proportions or for individual bone morphologies (except the mandible; Figs 2 and Extended Data Figures 3, 6 and 9). In contrast, waterbirds show overall high disparity, particularly for skeletal proportions and for overall skeletal form (Figs. 2-4; also found when ardeans and charadriiforms are analysed separately, Fig. S34) and exhibit strong evidence for a lack of partitioning of morphospace in the evolution of skeletal form and proportions (significantly positive MDI; Fig. 3).

Similar patterns of relative disparity are obtained for other water-linked groups when compared to closely related terrestrial groups. This includes comparisons of gruiforms (rails, finfoots, flufftails, limpkins, trumpeters, and cranes) to non-landbird terrestrial neoavians (a diverse assemblage including nightjars, swifts, hummingbirds, pigeons, bustards, cuckoos among others), and of anseriforms (ducks and geese) to galliforms (landfowl) (Figs. 2, Extended Data Figure 4 & Figs. S35 and S36). Although sample sizes are too small to rigorously investigate MDI, these water-linked groups exhibit significantly greater disparity in skeletal proportions than their terrestrial relatives, consistent with an association of broad environmental class with skeletal disparity in birds (Extended Data Figure 4).

We find that non-passerine landbirds are not simply less disparate or more constrained than waterbirds across all structural scales, contrary to their low disparity of skeletal proportions and most element shapes. Local shape variation was especially important to landbird diversification — differences between the disparities of waterbirds and non-passerine landbirds are substantially reduced when analysing local shape variation (Figs. 2, 4). Comparison of within-group disparity to expectations under a uniform model of morphological diversification for all birds (see Methods and Extended Data Figure 1) indicates that landbirds collectively have emphasised variation in the skeletal elements that interact most directly with the environment (skull/mandible, carpometacarpus, tarsometatarsus) (Fig. 4). This is more prominent in some subgroups; for instance, piciiforms (toucans, woodpeckers and kin) exhibit large variation in skull and mandible shapes while psittaciforms (parrots and cockatoos) demonstrate large variation in the local aspects of the morphology of the mandible and the tarsometatarsus, including articular facets of trochleae, with implications for foot function (Figs. S1 and S2). Conversely, waterbirds exhibit higher shape disparity in elements closer to the body core (sternum, coracoid, femur, tibiotarsus) (Fig. 4) which are functionally related with the lever mechanics of the wingstroke and stride<sup>8,38</sup>. Exceptions to these generalisations do exist. For example, important divergences of other elements did occur within waterbird lineages (e.g., extreme skull and mandible shape divergence between grebes and flamingos, Figs. S21 & S22), and strisoreans (nightjars, frogmouths, swifts, hummingbirds) exhibit a hyper-variable forelimb morphology contrasting with their extremely conservative hindlimb variation (Extended Data Figure 4 & Figs. S19 and S20). These observations illustrate a dazzling complexity of skeletal evolvability across the living radiation of birds (see Figs. S1-S34 for more detailed patterns of morphological evolution in other lineages).

Passerines, a landbird subclade that includes more than half of modern bird species, exhibit noticeably low disparity in all studied aspects of morphology, including local shape variation, and even when accounting for their relatively recent origins using a uniform model of morphological diversification (Figs. 2 & 4). This indicates that the low disparity of passerine morphology most likely results from a conservative evolutionary dynamic compared to other birds, and not from a lack of time to diversify. Therefore, morphological divergence was less important during the passerine super-radiation than in other birds. Instead, passerine diversification may be more related to other factors such as geographic differentiation (e.g., <sup>39</sup>), behavioural divergence, subtle ecomorphological differences related to finer-scale habitat partitioning (e.g., <sup>40</sup>), or variation in display signals such as plumage patterns or song (e.g., <sup>41,42</sup>).

Our results indicate remarkable variation in the dynamics of phenotypic evolution among major avian subgroups, suggesting fundamental differences in the structure of the macroevolutionary landscape experienced by birds evolving in water-related ecosystems compared to those in arboreal/terrestrial environments.

In summary, we found that landbirds established group-specific body forms, related to locomotor and foraging strategies, during their early history, documenting early-partitioning of avian morphospace by a major terrestrial group, but unique to landbird body proportions only, and not typical of patterns across birds. Landbirds subsequently emphasised lower-scale changes in the skull, mandible, carpometacarpus and tarsometatarsus,

terminal elements that show some of the strongest correlations with ecology across the bird skeleton<sup>32</sup>. For instance, variation in tarsometatarsus structure encodes important variation in the foot-use traits that vary markedly among landbirds, including digit orientations, arboreality and raptoriality<sup>43,44</sup>, and variation in skull and mandible shapes encodes dietary variation, although these relationships are complex<sup>32,35,45</sup>. One possible explanation for these patterns is that land-based environments, especially arboreal settings, are topologically complex and offer substantial opportunities for fine-grain niche partitioning among similar ecologies.

In contrast, waterbirds continually re-explored a larger space of body proportions and body core elements, and high disparity of body proportions is also seen in other water-linked groups (anseriforms, gruiforms). This suggests much greater evolutionary versatility of coarse-grained locomotory adaptations and greater discontinuities between water-related adaptive zones. For example, the divergence between penguins (wing-propelled divers) and tubenoses (mostly dynamic soarers) implies a complete re-organization of the muscle function in the trunk, fore- and hindlimbs<sup>38</sup>, which in fact occurred a second time during the origins of diving petrels (also wing-propelled divers) from within tubenoses, and in parallel within shorebirds, with the origin of wing-propelled diving in auks<sup>7</sup>.

Our findings resonate with a hypothesis of ‘interzonal’ diversification in waterbirds and early landbirds (i.e., diversification between widely distinct adaptive zones) versus ‘subzonal’ diversification in the subsequent evolution of landbirds (i.e., bounded diversification within adaptive zones). These modes of diversification were proposed qualitatively, and in the absence of a detailed knowledge of avian phylogeny more than 65 years ago<sup>1</sup>. ‘Subzonal’ diversification, possibly facilitated by behavioural differentiation, may have been even more important for the diversification of passerines, providing one potential explanation for the apparent paradox of high species diversity coupled with low morphological disparity. Differences in developmental constraints may also explain these patterns, and are not mutually exclusive of environmental explanations, but remain poorly understood.

Morphological macroevolution seeks to understand the processes that gave rise to the phenomenal disparity of extant species, encompassing their full phenotypic diversity. However, many previous studies have focussed on just specific aspects of phenotype, usually those with assumed links to particular ecological traits (e.g.,<sup>4,6,41</sup> although see<sup>46</sup>). We instead quantified phenotypic variation across much of the skeleton, permitting an unprecedented characterization of macroevolutionary patterns at multiple structural scales. Our results suggest that, even when early establishment of a wide morphospace is evident, associated with early partitioning of environmental space (as with deep divergences between water- and land/arboreal-related bird groups) this did not give rise to early partitioning of morphological traits.

Our findings therefore indicate a decoupling of morphospace partitioning from the partitioning of environmental space in crown-group birds, for which hypotheses have yet to be proposed. This potentially could reflect the importance of finer-scale ecological partitioning as a driver of morphological innovation during later avian evolution. Alternatively, patterns of morphological partitioning may not faithfully reflect underlying patterns of ecological partitioning given that morphology and ecology are only weakly correlated at large phylogenetic scales in birds<sup>32,35,45</sup>. Furthermore, although many studies have assumed that ecological partitioning occurs mainly during the early evolution of groups (e.g. this is implicit in the ‘early burst’ model of morphological evolution<sup>47</sup>), ecological shifts may continue to occur during later evolution, given that turnover events are common throughout the histories of most major groups<sup>47</sup>. Directly evaluating patterns of ecological evolution is therefore important but may be challenging due to difficulties fully quantifying the niches of organisms. Nevertheless, our observations question the widespread assumption of ‘niche-filling’ models, that saturation of ecological space occurs during the course of an evolutionary radiation and causes early partitioning of morphological space<sup>9,10,48</sup>.

We suggest instead that evolutionary shifts between major ecological types have structured the phenotypic disparity of organisms by altering the dynamics of morphological evolution — as evidenced by the very different patterns seen in waterbirds and landbirds and replicated to a certain extent between other water-linked and terrestrial sister lineages in our sample (Extended Data Figure 4, Figs. S17-S36). Our findings emphasise the potential for environmental factors to influence phenotypic macroevolution in a complex manner, beyond simply defining the niches available to evolving lineages, and resonate with similar contrasting patterns found between marine and freshwater teleostean fishes<sup>49</sup>. We propose a potential role for the physical or ecological structure of

environments in determining evolutionary variation among units of the avian skeleton and at different structural scales. It is also possible that differences in spatial and climatic heterogeneity between water- and land/arboreal-based environments, either through space or in time, may explain emergence of interzonal versus subzonal patterns in different groups of ancestrally terrestrial organisms. Incorporating these insights into macroevolutionary models and theory will be necessary in order to achieve a deeper understanding of evolutionary processes that control the distribution of disparity in space and time, in particular, to deepen in our understanding of the relationship among ecological opportunity and the diversification of species and their phenotypes.

## References (main text)

- 1 Simpson, G. G. *The major features of evolution*. (Columbia University Press, 1953).
- 2 Gould, S. J. *Ontogeny and phylogeny*. (Harvard University Press, 1985).
- 3 Jablonski, D. Approaches to macroevolution: 2. Sorting of variation, some overarching issues, and general conclusions. *Evolutionary Biology* **44**, 451-475 (2017).
- 4 Cooney, C. R. *et al.* Mega-evolutionary dynamics of the adaptive radiation of birds. *Nature* **542**, 344-347 (2017).
- 5 Felice, R. N. & Goswami, A. Developmental origins of mosaic evolution in the avian cranium. *Proceedings of the National Academy of Sciences*, 201716437 (2018).
- 6 Navalón, G., Marugán-Lobón, J., Bright, J. A., Cooney, C. R. & Rayfield, E. J. The consequences of craniofacial integration for the adaptive radiations of Darwin's finches and Hawaiian honeycreepers. *Nature Ecology & Evolution* **4**, 270-278 (2020).
- 7 Gill, F. B. *Ornithology*. (Macmillan, 1995).
- 8 Kardong, K. V. *Vertebrates: comparative anatomy, function, evolution*. (Heinle and Heinle Publishers, 1997).
- 9 Schluter, D. *The ecology of adaptive radiation*. (OUP Oxford, 2000).
- 10 Losos, J. B. Adaptive radiation, ecological opportunity, and evolutionary determinism: American Society of Naturalists EO Wilson Award address. *The American Naturalist* **175**, 623-639 (2010).
- 11 Harmon, L. J., Schulte, J. A., Larson, A. & Losos, J. B. Tempo and mode of evolutionary radiation in iguanian lizards. *Science* **301**, 961-964 (2003).
- 12 Hughes, M., Gerber, S. & Wills, M. A. Clades reach highest morphological disparity early in their evolution. *Proceedings of the National Academy of Sciences* **110**, 13875-13879 (2013).
- 13 Ackerly, D., Schilck, D. & Webb, C. Niche evolution and adaptive radiation: testing the order of trait divergence. *Ecology* **87**, S50-S61 (2006).
- 14 Gatesy, S. M. & Dial, K. P. Locomotor modules and the evolution of avian flight. *Evolution*, 331-340 (1996).
- 15 Dececchi, T. A. & Larsson, H. C. Body and limb size dissociation at the origin of birds: uncoupling allometric constraints across a macroevolutionary transition. *Evolution* **67**, 2741-2752 (2013).
- 16 Clarke, J. A. & Middleton, K. M. Mosaicism, modules, and the evolution of birds: results from a Bayesian approach to the study of morphological evolution using discrete character data. *Systematic biology* **57**, 185-201 (2008).
- 17 Prum, R. O. *et al.* A comprehensive phylogeny of birds (Aves) using targeted next-generation DNA sequencing. *Nature* (2015).
- 18 Oliveros, C. H. *et al.* Earth history and the passerine superradiation. *Proceedings of the National Academy of Sciences* **116**, 7916-7925 (2019).
- 19 Field, D. J. *et al.* Early evolution of modern birds structured by global forest collapse at the end-Cretaceous mass extinction. *Current Biology* **28**, 1825-1831. e1822 (2018).
- 20 Benito, J. *et al.* 40 new specimens of *Ichthyornis* provide unprecedented insight into the postcranial morphology of crownward stem group birds. *bioRxiv* (2022).
- 21 Field, D. J. *et al.* Timing the extant avian radiation: The rise of modern birds, and the importance of modeling molecular rate variation. *PeerJ Preprints* **7** (2019).
- 22 Feduccia, A. 'Big bang' for tertiary birds? *Trends in Ecology & Evolution* **18**, 172-176 (2003).
- 23 Chiappe, L. M. & Qingjin, M. *Birds of Stone: Chinese Avian Fossils from the Age of Dinosaurs*. (JHU Press, 2016).
- 24 Saupe, E. E. *et al.* Climatic shifts drove major contractions in avian latitudinal distributions throughout the Cenozoic. *Proceedings of the National Academy of Sciences* **116**, 12895-12900 (2019).
- 25 Nudds, R., Dyke, G. & Rayner, J. Forelimb proportions and the evolutionary radiation of Neornithes. *Proceedings of the Royal Society of London. Series B: Biological Sciences* **271**, S324-S327 (2004).
- 26 Wang, X. & Clarke, J. A. Phylogeny and forelimb disparity in waterbirds. *Evolution* **68**, 2847-2860 (2014).

- 294 27 Crouch, N. M. & Ricklefs, R. E. Speciation rate is independent of the rate of evolution of morphological  
295 size, shape, and absolute morphological specialization in a large clade of birds. *The American Naturalist*  
296 **193**, E78-E91 (2019).
- 297 28 Brocklehurst, N., Panciroli, E., Benevento, G. L. & Benson, R. B. Mammaliaform extinctions as a driver  
298 of the morphological radiation of Cenozoic mammals. *Current Biology* (2021).
- 299 29 Osborn, H. F. The law of adaptive radiation. *The American Naturalist* **36**, 353-363 (1902).
- 300 30 Felice, R. N. *et al.* Decelerated dinosaur skull evolution with the origin of birds. *PLoS biology* **18**,  
301 e3000801 (2020).
- 302 31 Felice, R. N., Tobias, J. A., Pigot, A. L. & Goswami, A. Dietary niche and the evolution of cranial  
303 morphology in birds. *Proceedings of the Royal Society B* **286**, 20182677 (2019).
- 304 32 Orkney, A., Bjarnason, A., Tronrud, B. C. & Benson, R. B. Patterns of skeletal integration in birds reveal  
305 that adaptation of element shapes enables coordinated evolution between anatomical modules. *Nature*  
306 *Ecology & Evolution* **5**, 1250-1258 (2021).
- 307 33 Chira, A. M. & Thomas, G. H. The impact of rate heterogeneity on inference of phylogenetic models of  
308 trait evolution. *Journal of evolutionary biology* **29**, 2502-2518 (2016).
- 309 34 Rombaut, L. M. *et al.* Allometric conservatism in the evolution of bird beaks. *Evolution letters* **6**, 83-91  
310 (2022).
- 311 35 Navalón, G., Bright, J. A., Marugán-Lobón, J. & Rayfield, E. J. The evolutionary relationship among  
312 beak shape, mechanical advantage, and feeding ecology in modern birds. *Evolution* **73**, 422-435 (2019).
- 313 36 Mayr, G. *Avian evolution: the fossil record of birds and its paleobiological significance*. (John Wiley &  
314 Sons, 2016).
- 315 37 Foote, M. The evolution of morphological diversity. *Annual Review of Ecology and Systematics* **28**, 129-  
316 152 (1997).
- 317 38 Bribiesca-Contreras, F., Parslew, B. & Sellers, W. I. Functional morphology of the forelimb musculature  
318 reflects flight and foraging styles in aquatic birds. *Journal of Ornithology*, 1-15 (2021).
- 319 39 Phillimore, A. B. *et al.* Sympatric speciation in birds is rare: insights from range data and simulations.  
320 *The American Naturalist* **171**, 646-657 (2008).
- 321 40 MacArthur, R. H. Population ecology of some warblers of northeastern coniferous forests. *Ecology* **39**,  
322 599-619 (1958).
- 323 41 Cooney, C. R. *et al.* Sexual selection predicts the rate and direction of colour divergence in a large avian  
324 radiation. *Nature communications* **10**, 1-9 (2019).
- 325 42 Tobias, J. A. *et al.* Species coexistence and the dynamics of phenotypic evolution in adaptive radiation.  
326 *Nature* **506**, 359 (2014).
- 327 43 Del Hoyo, J. *et al.* Handbook of the Birds of the World Alive. Lynx Editions, Barcelona. (2017).
- 328 44 Botelho, J. F., Smith-Paredes, D. & Vargas, A. O. Altriciality and the evolution of toe orientation in  
329 birds. *Evolutionary Biology* **42**, 502-510 (2015).
- 330 45 Natale, R. & Slater, G. J. The effects of foraging ecology and allometry on avian skull shape vary across  
331 levels of phylogeny. (2022).
- 332 46 Pigot, A. L. *et al.* Macroevolutionary convergence connects morphological form to ecological function  
333 in birds. *Nature Ecology & Evolution* **4**, 230-239 (2020).
- 334 47 Slater, G. J. Iterative adaptive radiations of fossil canids show no evidence for diversity-dependent trait  
335 evolution. *Proceedings of the National Academy of Sciences* **112**, 4897-4902 (2015).
- 336 48 Rabosky, D. L. & Lovette, I. J. Density-dependent diversification in North American wood warblers.  
337 *Proceedings of the Royal Society B: Biological Sciences* **275**, 2363-2371 (2008).
- 338 49 Friedman, S., Collyer, M., Price, S. & Wainwright, P. Divergent processes drive parallel evolution in  
339 marine and freshwater fishes. *Systematic Biology* (2021).

## 341 Material and Methods

### 342 Dataset, phylogenetic hypothesis, and morphological variables

343 Our dataset comprises 3D morphometric data for 13 skeletal units in 228 species, providing a phylogenetically-  
344 and ecologically broad sample of extant avian diversity (see Table S1 for full list of species and specimens). It is  
345 substantially expanded from the recent dataset of Orkney *et al.*,<sup>32</sup> by adding 79 species, improving the  
346 representation of many groups, especially passerines. To illustrate that our sample of extant bird species (N = 228)  
347 provides an effective sample of ancient bird divergences, we compared the count of phylogenetic lineages through  
348 time for a supertree of 9,993 extant bird species sourced from<sup>4</sup> (complete supertree from<sup>50</sup>, using backbone from  
349 <sup>17</sup>) to the count of lineages in a pruned tree that includes only those species that we sampled. Results show that  
350 our species sample achieves a near-complete coverage of deep bird divergences up to around 30 million years ago

(Fig. S37) and only missing out a significant portion of bird diversity (half the lineages) at about 20 million years ago onwards.

Digital skeletal models were segmented from high-resolution micro-CT (computed-tomography) scans of complete skeletons in Avizo 9.3 (Thermo Fisher Scientific, Zuse Institute). We placed landmarks and curve semilandmarks on these models, yielding a dense, quantitative representation of each element's geometry (File S1. full landmark, for details on landmarking scheme, including consideration of homology, see <sup>51</sup>), and thereby providing a broad representation skeletal form (shape and size) compared to previous studies (e.g., <sup>5</sup>). Some elements of the skeleton, like the pedal phalanges, were not landmarked for practical reasons (e.g., availability in skeletal museum collections) despite their ecological relevance<sup>52</sup>. Our analyses were conducted in R version 4.0.2<sup>53</sup> using functions primarily from the packages ape version 5.5, geomorph version 4.0.1<sup>54</sup>, RRPP version 0.6.2<sup>55</sup>, and geiger version<sup>56</sup>, as well as custom code (Files S3 and S4). We use a composite phylogenetic framework combining recent phylogenetic hypotheses for non-passerines<sup>17</sup> and passerines<sup>18</sup> (see File S2 for tree files and Table S1 taxonomic match between source phylogenies and our morphological data).

Shape data (Procrustes residuals) were isolated from size, position and rotational information by applying Generalised Procrustes Analysis (GPA<sup>57</sup>) to the 3D landmark coordinates of each element using the gpagen function from geomorph, sliding semilandmarks to minimise bending energy differences from the mean shape<sup>58</sup>. Common allometric information was factored out from element shapes by taking residuals from a phylogenetic generalised least squares (pGLS) regression of Procrustes residuals on log<sub>10</sub>-transformed body mass, using the function procD.pgls of geomorph. The 'allometry-free' residual shape matrix was added to the mean shape for use as 'shape' in subsequent analyses. Element size was indexed as the centroid size from our landmark/semilandmark constellations and relative element sizes were taken as the residuals from a pGLS regression of log<sub>10</sub>-element size on log<sub>10</sub>-transformed body mass. The 'form' of individual elements is represented by shape multiplied by relative size.

We analysed data representing structure at four hierarchical levels of organisation: 1) Overall skeletal form, as the combined relative sizes and allometry-corrected shapes (= 'forms') of all skeletal elements, or subsets representing the head (skull, mandible), pectoral limb (scapula, coracoid, sternum, humerus, ulna, radius, carpometacarpus), and pelvic limb (synsacrum, femur, tibia, tarsometatarsus); 2) Overall skeletal proportions represented by a matrix containing the relative sizes of individual elements across the skeleton and for subsets (head, pectoral limb, pelvic limb); 3) The allometry-corrected shapes of individual skeletal elements; and 4) Local shape variation of elements, both individually and combined together per region, calculated as explained below. Combined configurations were generated by overlying landmark configurations for individual elements in the same space, centring them on the origin then rescaling the combined configuration to unit centroid size following recent recommendations for best practices<sup>59</sup>, using custom code and the function gpagen.

Therefore, for individual elements we studied 1) allometry-free shape and 2) proportions-normalised shape, while for combined elements (whole skeleton, head, pectoral limb, and pelvic limb) we studied 1) skeletal proportions, 2) allometry-free form (shape plus size) and 3) proportions-normalised combined shapes.

### **Local shape variation (proportion-normalised shape)**

Local shape variation for each element was calculated by normalising element shapes according to element proportions. This was done by taking the residuals from a pGLS regression of Procrustes residuals (shape) against log<sub>10</sub> body mass and the maximum length, breadth and depth of each element, measured along standard anatomical axes, and subsequently called 'x-y-z distances'. X-y-z distances were calculated as the distance between selected pairs of landmarks in the Procrustes residuals (Table S1 for all distances and Table S3 for all pairs of landmarks per axis and element). This novel approach is intended to remove aspects of shape variation that are correlated only to overall stretching or squashing of the aspect ratios or proportional lengths of skeletal units (i.e., elongation, widening, or deepening of an anatomical structure), which may primarily be related to changes in overall skeletal proportions. The residual variation reflects local-scale shape variation. For example, variation in articular facets or processes for attachment of muscles or tendons which may hold important functional information.

For each skeletal element, we built additive pGLS models for all the combinations of x-y-z distances, analysed as covariates (e.g., ‘shape ~ log<sub>10</sub> body mass + x + y’; shape ~ log<sub>10</sub> body mass + x + y + z). We then retained as proportions-normalised shapes the residuals from the pGLS model that satisfies two conditions: 1) The model with the highest effect size and 2) whose individual terms are all statistically significant (Table S2 for the all the ANOVA tables). The only bone whose full model (e.g., ‘shape ~ log<sub>10</sub>-body mass + x + y + z’) failed to meet the three conditions is the carpometacarpus in which maximum length in the z axis is not statistically significant and therefore, the PGLS model including only maximum lengths in the x and the y axes was used to generate the proportions-normalised shape of this element.

Visual inspection of the residual shapes confirmed our expectations for an approach intended to remove proportional variation and preserve local shape variation (see Extended Data Figure 1 and Figs. S1-S14).

## **Quantifying disparity**

For all the morphological variables (size proportions, form, and shape) and partitions (whole skeleton, regions and individual elements), including both empirical data and our simulations (see below) we quantified morphological disparity as the mean pairwise squared Euclidean distances among species within the subclade. This was chosen as an estimator of the spread of species in multivariate shape space in favour of other measures, because it has been shown to be robust to variation in sampling proportion and sample size by both theoretical and empirical studies, with properties similar to variance-based measures of disparity<sup>37,60,61</sup>.

## **Patterns of morphospace establishment**

To evaluate how extant bird lineages established their morphospace through time, we used ancestral character estimation in the R package mvMORPH version 1.1.4<sup>62</sup> for all our morphological variables (size proportions, form and shape) and partitions (whole skeleton, regions and individual elements), based on principal component axes representing > 95% of variation. We then calculated morphological disparity for all edges of our phylogeny that cut through each in a series of census times, spaced by 1 Ma intervals from the origin of the bird crown group to the present. This provided a time series of the estimated disparity of Neornithes from their time of origin to the present, based on those lineages that are extant today. This was compared to the time series resulting from multivariate Brownian motion simulations (100 iterations, due to the extensive computational time required), using parameters estimated from our empirical datasets, also using functions from mvMORPH<sup>62</sup>. When the empirical line falls above the 95% confidence intervals of the simulated values, that suggests that birds established higher disparity at that time than would be expected under a gradual, diffusive model of evolution. Our approach is similar to that of by Cooney et al.<sup>4</sup>, who used univariate simulations of individual principal component axes, also representing >95% of variation. For direct comparison to Cooney et al.<sup>4</sup>, we also therefore present analyses using univariate simulations of individual axes based on functions in ape version 5.0<sup>63</sup> and phytools version 1.0-1<sup>64</sup>, showing that our multivariate approach is more conservative (i.e. has wider 95% confidence intervals, and so is more likely to reject a hypothesis of early establishment of morphospace; see Fig. S15 for comparison).

## **Patterns of morphospace partitioning**

To evaluate patterns of morphospace partitioning through time, we calculated morphological disparity for all the subclades in our tree for all our morphological variables (size proportions, form and shape) and partitions (whole skeleton, regions and individual elements). This was expressed as a proportion of the mean disparity of the whole clade (Neornithes). We used these subclade disparities to document the relationship between subclade disparities and subclade ages among birds, and within waterbirds, non-passerine landbirds, and passerines, using a modified version of the ‘disparity through time’ approach<sup>11</sup>. We avoid using this terminology (‘disparity through time’) because these analyses evaluate morphospace partitioning among progressively younger subclades, differing from the quantification of how disparity accumulated through time in our analysis of morphospace establishment, described above. We therefore call these ‘subclade disparity–age’ plots, or morphospace partitioning analyses. These provide a test of the mode of evolution, testing the hypothesised importance of early partitioning of morphospace in birds and bird subgroups.

We summarised subclade disparity as the mean value for all subclades whose stem (branch ending directly in the basal node for that clade) existed at that time. Connecting all these time-binned values creates mean empirical

disparity-through-time curves from the origin of a clade to the most recent branching event it experienced (Extended Figure 2).

To establish a macroevolutionary baseline to compare empirical values with, we calculated subclade disparity for 200 simulations of morphological evolution under a uniform, single-rate Brownian Motion model (constant diffusive trait evolution) for each kind of morphological data (proportions, form, shape and local shape) and each partition (whole skeleton, regions and individual bones). For this, we used the function `mvgl` to fit a single rate Brownian Motion model to each kind of data/partition to estimate the adequate trait-covariance matrix and the ancestral states at the root of the tree, then, we fed these values to the function `mvSIM` which we used to generate 200 iterations of simulated morphological data. This simulated morphological data represents a diffusive, Brownian motion, model of evolution with a single set of parameters shared across all Neornithes ('all Neornithines' simulations) and was used to evaluate relative disparities of each group across all anatomical data types. We also repeated this process for each subclade (waterbirds, non-passerine landbirds and passerines) by fitting only species data belonging to each of the clades. These were used to evaluate the mode of evolution for each group (i.e. early partitioning versus diffusive or constrained evolution; see below).

We interrogated the mode of morphological evolution by calculating the Morphological Disparity Index (MDI<sup>11</sup>) for each of the four target groups (Neornithes, Aequolithornithes, non-passerine Inopinaves and Passeriformes). MDI is calculated as the area between the empirical subclade disparity-through-time curve and the disparity-through-time curve simulated under Brownian Motion. MDI therefore informs about how disparity among subclades compares with disparity of the total group and at which phylogenetic level constraints in morphological evolution might be acting. Negative MDI values indicates that the empirical curve exhibits lower subclade disparities than the simulated curve and indicates that subclades explore smaller morphospaces than expected given the diversity of the full clade, suggesting early partitioning of trait space, or constrained subclade evolution. Positive MDI indicates that subclades explore larger morphospaces than expected given the diversity of the full clade, suggesting little partitioning of avian trait space, and/or that constraints on evolution at the level of all birds are similar to those of its subgroups<sup>11</sup>. Confidence intervals use the 95% and 5% percentiles of simulated disparities in place of the mean. We calculated MDI using `area.between.curves` internal function of the `dt` function in the R package `geiger`.

For display, we calculated the relative subclade disparities compared to expectations under a uniform model of all-bird evolution by subtracting  $\log_{10}$ -transformed empirical group disparities from mean  $\log_{10}$ -transformed simulated subclade disparity values from our 'all Neornithines' simulations. We plotted these values as colours in the basal nodes for all clades in our phylogeny to visually inspect patterns of disparity across phylogeny for each data/partition (Fig. 2 and Extended Data Figures 5-10).

We also summarised patterns of pan-skeletal variation (whole skeletal proportions, allometry-free combined form and proportions-normalised combined shapes) other water-linked groups: Gruiformes (cranes, rails and akin), Charadriiformes (shorebirds), Ardea ('core waterbirds'), Anseriformes (ducks and geese); and all the other land-linked groups which are not members of Inopinaves.

## Relative disparity

We compared the relative disparity of our target groups (Aequolithornithes, non-passerine Telluraves and Passeriformes) to expectations under a uniform model across all Neornithes, for all anatomical data types. Relative disparity was calculated as the empirical disparity minus the simulated disparity across 200 Brownian Motion simulations ('all Neornithines' simulations). These 200 values were summarised by calculating the minimum, maximum, mean and first and third quantiles. Relative disparities provide information about the difference in a group's disparity compared to what would be expected given the duration and topology of phylogenetic history if all birds evolved in the same way. We repeated this for four additional groups: Anseriformes, Galliformes, Gruiformes and a diverse assemblage of non-landbird mainly terrestrial clades (Strisores + Otidimorphae).



## 493      **References (material and methods section)**

- 494      50      Jetz, W., Thomas, G., Joy, J., Hartmann, K. & Mooers, A. The global diversity of birds in space and  
495      time. *Nature* **491**, 444-448 (2012).
- 496      51      Bjarnason, A. & Benson, R. A 3D geometric morphometric dataset quantifying skeletal variation in birds.  
497      *MorphoMuseuM* **7** (2021).
- 498      52      Abourachid, A., Fabre, A. C., Cornette, R. & Höfling, E. Foot shape in arboreal birds: two morphological  
499      patterns for the same pincer-like tool. *Journal of anatomy* **231**, 1-11 (2017).
- 500      53      Team, R. C. 2020. *R: A Language and Environment for Statistical Computing. R Foundation for*  
501      *Statistical Computing, Vienna, Austria: Available at: <https://www.R-project.org/>.*[Google Scholar]  
502      (2019).
- 503      54      Adams, D., Collyer, M., Kaliontzopoulou, A. & Baken, E. (2021).
- 504      55      Collyer, M., Adams, D. & Collyer, M. M. Package ‘RRPP’. (2021).
- 505      56      Harmon, L. *et al.* Package ‘geiger’. *R package version 2* (2020).
- 506      57      Bookstein, F. L. in *Advances in morphometrics* 131-151 (Springer, 1996).
- 507      58      Gunz, P. & Mitteroecker, P. Semilandmarks: a method for quantifying curves and surfaces. *Hystrix, the*  
508      *Italian journal of mammalogy* **24**, 103-109 (2013).
- 509      59      Collyer, M. L., Davis, M. A. & Adams, D. C. Making heads or tails of combined landmark configurations  
510      in geometric morphometric data. *Evolutionary Biology* **47**, 193-205 (2020).
- 511      60      Ciampaglio, C. N., Kemp, M. & McShea, D. W. Detecting changes in morphospace occupation patterns  
512      in the fossil record: characterization and analysis of measures of disparity. *Paleobiology* **27**, 695-715  
513      (2001).
- 514      61      Wills, M. A., Briggs, D. E. & Fortey, R. A. Disparity as an evolutionary index: a comparison of Cambrian  
515      and Recent arthropods. *Paleobiology* **20**, 93-130 (1994).
- 516      62      Clavel, J., Escarguel, G. & Merceron, G. mvMORPH: an R package for fitting multivariate evolutionary  
517      models to morphometric data. *Methods in Ecology and Evolution* **6**, 1311-1319 (2015).
- 518      63      Paradis, E. & Schliep, K. ape 5.0: an environment for modern phylogenetics and evolutionary analyses  
519      in R. *Bioinformatics* **35**, 526-528 (2019).
- 520      64      Revell, L. J. phytools-package 5. Package ‘phytools’, 5 (2015).

521

## 522      **Data availability**

523      Raw landmark coordinates can be accessed as Supplementary Files linked to this article and accessing our project  
524      in OSF Public Repository following this link: <https://osf.io/wjk3m/>. All three-dimensional meshes can be freely  
525      downloaded following the links to Morphosource in SM.Table 1.

## 526      **Code availability**

527      Custom code can be accessed in our project in OSF Public Repository following this link: <https://osf.io/wjk3m/>.

## 528      **Acknowledgements**

529      For access to specimens, we thank J. White and J. Cooper (NHMUK), J. Hinshaw (UMMZ), M. Lowe and M.  
530      Brooke (UMZC), M. Carnall and E. Westwig (OUMNH), K. Zyskowski (YPM), and B. Marks and J. Bates  
531      (FMNH). For access to CT scanning facilities, we thank K. Smithson (Cambridge Biotomography Centre); T.  
532      Davies, B. Moon and L. Martin-Silverstone (University of Bristol); V. Fernandez (Natural History Museum); A.  
533      Neander and Z.-X. Luo (University of Chicago PaleoCT); and M. Friedman (University of Michigan). We thank  
534      E. Griffiths, S. Wright, S. Poindexter, A. Wolniewicz and S. Evers for segmenting digital bone models from the  
535      CT scan data. We are grateful to Alberto Martin-Serra, Juan L. Cantalapiedra, Fernando Blanco, Matteo Fabbri,  
536      Iris Menéndez, Sergio M. Nebreda, Julien Clavel, Elizabeth M. Steell, Jesús Marugán-Lobón and César Navalón  
537      for enlightening discussion on contents, narrative and analytical approaches. We thank Lucía Balsa Pascual and  
538      Óscar Sanisidro for discussion on design choices. This work was funded by the European Union’s Horizon 2020  
539      research and innovation programme 2014–2018 under grant agreement no. 677774 (European Research Council  
540      Starting Grant: TEMPO). Grant no. 677774 applies to the work of G.N, A.B and R.B.J.B. GN acknowledge  
541      support from UKRI Future Leaders Fellowship MR/S032177/1.

## Competing Interest statement

The authors declare no competing interests.

## Author's contributions

GN and RBJB conceptualised the study and design the analytical approach. GN, AB, EG and RBJB collected and curated the data. GN and RBJB undertook the formal analyses. GN and RBJB wrote the manuscript. GN made the figures; GN, AB, EG and RBJB edited the text. RBJB acquired the funding used for this research.

## Main text figure captions

**Figure 1. Early establishment of the morphospace for skeletal form (a) and beak shape (b) during the diversification of Neornithes.** Empirical disparity time series based on ancestral character estimation for Neornithes (brown, continuous line) is compared to expectation under a set of 100 simulations under diffusive, multivariate Brownian motion model (blue shaded area indicating 95% confidence intervals; red shaded area for univariate simulations for beak shape as in<sup>4</sup>). Timing of the K-Pg mass extinction event is indicated by the dotted vertical line. Analyses of other elements and anatomical regions across all our data types are shown in Figs S15 & S16.

**Figure 2. Whole skeletal subclade disparity–age plotted across avian phylogeny and through time.** a) Whole skeleton subclade disparity values colour-coded based on difference from expectations under a constant diffusive model of evolution (Brownian motion, BM), plotted at the basal node of each clade in the phylogeny for three kinds of morphological data: skeletal proportions (top), combined overall form for the whole skeleton (middle, combined element shapes after correcting for body mass, plus relative sizes among elements) and local shapes from all skeletal elements combined together (proportions-free combined shapes; bottom, combined shapes of elements corrected for body mass and main axes proportional changes in shape, see Methods). Subclade disparity values are log<sub>10</sub>-transformed deviations of empirical values from means of 200 simulations of morphological evolution under BM. Purples represent lower disparities than expected under BM for that clade, ochres represent higher disparities than expected under BM. b) Patterns of mean binned subclade disparity against subclade age for all birds (Neornithes) and three target lineages. Only the empirical curved of Neornithes (brown) relates to the null expectations for BM, the three subclade curves (Aequorlithornithes, Inopinaves, Passeriformes) are only plotted for reference (for similar curves for other subclades see Extended Data Figures 5-10). Grey envelope represents the maximum and minimum values for each bin of the 200 simulations of morphological evolution under BM. Individual colour coded clade values are plotted and some extreme values are labelled. Time scale in million years apply for both parts of the figure and the dashed horizontal line at 67 MYA indicates the timing of K-Pg extinction. Clades in a) indicated as numbers: 1. Palaeognathae, 2. Galloanserae, 3. Strisores, 4. Columbaves, 5. Gruiformes, 6. Mirandornithes + Charadriiformes, 7. Ardeae, 8. Accipitriformes, 9. Strigiformes, 10. Eucavitaves, 11. Cariamiformes, 12. Falconiformes, 13. Psittaciformes, 14. Suboscines (Passeriformes), 15. Oscines (Passeriformes).

**Figure 3. Tests of early partitioning of avian skeletal space using the morphological diversity index (MDI).** MDI means and confidence intervals are derived from comparison of subclade disparities to simulations under Brownian motion (see Methods), shown here for all aspects of morphological variation of the whole skeleton and the three main anatomical regions in all Neornithes, and in Aequorlithornithes, Inopinaves and Passeriformes (see Extended Data Figure 2, for the patterns of individual skeletal elements). Mean Morphological Disparity Index (MDI) values for each partition/lineage/data type represented by a dot and associated 95% confidence intervals are represented as whiskers. See Extended Data Figure 2 for a detailed account of the idealised patterns associated with each mode of evolution of disparity through time.

**Figure 4. Deviations of group-specific disparities from the disparity expected if all birds were evolving under a uniform Brownian motion model of evolution.** Boxplots summarise the distribution of values, calculated as empirical disparities minus disparities for the 200 simulated values for Aequorlithornithes, Inopinaves and Passeriformes. High values indicate higher-than-expected disparity and low values indicate lower-than-expected disparity. All partitions and data types are displayed, namely, the whole skeleton, three main skeletal regions and individual bones and the four different aspects of morphological variation. Arrows highlight the lineage/partition/data type which shows particularly high (up pointing arrows) or low (down pointing arrows) values. Values are normalised by interquartile range.

592 **Extended Data Figure captions**

593 **Extended Data Figure 1. Infographic displaying the data and the methods' pipeline used in this study.** A  
594 detailed account of the Material and Methods used in our study can be found in the main text.

595 **Extended Data Figure 2. Diagram showing how subclade disparity through time is calculated as test of**  
596 **early partitioning of morphospace, showing idealised contrasting patterns of morphological evolution.** a)  
597 Example time-calibrated phylogeny and points in time (cladogenesis events) for which b) subclade disparities  
598 values are calculated for a Brownian model of diffusive evolution and two alternative modes of morphological  
599 evolution. c) Corresponding patterns in morphospace exploration over time for two idealised patterns of  
600 morphological evolution: early partitioning of trait space (morphospace) in which morphological evolution is  
601 constrained at the level of subclades, and a non-partitioned pattern in which constraints are similar in the total  
602 group and within subclades.

603 **Extended Data Figure 3. Tests of early-partitioning of avian allometry-free shape and local shape variation**  
604 **of the individual elements in Aequorlithornithes, Inopinaves and Passeriformes.** See Extended Data Figure  
605 2 for a detailed account of the idealised patterns associated with each mode of evolution of disparity through time.

606 **Extended Data Figure 4. Deviations of group-specific disparities from the disparity expected if all birds**  
607 **were evolving under a uniform Brownian motion model of evolution for additional groups of water-based**  
608 **(Gruiformes, Anseriformes) and land-based (non-landbird terrestrial Neoaves, Galliformes) birds.**  
609 Boxplots summarise the distribution of delta disparities, calculated as empirical disparities minus disparities for  
610 the 200 simulated values for each of the three target clades. All partitions and data types are displayed, namely,  
611 the whole skeleton, three main skeletal regions and individual bones and the four different aspects of  
612 morphological variation in the three target lineages of birds. Arrows highlight the lineage/partition/data type  
613 which shows particularly high (up pointing arrows) or low (down pointing arrows) values. Values are normalised  
614 by interquartile range.

615 **Extended Data Figure 5. Subclade disparity–age plots for the whole skeleton and body regions for**  
616 **Aequorlithornithes (waterbirds).** X axes represent subclade disparities while y axes represent time in millions of  
617 years from the present time. Solid coloured lines represent mean empirical disparities through time, dashed lines  
618 represent mean BM-simulated disparities through time, shaded polygons display the space between 95%  
619 percentile and 5% percentiles of disparities through time for BM-simulated data. Colour code of individual  
620 subclade disparities (dots) as in Figure 2.

621 **Extended Data Figure 6. Subclade disparity–age plots for the whole skeleton and body regions for**  
622 **Inopinaves (landbirds).** X axes represent subclade disparities while y axes represent time in millions of years  
623 from the present time. Solid coloured lines represent mean empirical disparities through time, dashed lines  
624 represent mean BM-simulated disparities through time, shaded polygons display the space between 95%  
625 percentile and 5% percentiles of disparities through time for BM-simulated data. Colour code of individual  
626 subclade disparities (dots) as in Figure 2.

627 **Extended Data Figure 7. Subclade disparity–age plots for the whole skeleton and body regions for**  
628 **Passeriformes (passerines).** X axes represent subclade disparities while y axes represent time in millions of years  
629 from the present time. Solid coloured lines represent mean empirical disparities through time, dashed lines  
630 represent mean BM-simulated disparities through time, shaded polygons display the space between 95%  
631 percentile and 5% percentiles of disparities through time for BM-simulated data. Colour code of individual  
632 subclade disparities (dots) as in Figure 2.

633 **Extended Data Figure 8. Subclade disparity–age plots for the individual elements for Aequorlithornithes**  
634 **(waterbirds).** X axes represent subclade disparities while y axes represent time in millions of years from the  
635 present time. Solid coloured lines represent mean empirical disparities through time, dashed lines represent mean  
636 BM-simulated disparities through time, shaded polygons display the space between 95% percentile and 5%  
637 percentiles of disparities through time for BM-simulated data. Colour code of individual subclade disparities  
638 (dots) as in Figure 2.

639 **Extended Data Figure 9. Subclade disparity–age plots for the individual elements for Inopinaves**  
640 **(landbirds).** X axes represent subclade disparities while y axes represent time in millions of years from the present  
641 time. Solid coloured lines represent mean empirical disparities through time, dashed lines represent mean BM-

642 simulated disparities through time, shaded polygons display the space between 95% percentile and 5% percentiles  
643 of disparities through time for BM-simulated data. Colour code of individual subclade disparities (dots) as in  
644 Figure 2.

645 **Extended Data Figure 10. Subclade disparity–age plots for the individual elements for Passeriformes**  
646 **(passerines).** X axes represent subclade disparities while y axes represent time in millions of years from the  
647 present time. Solid coloured lines represent mean empirical disparities through time, dashed lines represent mean  
648 BM-simulated disparities through time, shaded polygons display the space between 95% percentile and 5%  
649 percentiles of disparities through time for BM-simulated data. Colour code of individual subclade disparities  
650 (dots) as in Figure 2.

## 651 **Supplementary Information**

652 **Figures S1-S37**

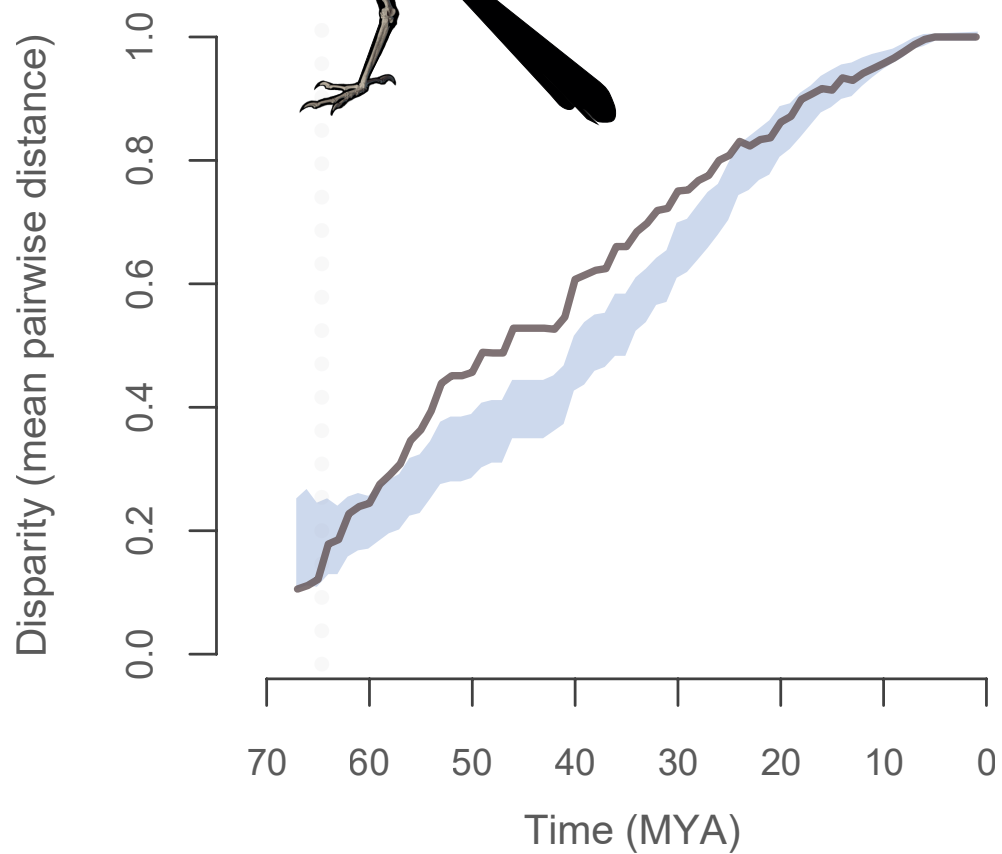
653 **Supplementary Materials (description in Supplementary Information)**

654 **Tables S1-S3 and Files S1-S7**

655

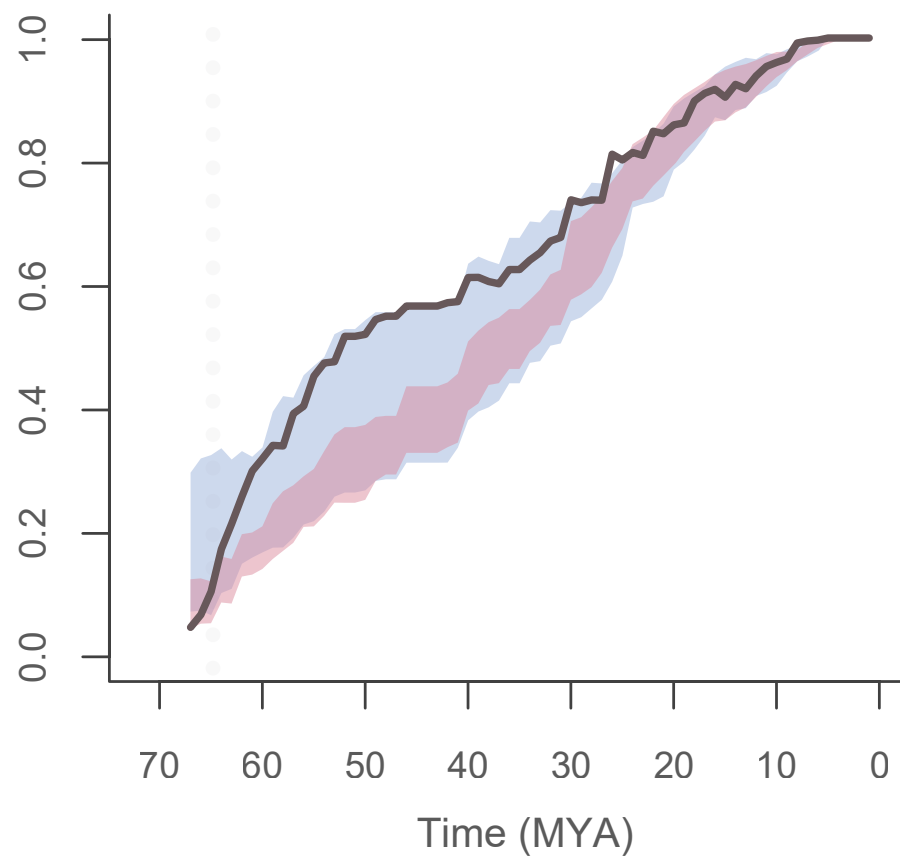
656

a)



95% CI for BM simulations (multivariate)

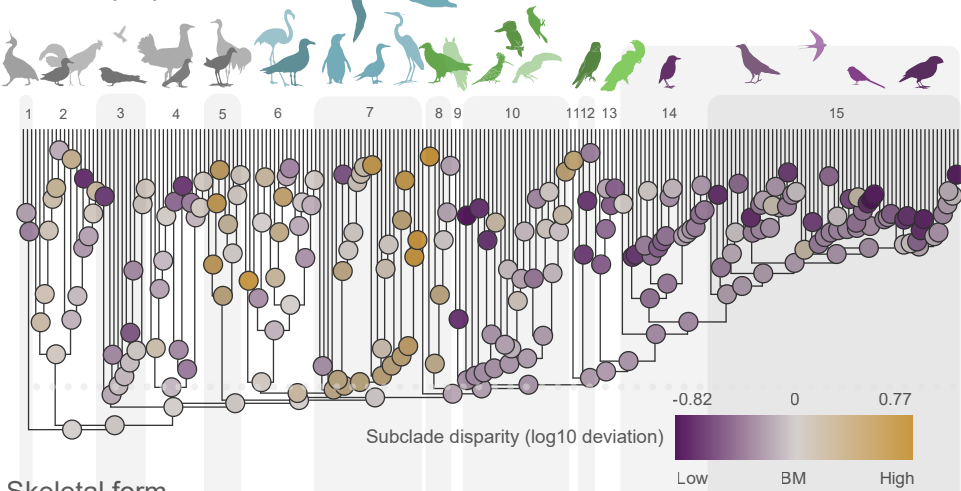
b)



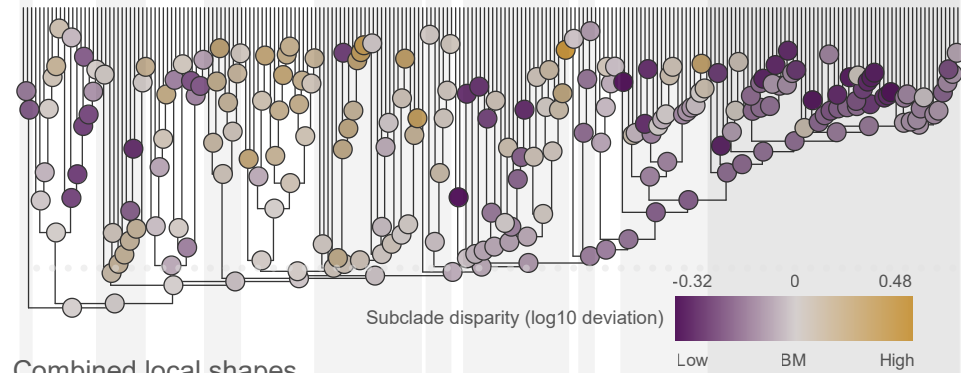
95% CI for BM simulations (univariate)

a) Whole skeleton

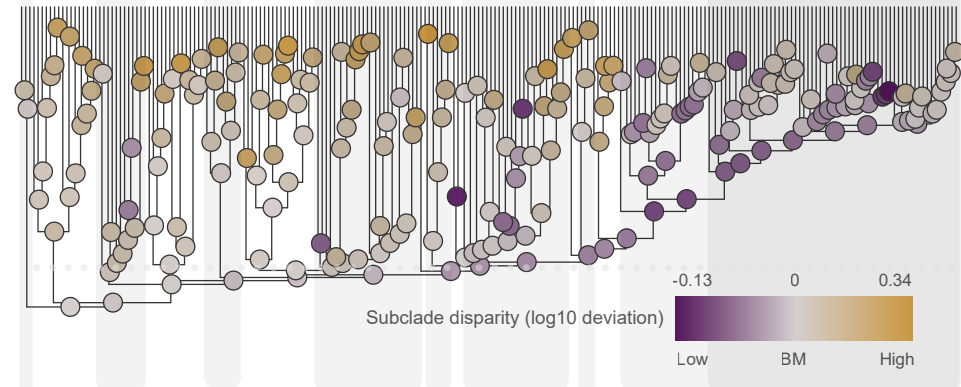
Skeletal proportions



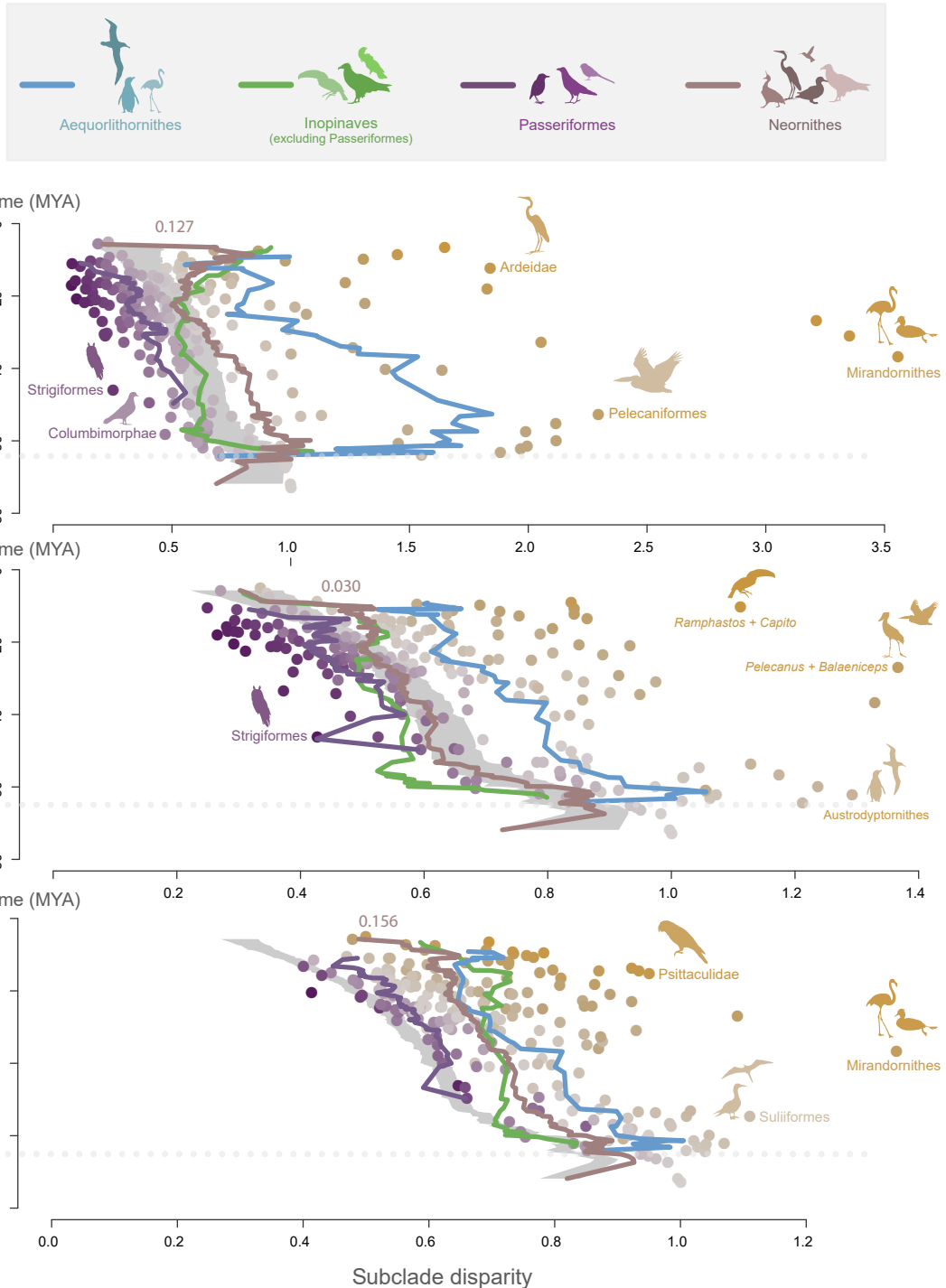
Skeletal form

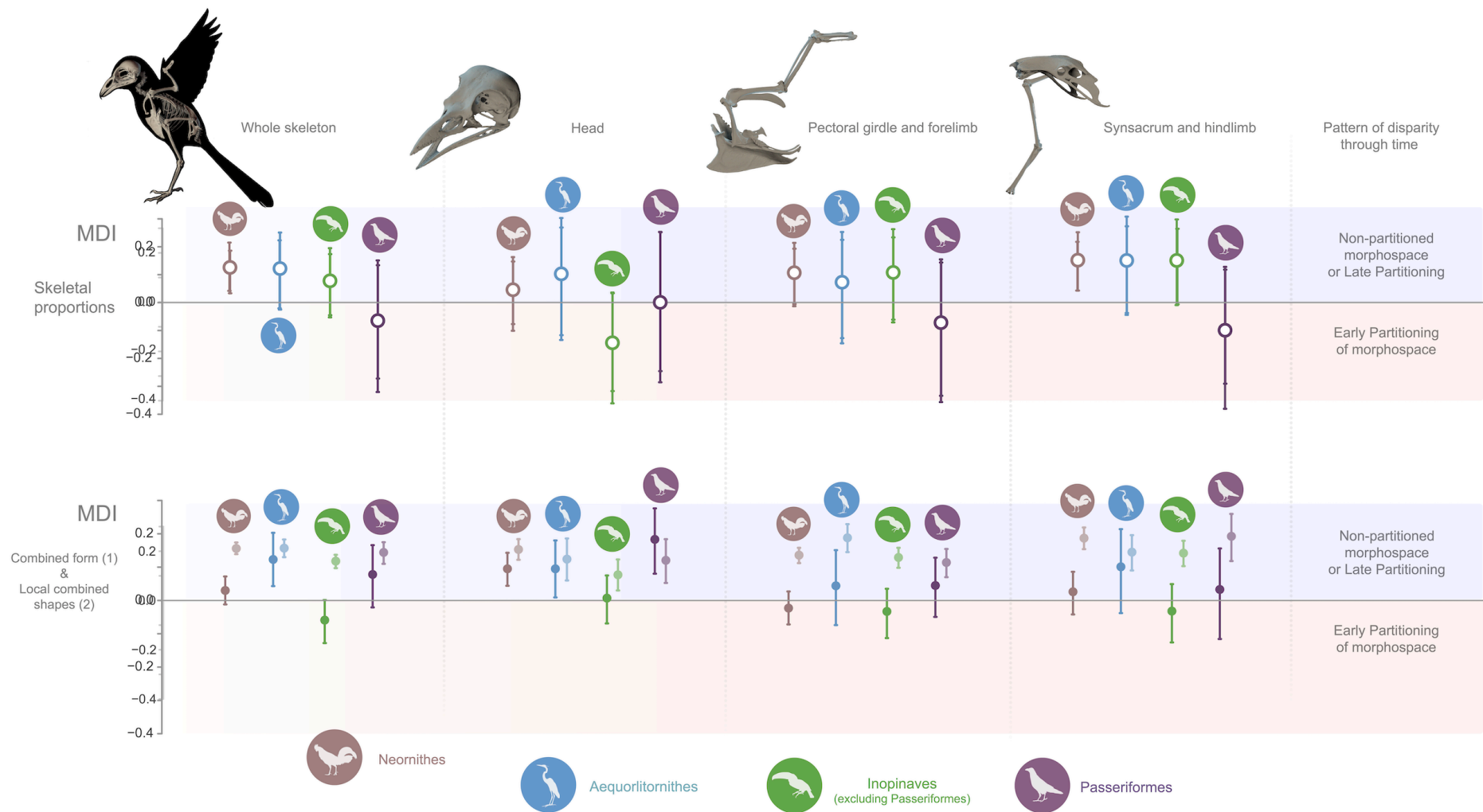


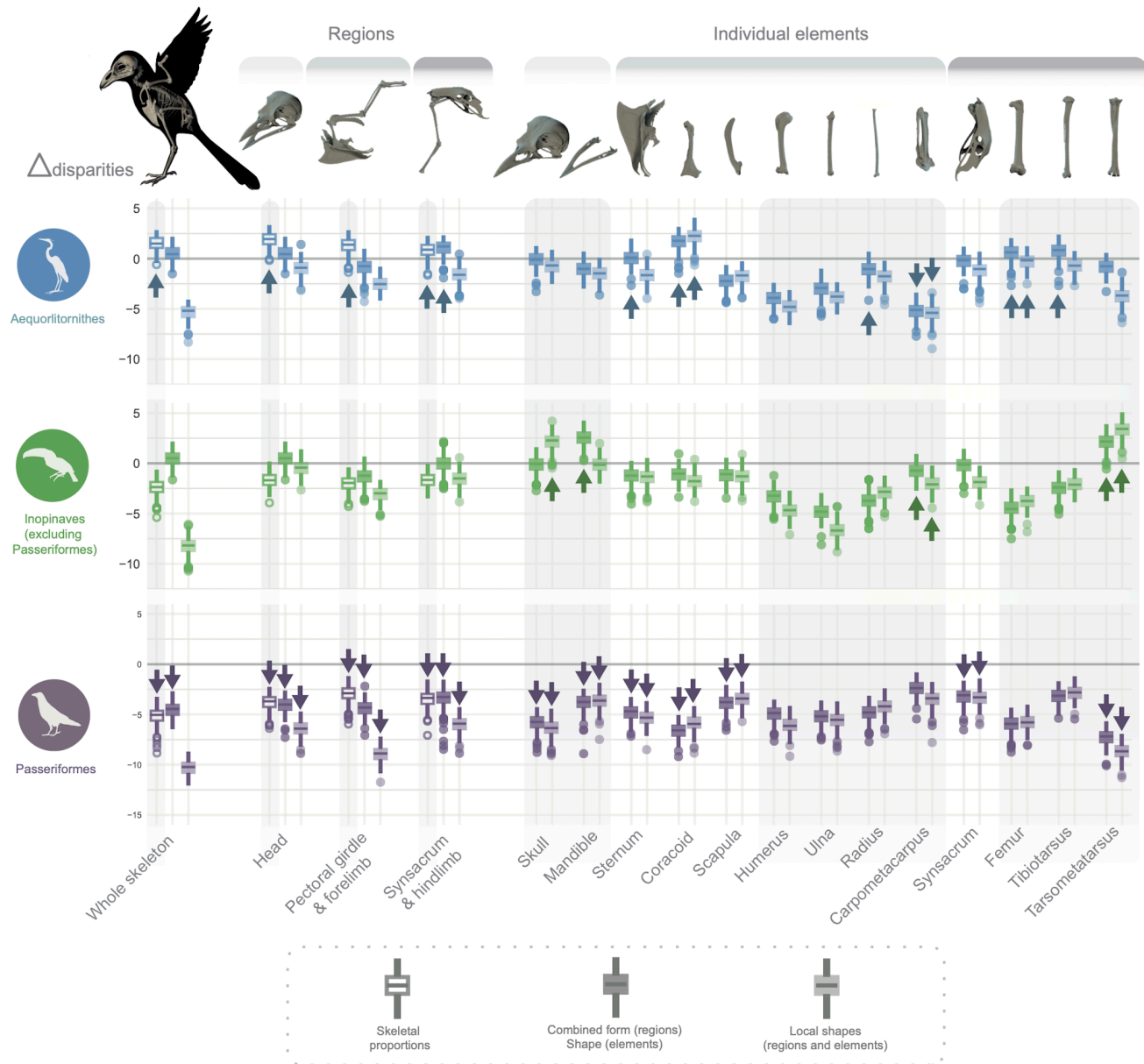
Combined local shapes



b)









# **Supplementary Information from**

## **Environmental signal in the evolutionary diversification of bird skeletons**

**Guillermo Navalón<sup>1,2,3\*</sup>, Alexander Bjarnason<sup>2</sup>, Elizabeth Griffiths<sup>2</sup>, Roger B. J. Benson<sup>2\*</sup>**

1. Department of Earth Sciences, University of Cambridge, Cambridge, UK.

2. Department of Earth Sciences, University of Oxford, Oxford, UK.

3. Unidad de Paleontología, Departamento de Biología, Universidad Autónoma de Madrid, Madrid, Spain.

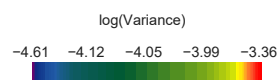
\*Corresponding authors: gn315@cam.ac.uk, roger.benson@earth.ox.ac.uk.

**Consisting of Figs. S1-S37. Presents extensive data on detailed patterns of skeletal evolution in birds per different regions and clades.**

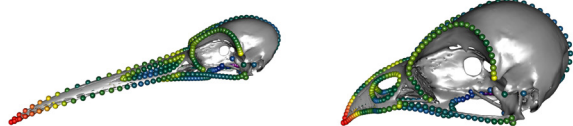
**Also see Supplementary Materials (available online):**

- **Table S1. List of specimens used in this study.**
- **Table S2. ANOVA tables used for proportions-normalising individual elements.**
- **Table S3. Pairs of landmarks used to calculate maximum distances in each of the spatial axes**
- **File S1. Bird\_landmarks\_Navalon\_2022. Raw landmark coordinates for all specimens used in this study.**
- **File S2. Read\_bird\_landmarks\_Navalon\_2022. R code to read the raw landmarks coordinates in File S1.**
- **File S3. Bird\_processed\_landmarks\_Navalon\_2022. Allometry free and proportions free landmark coordinates for all specimens used in this study.**
- **File S4. Read\_bird\_processed\_landmarks\_Navalon\_2022. R code to read the raw landmarks coordinates in File S3.**
- **File S5. Combined phylogeny used in this study.tre**
- **File S6. Custom R functions used in this study.**
- **File S7. Custom R code used in this study**

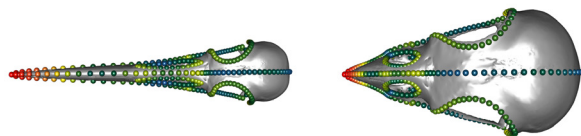
## Allometry-free shape



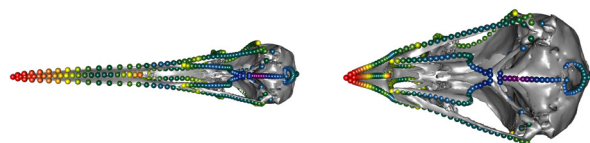
PC1



Lateral view

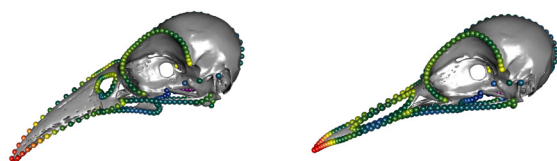


Dorsal view

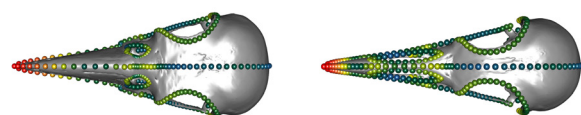


Palatal view

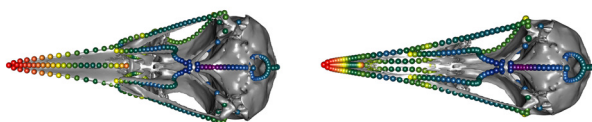
PC2



Lateral view



Dorsal view

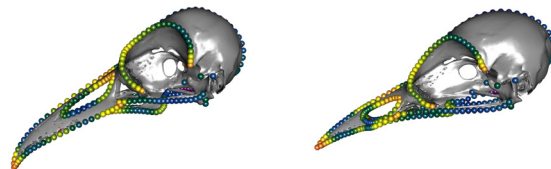


Palatal view

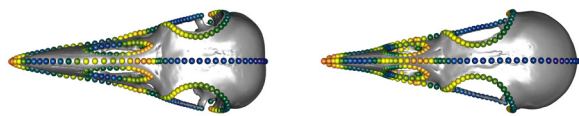
## Proportions-normalised shape



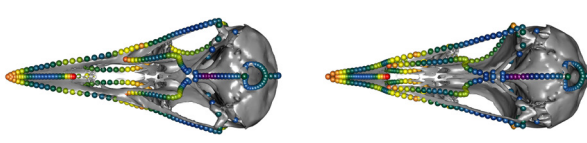
PC1



Lateral view

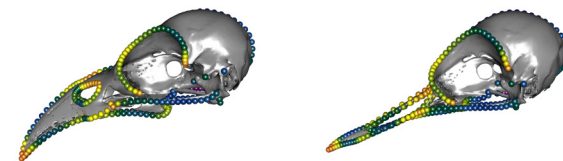


Dorsal view

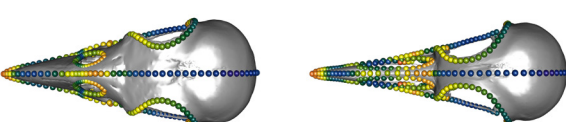


Palatal view

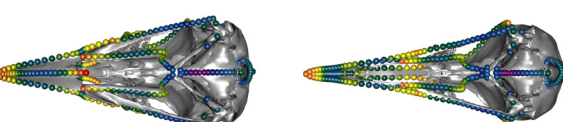
PC2



Lateral view



Dorsal view



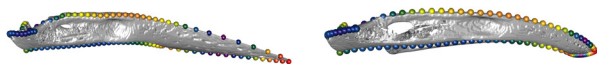
Palatal view

**Figure S1. Main shape (size normalized shape; left panel) and local shape variation (proportions normalized shape; right panel) for the skull.** Per landmark variances are color coded and placed on top of warped meshes for extreme shapes in each major axis of shape variation. Warped original mesh after the individual closer to mean shape.

## Allometry-free shape



PC1



Lateral view



Dorsal view



Palatal view

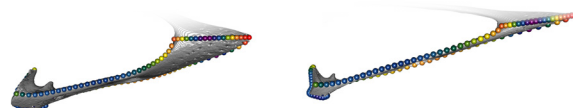
PC2



Lateral view

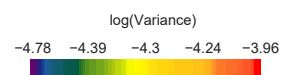


Dorsal view

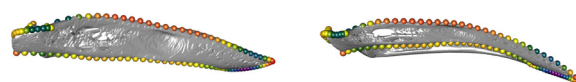


Palatal view

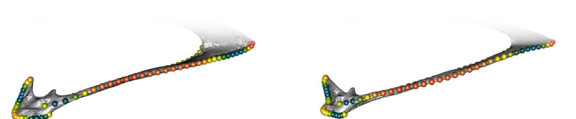
## Proportions-normalised shape



PC1



Lateral view



Dorsal view

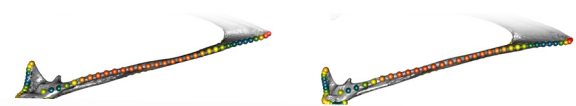


Palatal view

PC2



Lateral view



Dorsal view



Palatal view

**Figure S2. Main shape (size normalized shape; left panel) and local shape variation (proportions normalized shape; right panel) for the mandible.** Per landmark variances are color coded and placed on top of warped meshes for extreme shapes in each major axis of shape variation. Warped original mesh after the individual closer to mean shape.

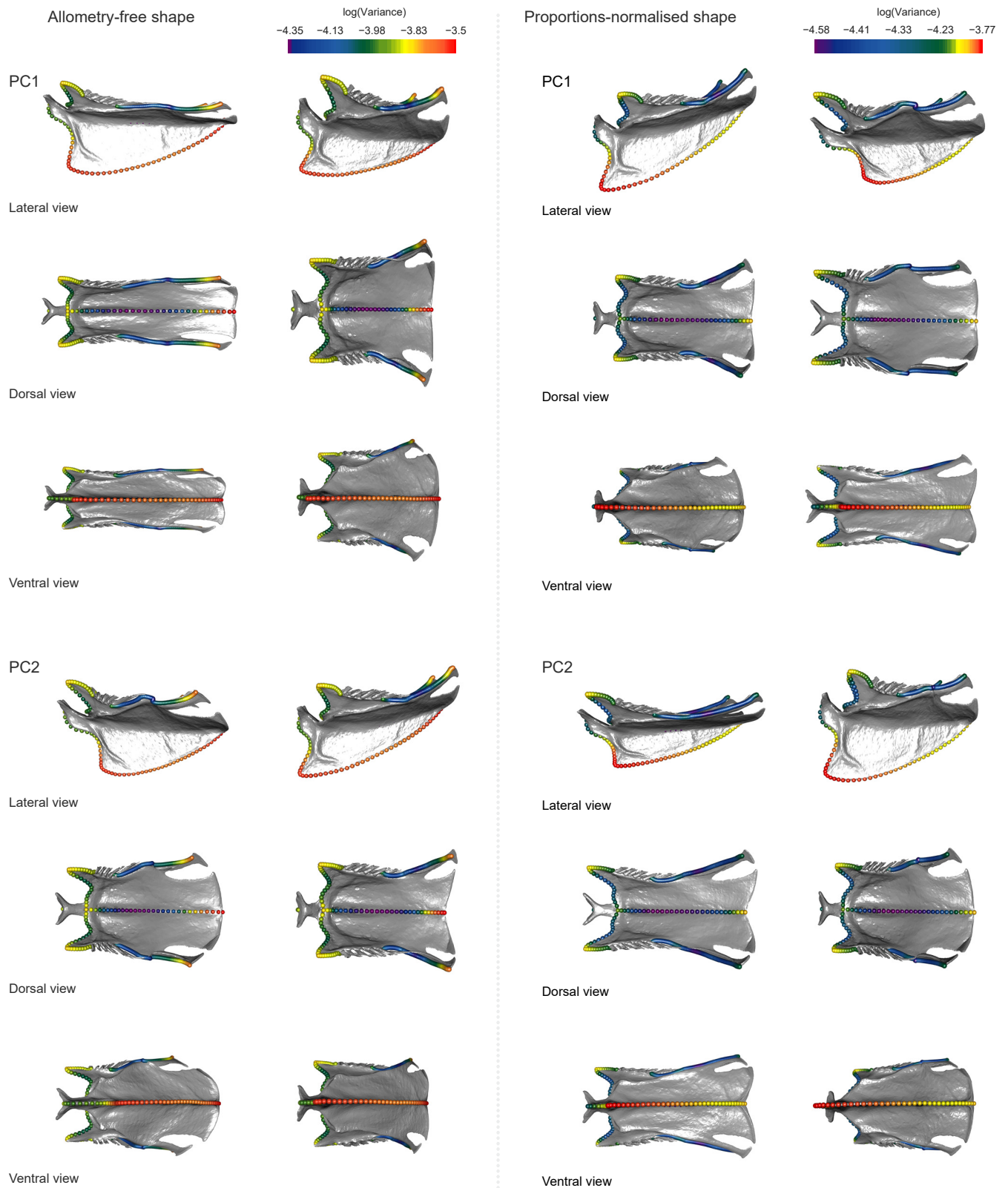


**Figure S3. Main shape (size normalized shape; left panel) and local shape variation (proportions normalized shape; right panel) for the sternum.** Per landmark variances are color coded and placed on top of warped meshes for extreme shapes in each major axis of shape variation. Warped original mesh after the individual closer to mean shape.

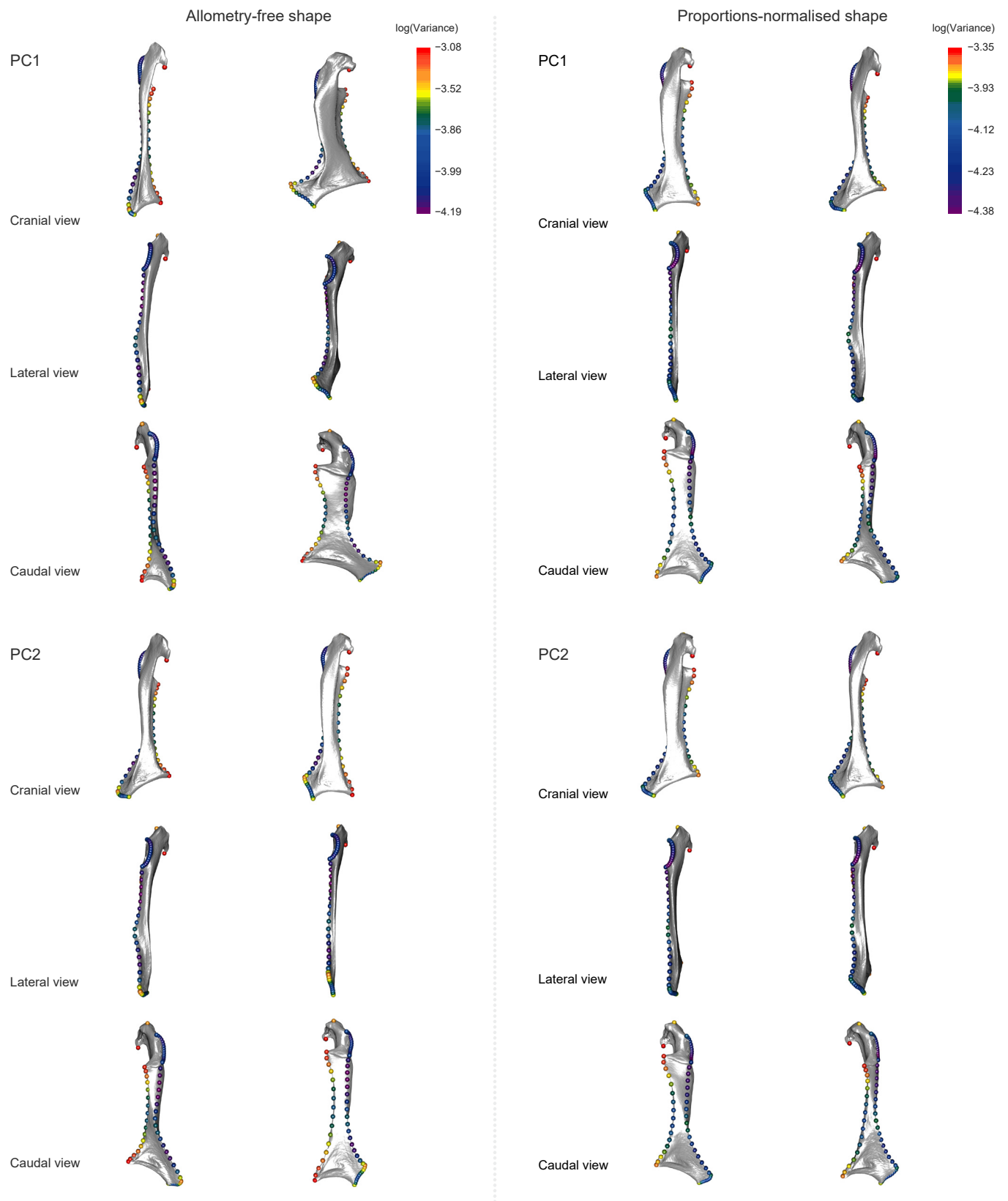


**Figure S4. Main shape (size normalized shape; left panel) and local shape variation (proportions normalized shape; right panel) for the coracoid.** Per landmark variances are color coded and placed on top of warped meshes for extreme shapes in each major axis of shape variation. Warped original mesh after the individual closer to mean shape.

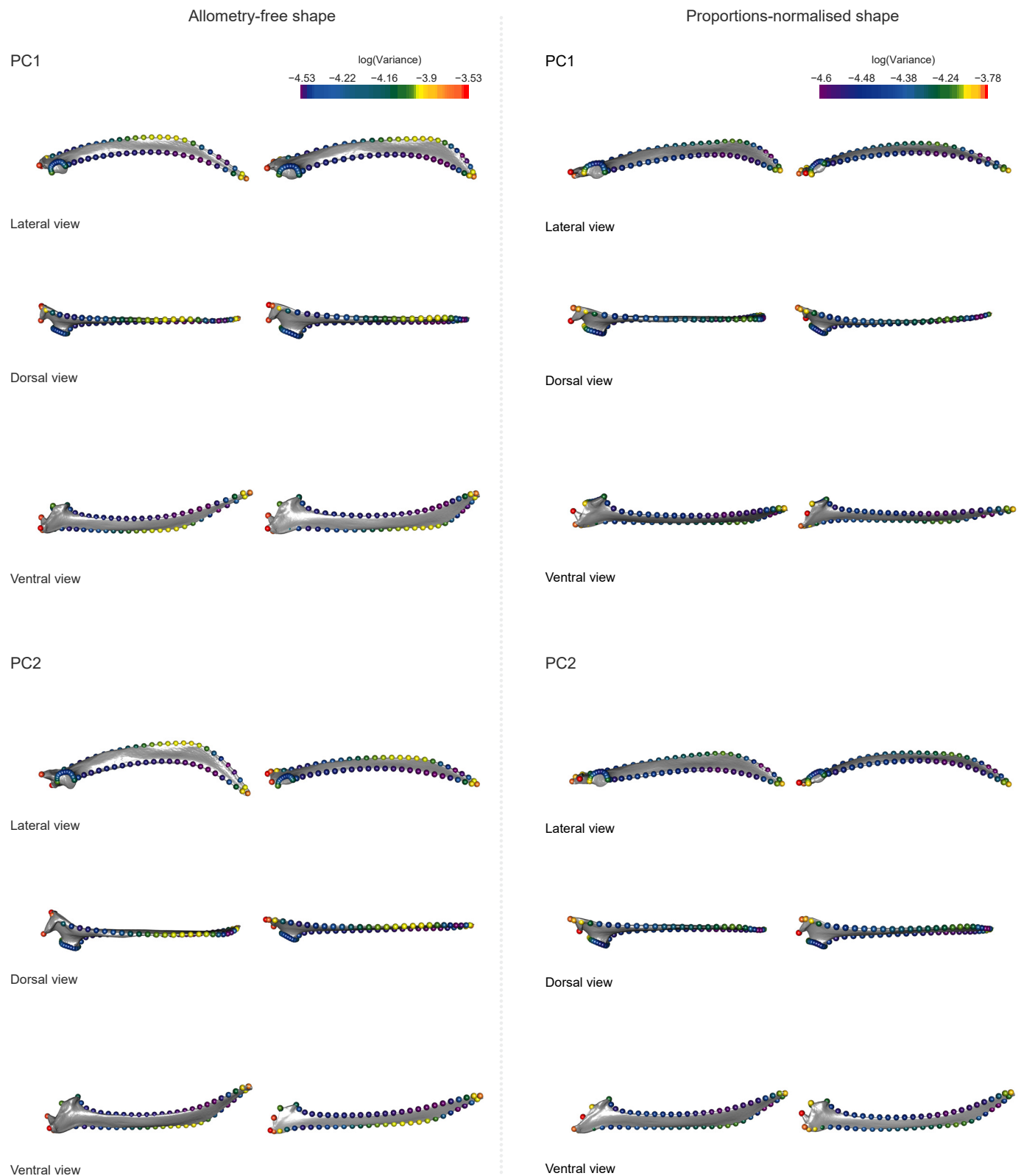


**Figure S5. Main shape (size normalized shape; left panel) and local shape variation (proportions normalized shape; right panel) for the scapula.** Per landmark variances are color coded and placed on top of warped meshes for extreme shapes in each major axis of shape variation. Warped original mesh after the individual closer to mean shape.



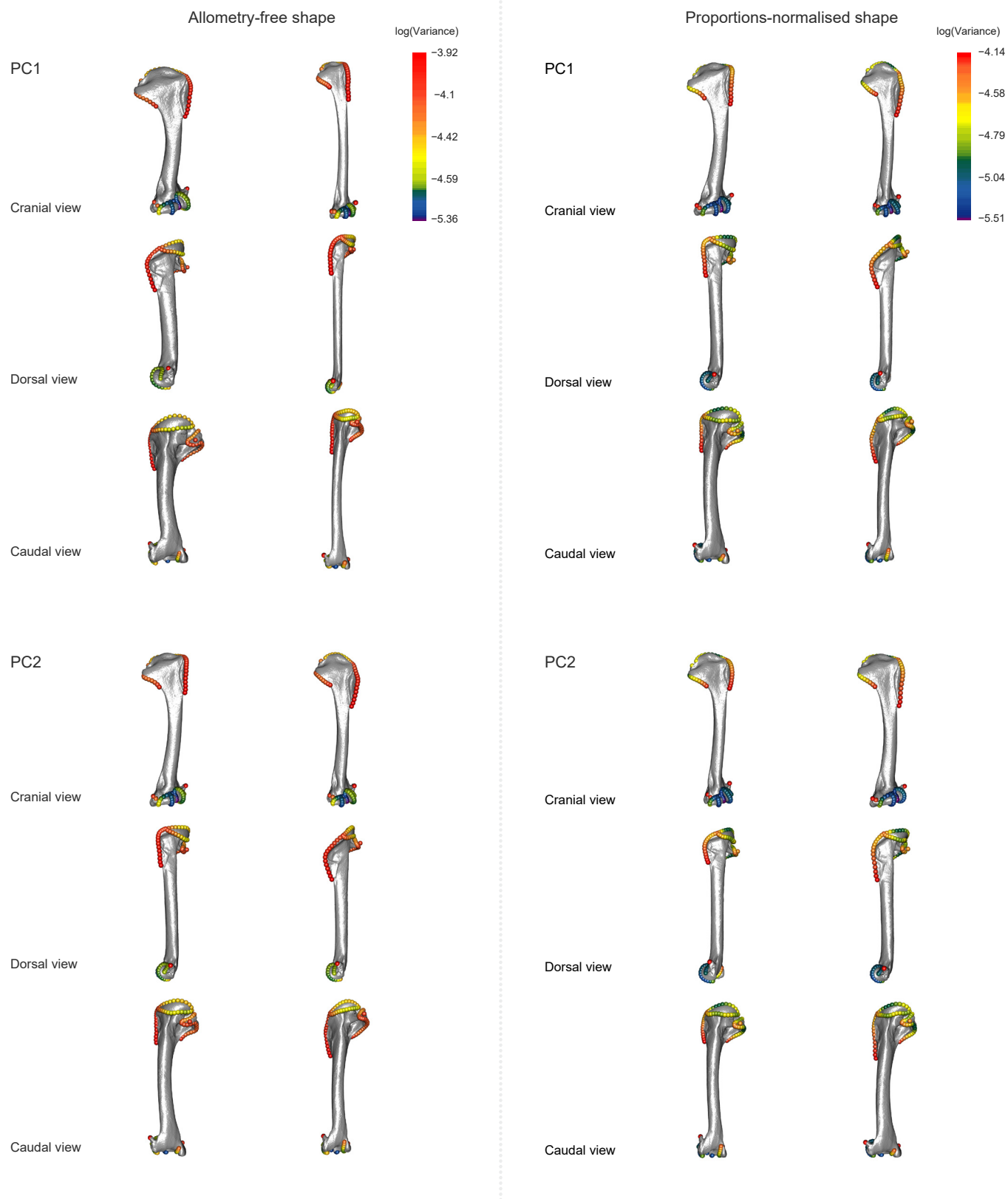


**Figure S6. Main shape (size normalized shape; left panel) and local shape variation (proportions normalized shape; right panel) for the humerus.** Per landmark variances are color coded and placed on top of warped meshes for extreme shapes in each major axis of shape variation. Warped original mesh after the individual closer to mean shape.



**Figure S7. Main shape (size normalized shape; left panel) and local shape variation (proportions normalized shape; right panel) for the ulna.** Per landmark variances are color coded and placed on top of warped meshes for extreme shapes in each major axis of shape variation. Warped original mesh after the individual closer to mean shape.



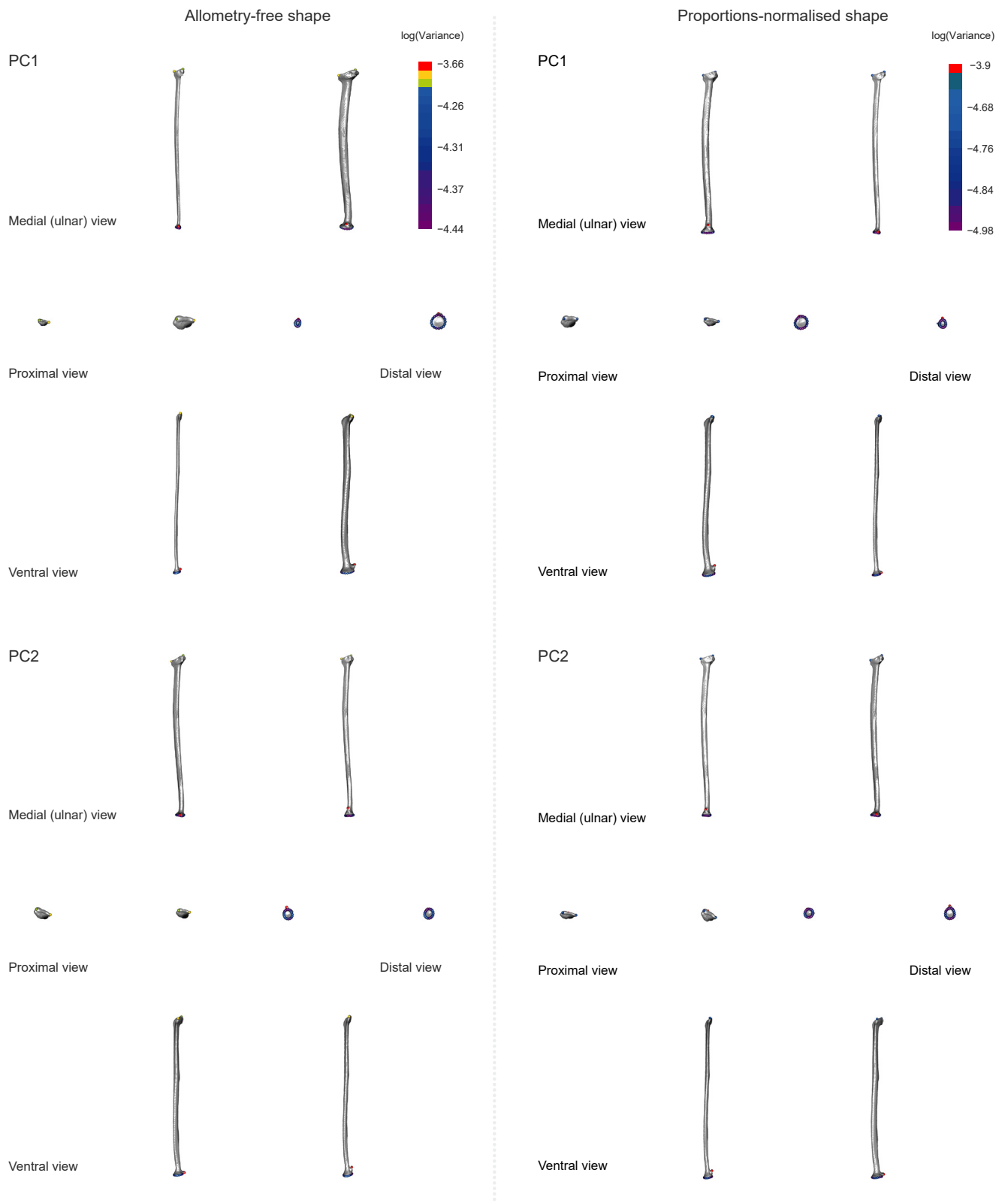
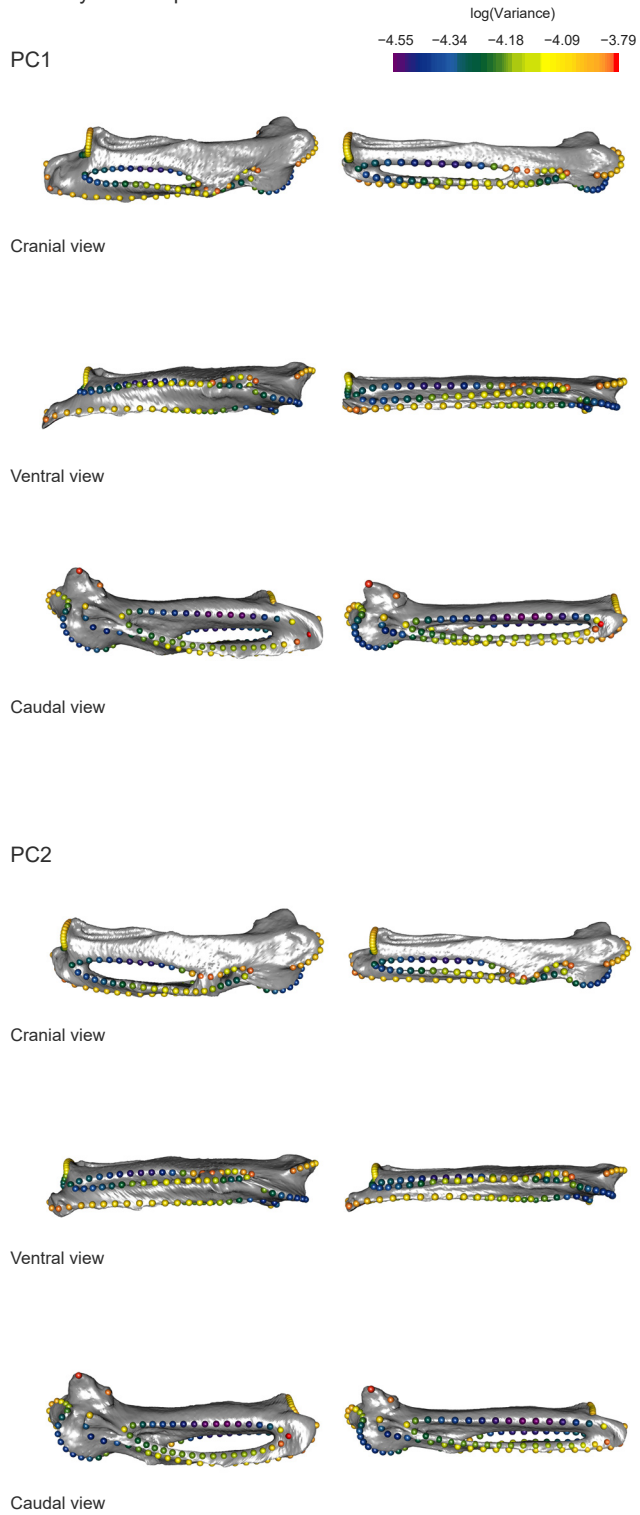


**Figure S8. Main shape (size normalized shape; left panel) and local shape variation (proportions normalized shape; right panel) for the radius.** Per landmark variances are color coded and placed on top of warped meshes for extreme shapes in each major axis of shape variation. Warped original mesh after the individual closer to mean shape.

## Allometry-free shape



## Proportions-normalised shape

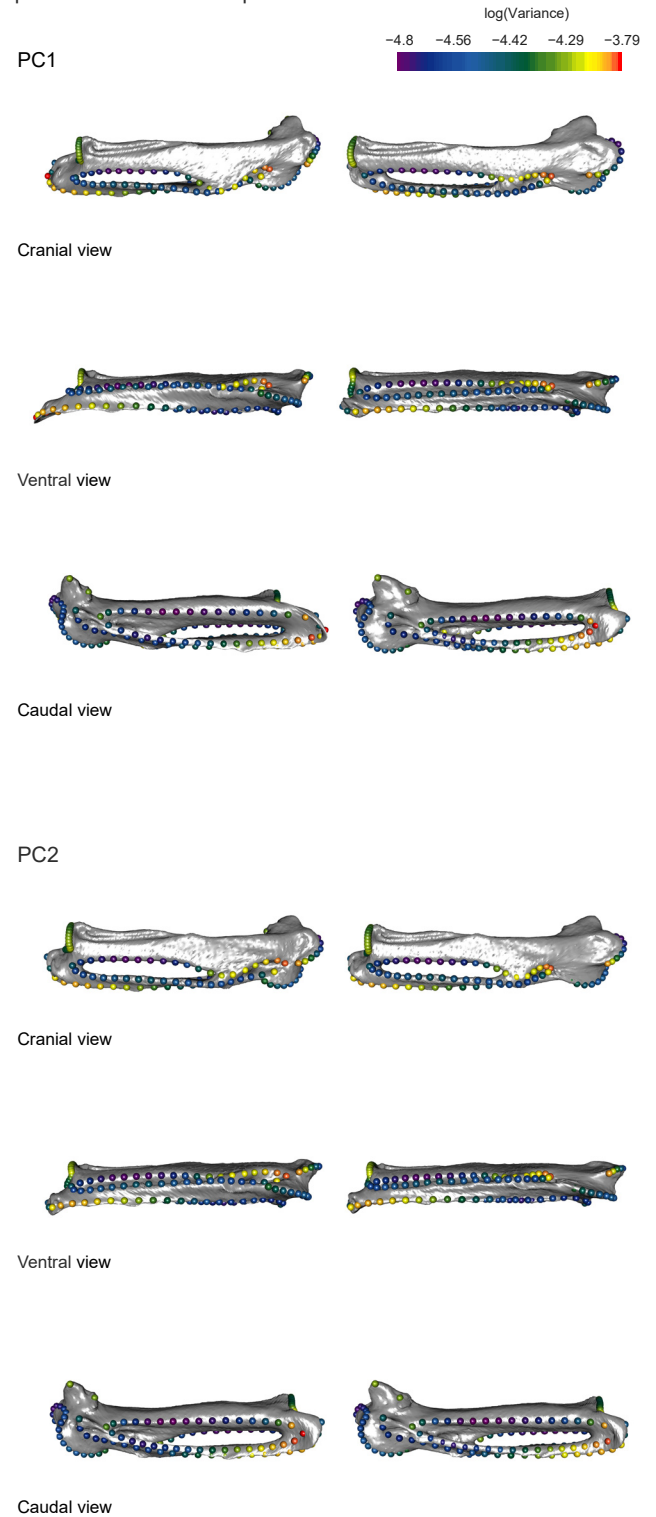
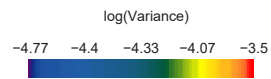
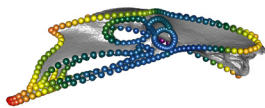


**Figure S9. Main shape (size normalized shape; left panel) and local shape variation (proportions normalized shape; right panel) for the carpometacarpus.** Per landmark variances are color coded and placed on top of warped meshes for extreme shapes in each major axis of shape variation. Warped original mesh after the individual closer to mean shape.

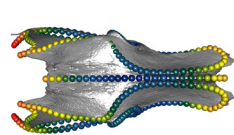
# Allometry-free shape



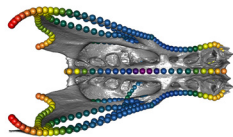
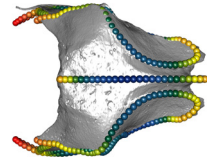
PC1



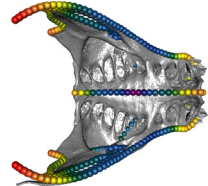
Lateral view



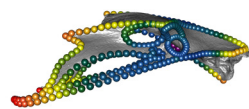
Dorsal view



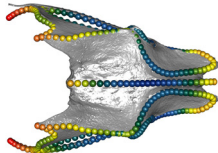
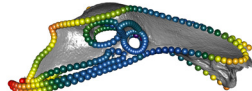
Palatal view



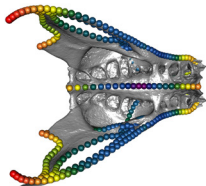
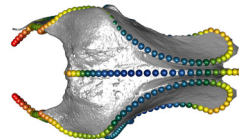
PC2



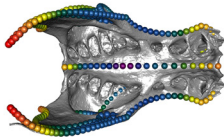
Lateral view



Dorsal view



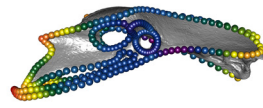
Palatal view



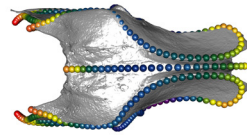
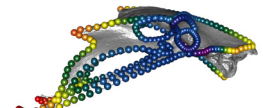
# Proportions-normalised shape



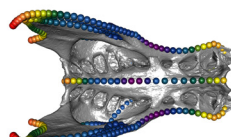
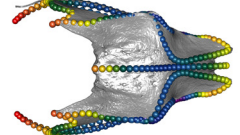
PC1



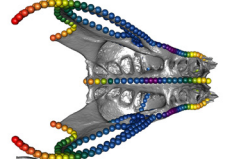
Lateral view



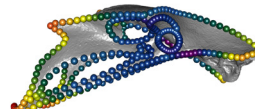
Dorsal view



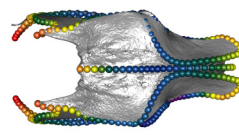
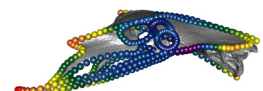
Palatal view



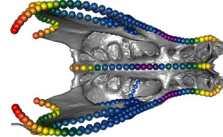
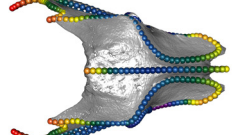
PC2



Lateral view



Dorsal view



Palatal view

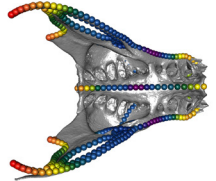


**Figure S10. Main shape (size normalized shape; left panel) and local shape variation (proportions normalized shape; right panel) for the synsacrum.** Per landmark variances are color coded and placed on top of warped meshes for extreme shapes in each major axis of shape variation. Warped original mesh after the individual closer to mean shape.

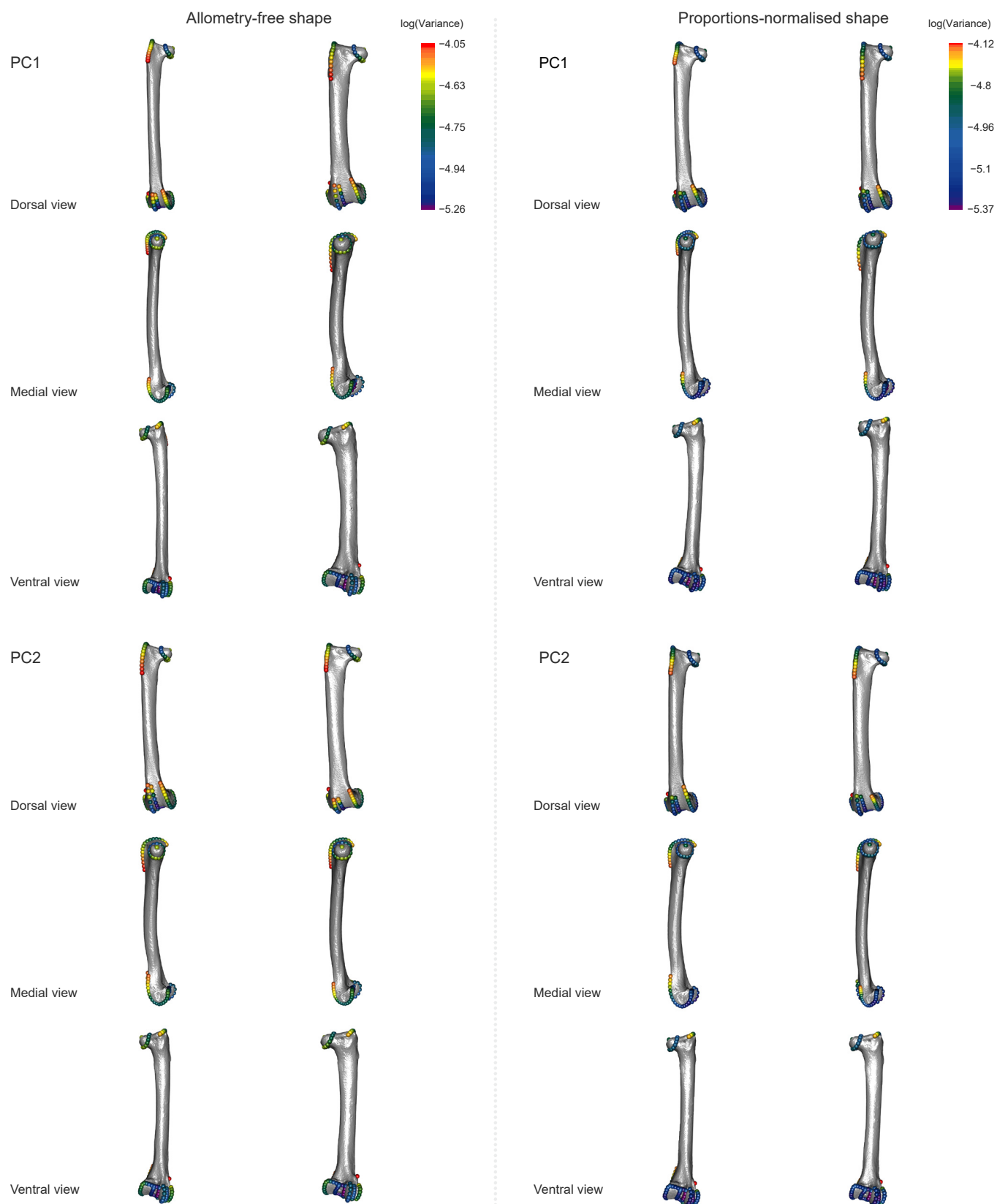


**Figure S11. Main shape (size normalized shape; left panel) and local shape variation (proportions normalized shape; right panel) for the femur.** Per landmark variances are color coded and placed on top of warped meshes for extreme shapes in each major axis of shape variation. Warped original mesh after the individual closer to mean shape.



**Figure S12. Main shape (size normalized shape; left panel) and local shape variation (proportions normalized shape; right panel) for the tibiotarsus.** Per landmark variances are color coded and placed on top of warped meshes for extreme shapes in each major axis of shape variation. Warped original mesh after the individual closer to mean shape.

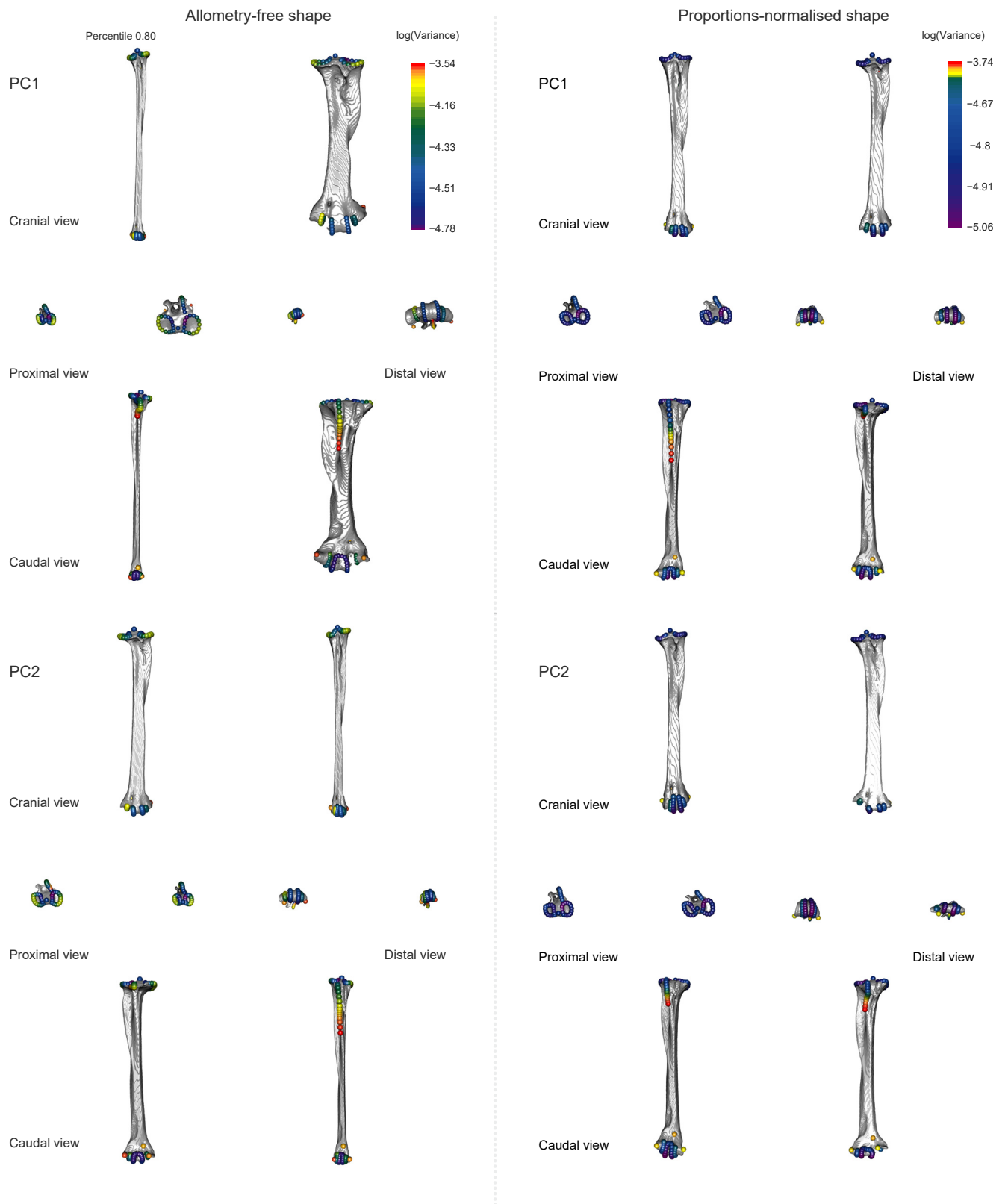
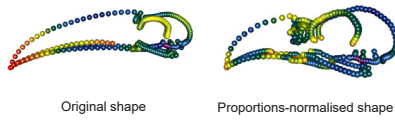


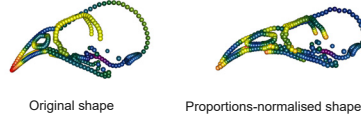
**Figure S13. Main shape (size normalized shape; left panel) and local shape variation (proportions normalized shape; right panel) for the tarsometatarsus.** Per landmark variances are color coded and placed on top of warped meshes for extreme shapes in each major axis of shape variation. Warped original mesh after the individual closer to mean shape.



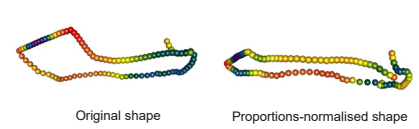
a. *Ramphastos ambiguus* (skull, lateral)



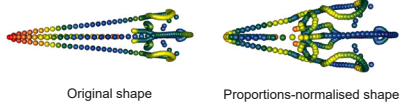
c. *Geospiza fuliginosa* (skull, lateral)



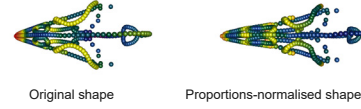
e. *Probosciger aterrimus* (mandible, lateral)



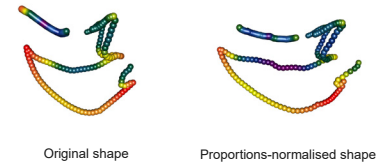
b. *Ramphastos ambiguus* (skull, dorsal)



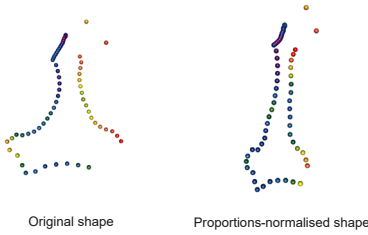
d. *Geospiza fuliginosa* (skull, dorsal)



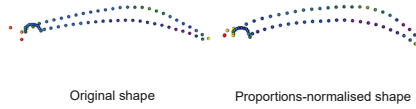
h. *Fregata aquila* (sternum, lateral)



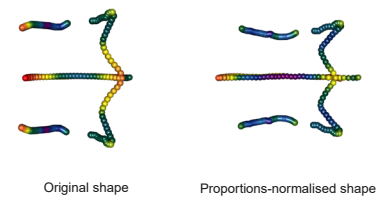
f. *Diomedea irrorata* (right coracoid, cranial )



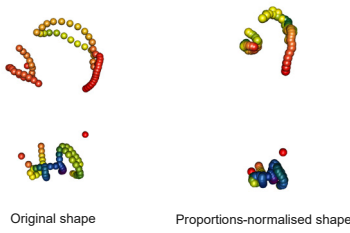
g. *Eremophila alpestris* (left scapula, lateral )



i. *Fregata aquila* (sternum, dorsal)



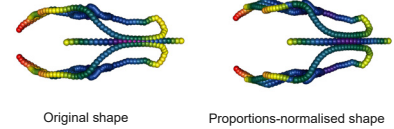
j. *Topaza pyra* (left humerus, cranial )



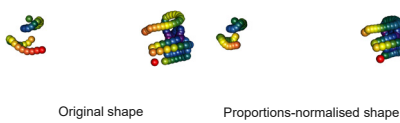
k. *Psaltriparus minimus* (left carpometacarpus, caudal)



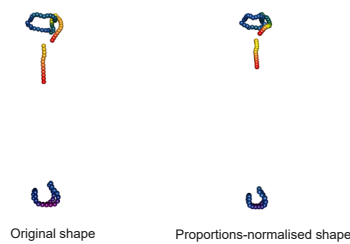
l. *Vultur gryphus* (synsacrum, dorsal)



m. *Phoenicopterus roseus*  
(right femur, cranial)



n. *Leipoa ocellata* (right tibiotarsus, lateral)



o. *Spheniscus humboldti*  
(tarsometatarsus, cranial)

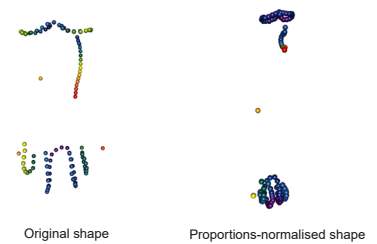


**Figure S14. Effects of normalisation for proportions in selected taxa for all 13 skeletal elements.**



## Neornithes (Regions)

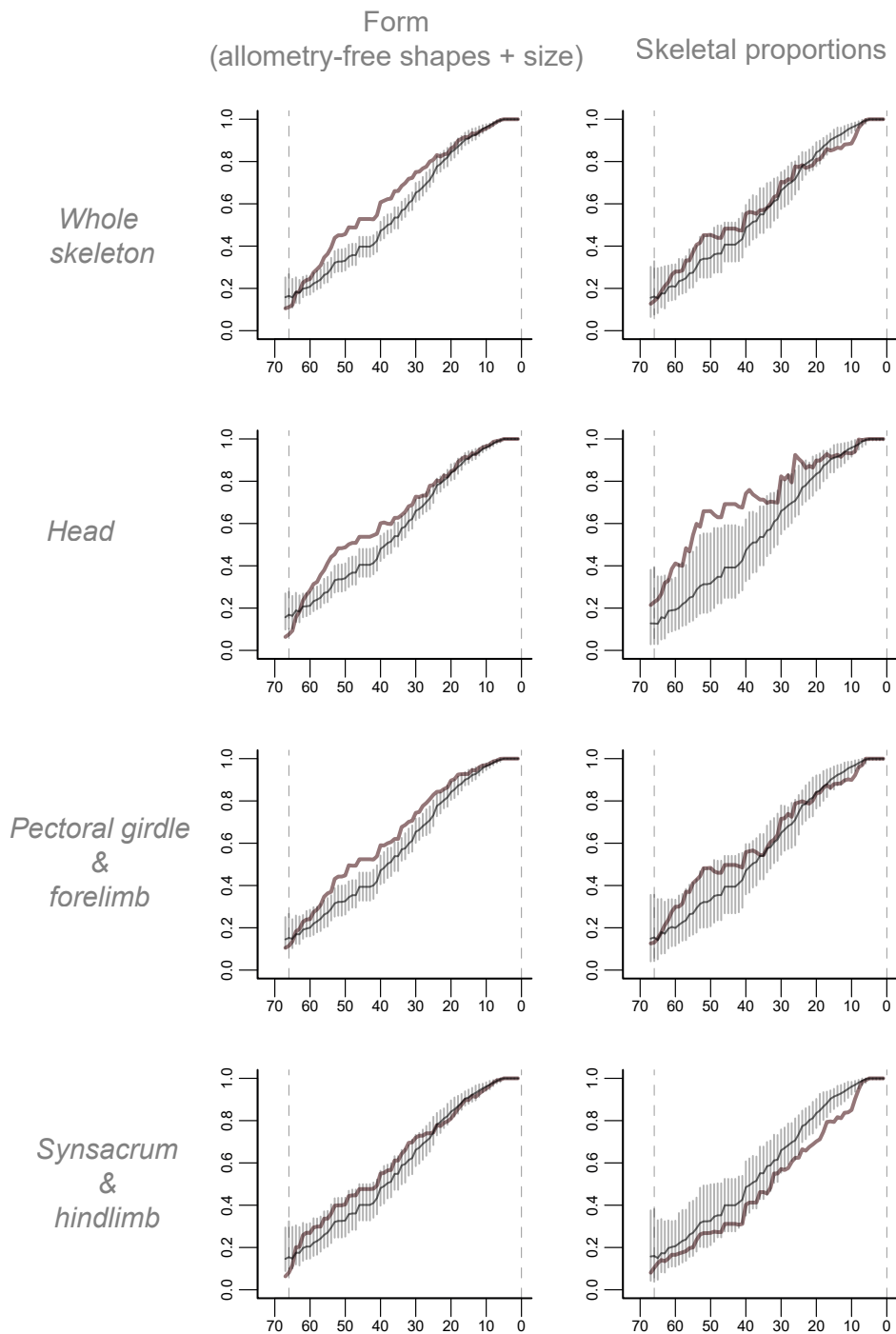


**Figure S15. Whole clade disparity-time plots (patterns of morphospace establishment) for the three studied aspects of morphological variation for the whole skeleton and body regions for Neornithes.** Empirical 1-million-year time bin disparity values for Neornithes indicated by the brown continuous line. Confidence intervals (grey vertical lines) and mean values (dark grey continuous line) for the 1-million-year time binned disparities for multivariate simulations under a Brownian Motion model of evolution. X axes represent disparity (mean pairwise distance) and Y axes represent time in million years before the present.





## Neornithes (Individual bones)

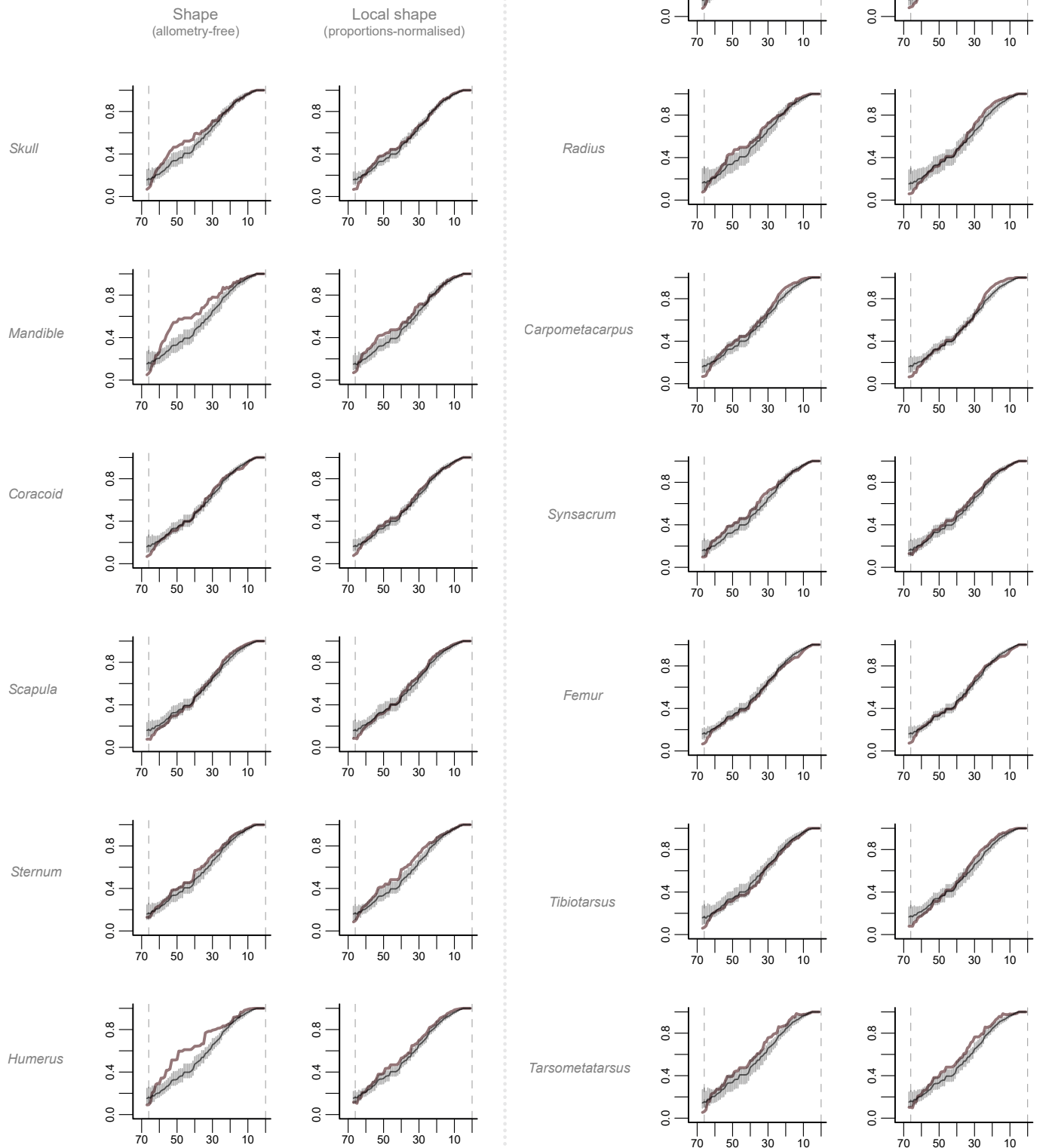


**Figure S16.** Whole clade disparity-time plots (patterns of morphospace establishment) for the two studied aspects of morphological variation for the individual elements for Neornithes. Legend as in Figure S15.

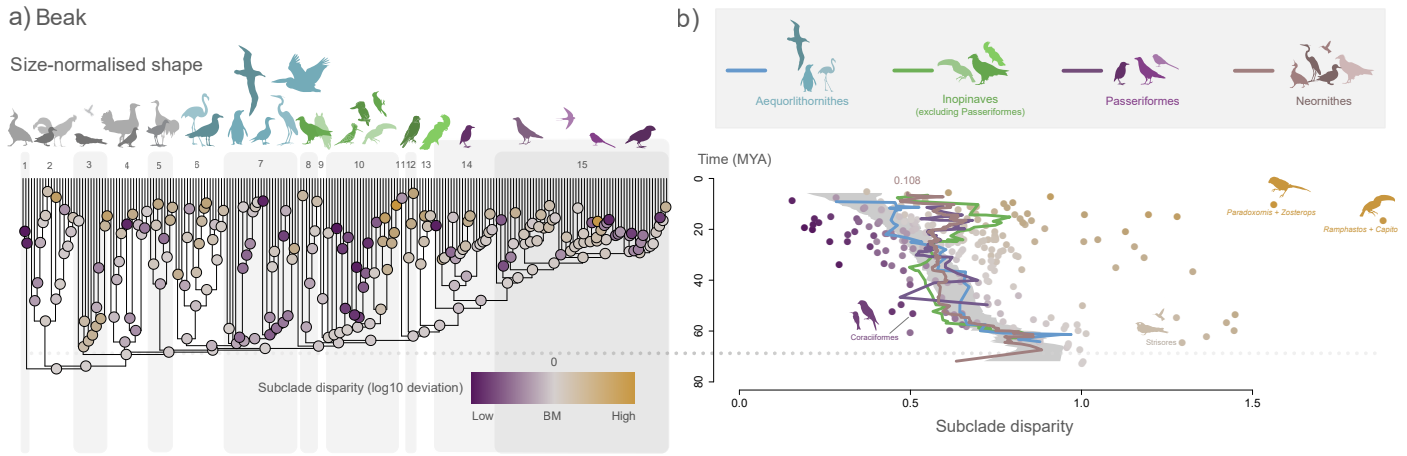


**Figure S17. Subclade disparity–age plotted across avian phylogeny and through time for beak shape.** a) Subclade disparity values colour-coded and plotted for each of the studied clades in their basal nodes. Subclade disparity values are log-10 transformed deviations of empirical values from means of 200 simulations of morphological evolution under a constant diffusive model of evolution (Brownian Motion, BM). Purples represent lower disparities than expected under BM, ochres represent higher disparities than expected under BM. b) Patterns of mean binned values of disparity through time for all birds (Neornithes) and three target lineages. Grey envelope represents the maximum and minimum values for each bin of the 200 simulations of morphological evolution under BM. Individual colour coded lineage values are plotted and some extreme values are labelled. Time scale in million years apply for both parts of the figure and the dotted horizontal line at 67 MYA indicates the timing of K-Pg extinction. Clades in a) indicated as numbers: 1. Palaeognathae, 2. Galloanserae, 3. Strisores, 4. Columbaves, 5. Gruiformes, 6. Mirandornithes + Charadriiformes, 7. Ardeae, 8. Accipitriformes, 9. Strigiformes, 10. Eucavitaves, 11. Cariamiformes, 12. Falconiformes, 13. Psittaciformes, 14. Suboscines (Passeriformes), 15. Oscines (Passeriformes).

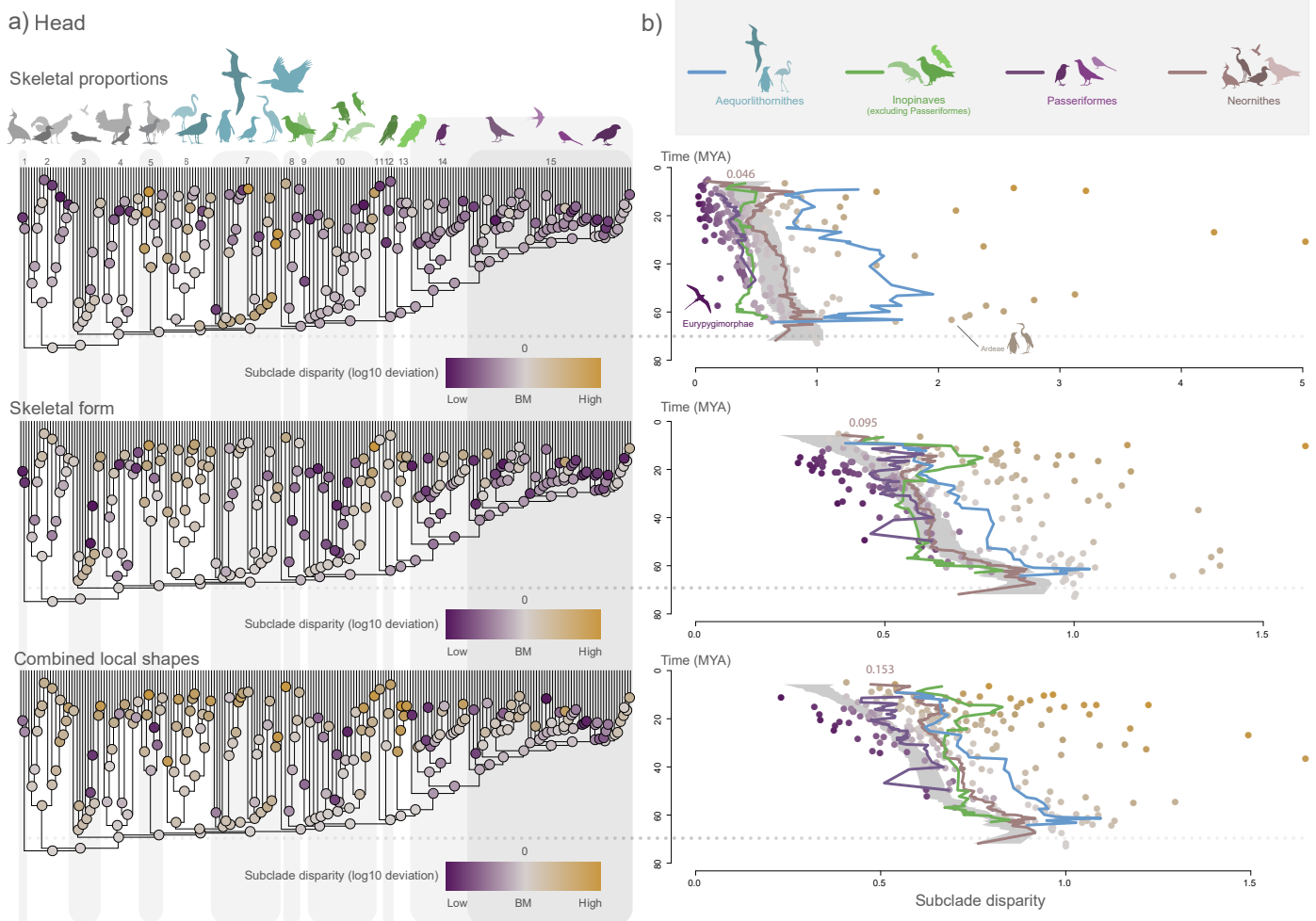


**Figure S18. Subclade disparity–age plotted across avian phylogeny and through time for head skeletal proportions, form and combined local shape.** Legend as in Figure S15 and Figure 1 in the main text.

a) Pectoral girdle and forelimb

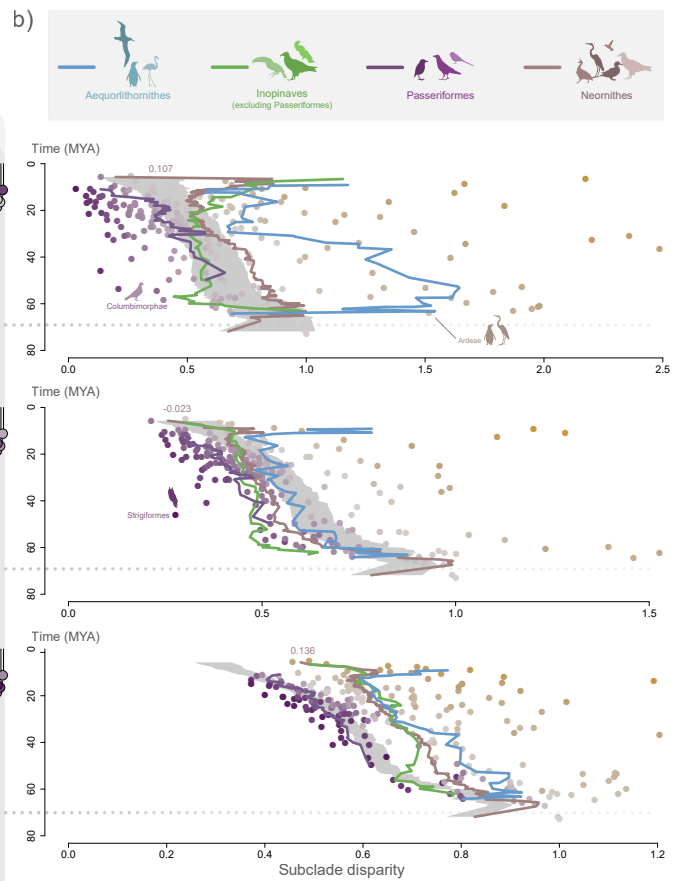
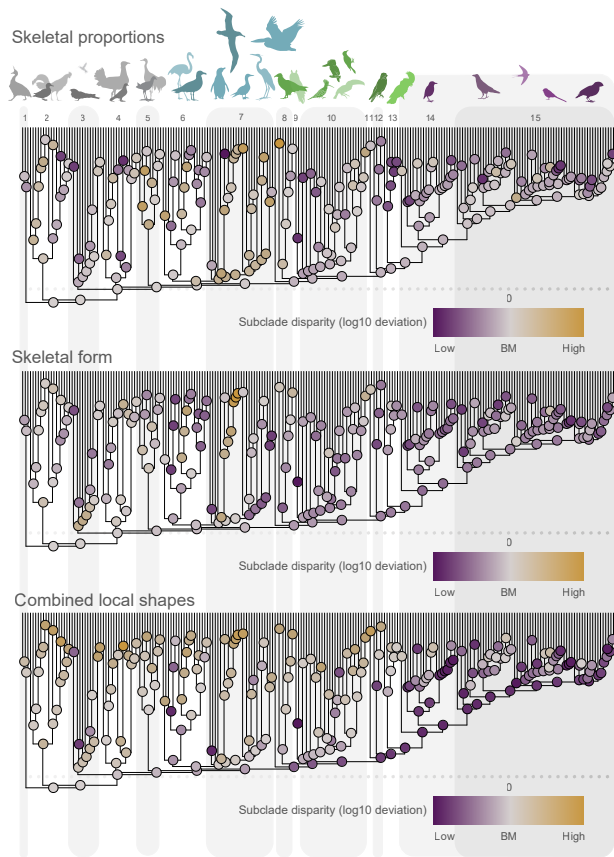


**Figure S19.** Subclade disparity–age plotted across avian phylogeny and through time for pectoral girdle and forelimb’s skeletal proportions, form and combined local shape. Legend as in Figure S15 and Figure 1 in the main text.

a) Synsacrum and hindlimb

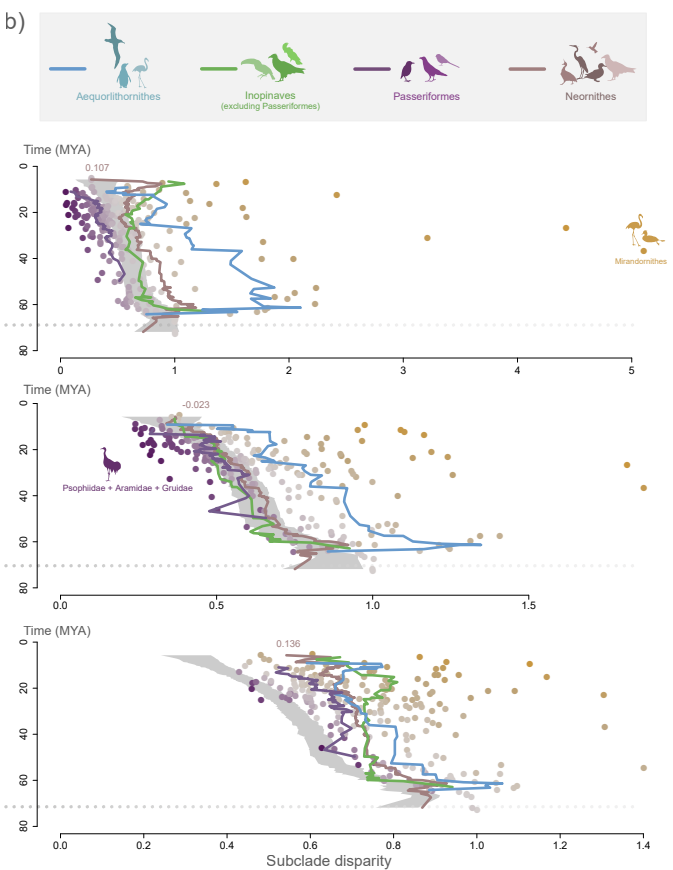
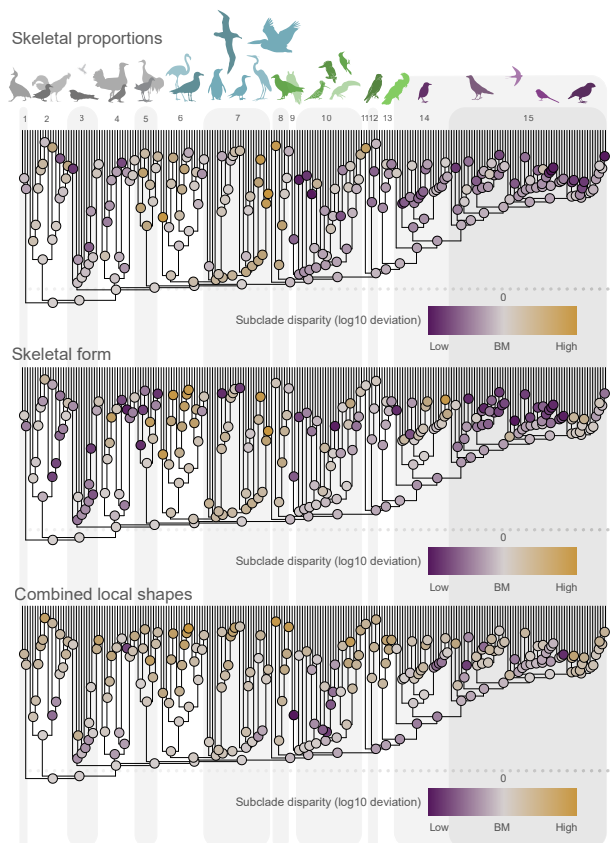
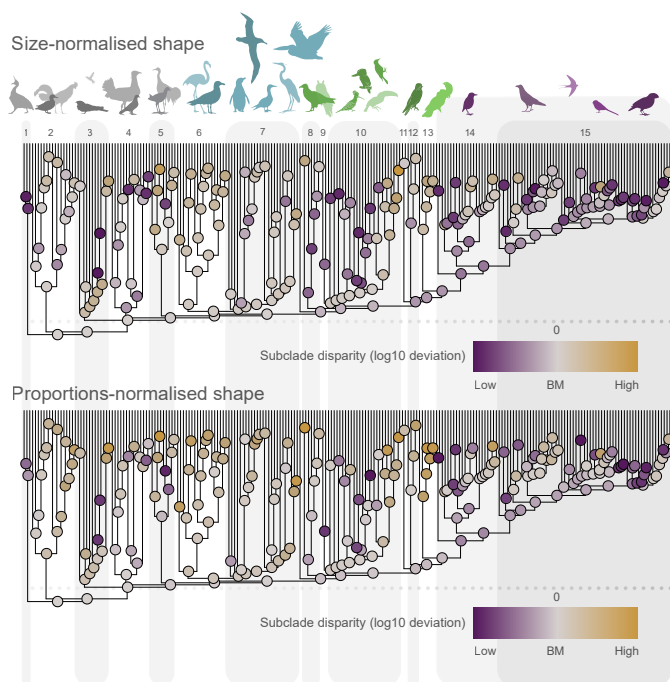


**Figure S20.** Subclade disparity–age plotted across avian phylogeny and through time for synsacrum and hindlimb’s skeletal proportions, form and combined local shape. Legend as in Figure S15 and Figure 1 in the main text.

a) Skull



b)

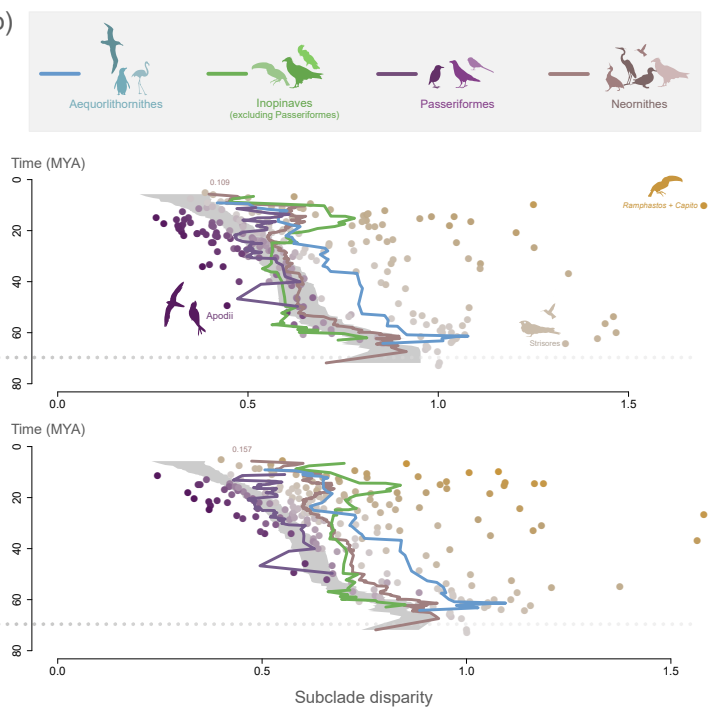
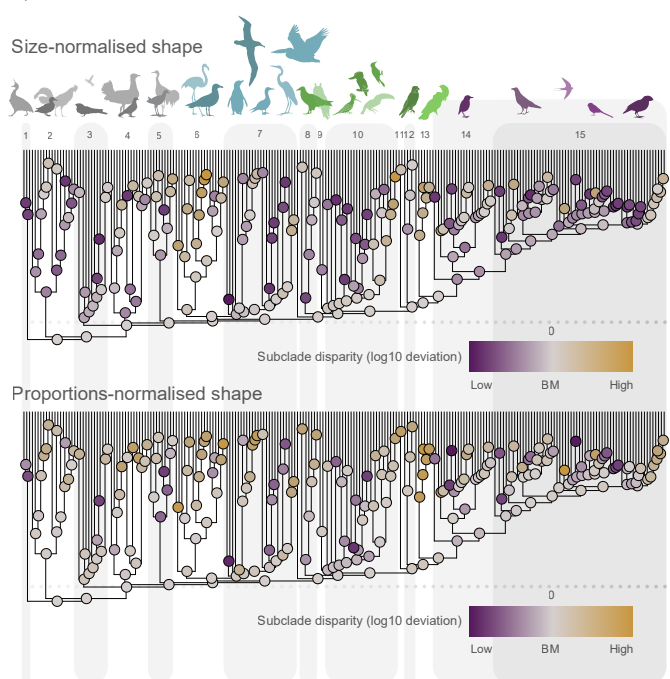


**Figure S21. Subclade disparity–age plotted across avian phylogeny and through time for skull shape (size-normalised shape) and local shape (proportions-normalised shape).** Legend as in Figure S15 and Figure 1 in the main text.

a) Mandible



b)

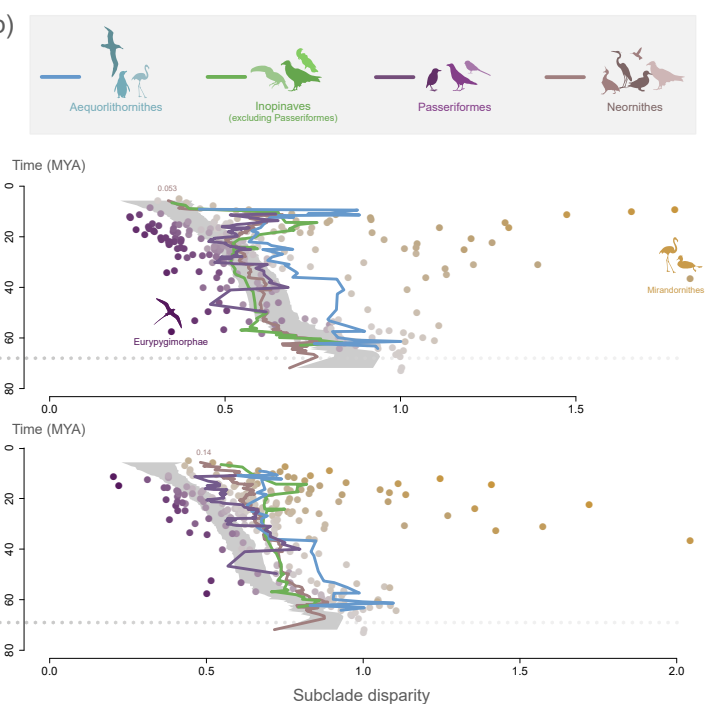
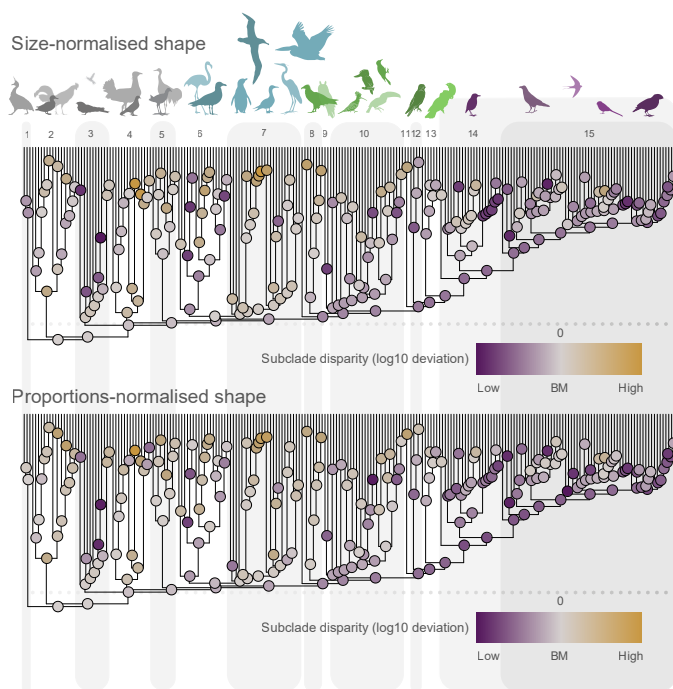


**Figure S22. Subclade disparity–age plotted across avian phylogeny and through time for mandible shape (size-normalised shape) and local shape (proportions-normalised shape).** Legend as in Figure S15 and Figure 1 in the main text.

a) Sternum



b)

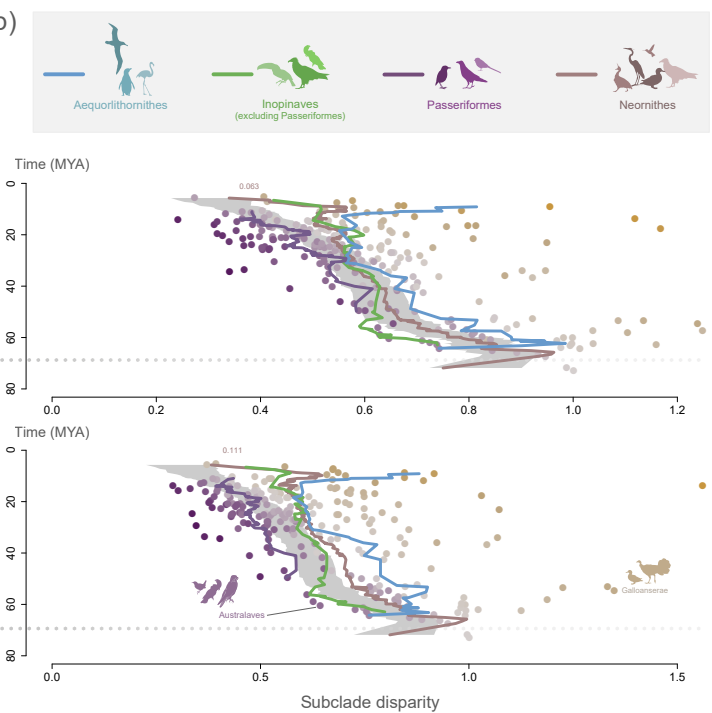
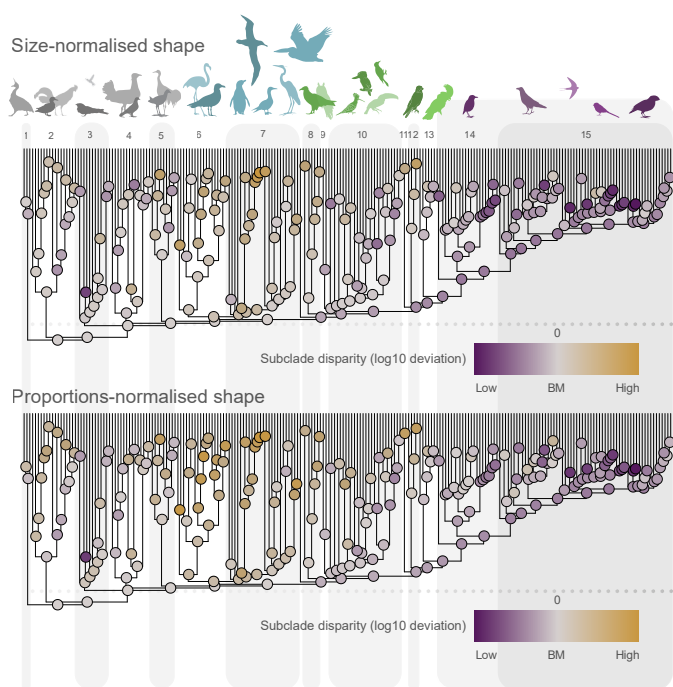


**Figure S23. Subclade disparity–age plotted across avian phylogeny and through time for sternum shape (size-normalised shape) and local shape (proportions-normalised shape).** Legend as in Figure S15 and Figure 1 in the main text.

a) Coracoid



b)

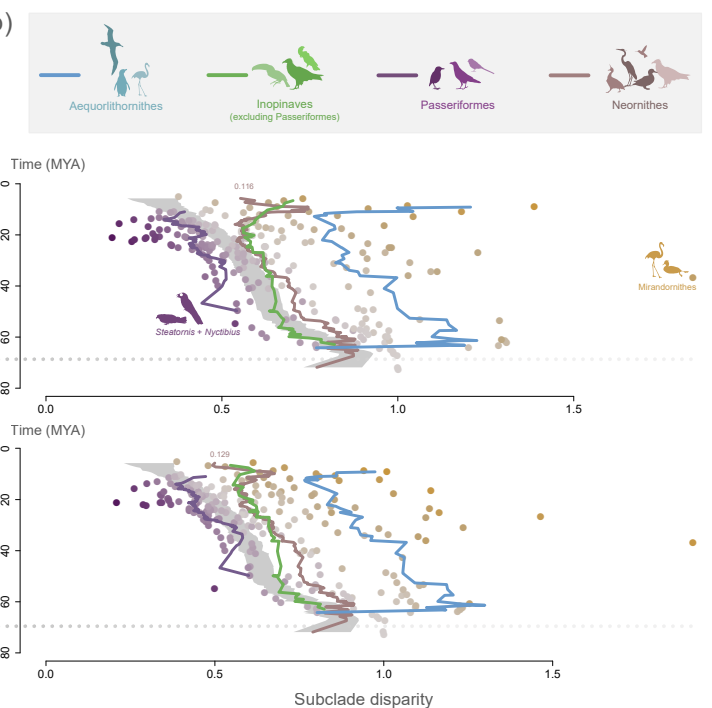
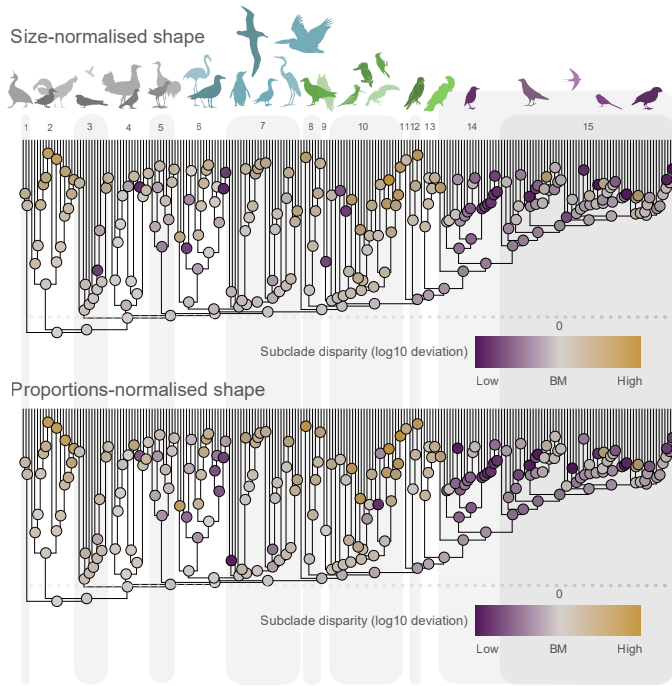


**Figure S24. Subclade disparity–age plotted across avian phylogeny and through time for coracoid shape (size-normalised shape) and local shape (proportions-normalised shape).** Legend as in Figure S15 and Figure 1 in the main text.



a) Scapula



b)

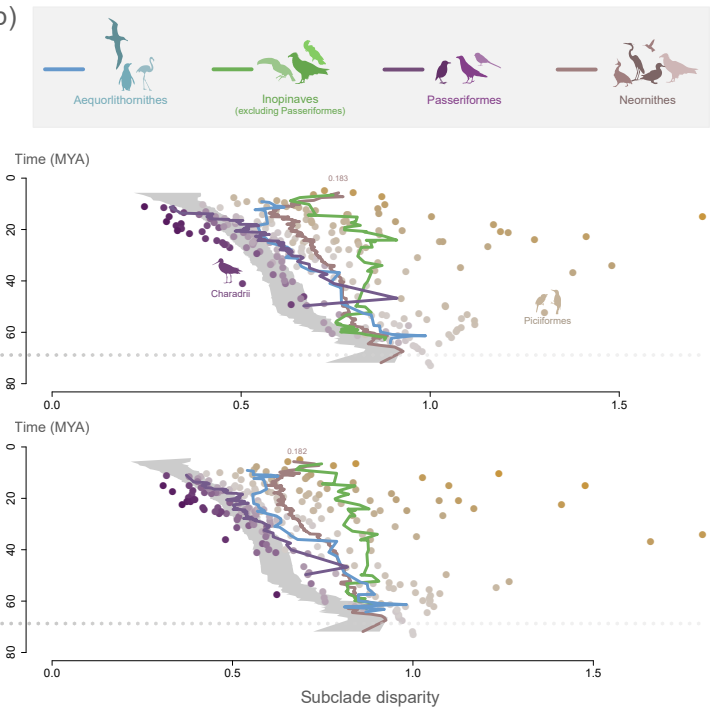
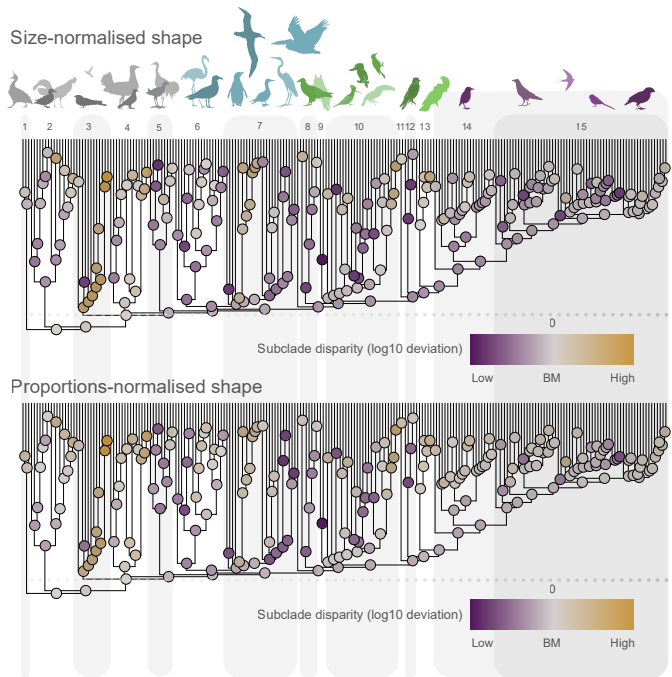


**Figure S25. Subclade disparity–age plotted across avian phylogeny and through time for scapula shape (size-normalised shape) and local shape (proportions-normalised shape).** Legend as in Figure S15 and Figure 1 in the main text.

a) Humerus



b)

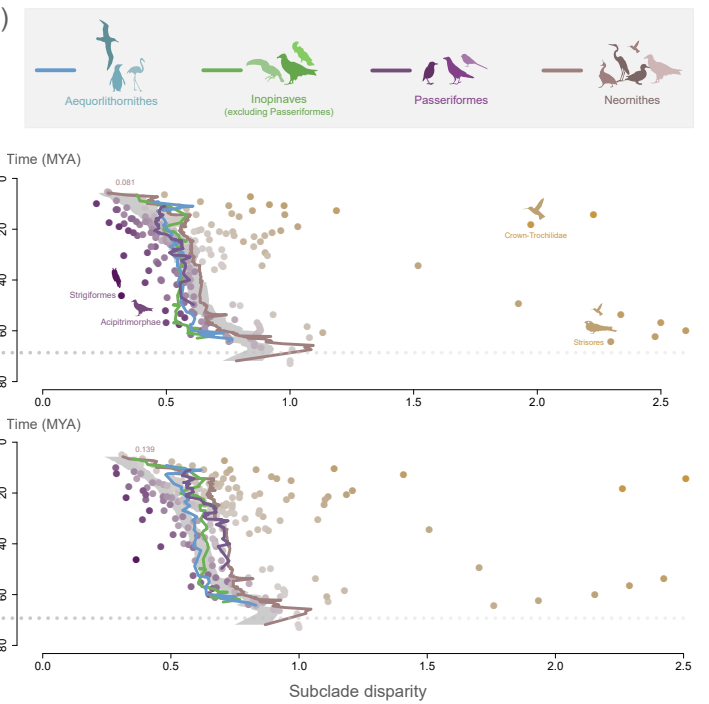


**Figure S26. Subclade disparity–age plotted across avian phylogeny and through time for humerus shape (size-normalised shape) and local shape (proportions-normalised shape).** Legend as in Figure S15 and Figure 1 in the main text.

a) Ulna

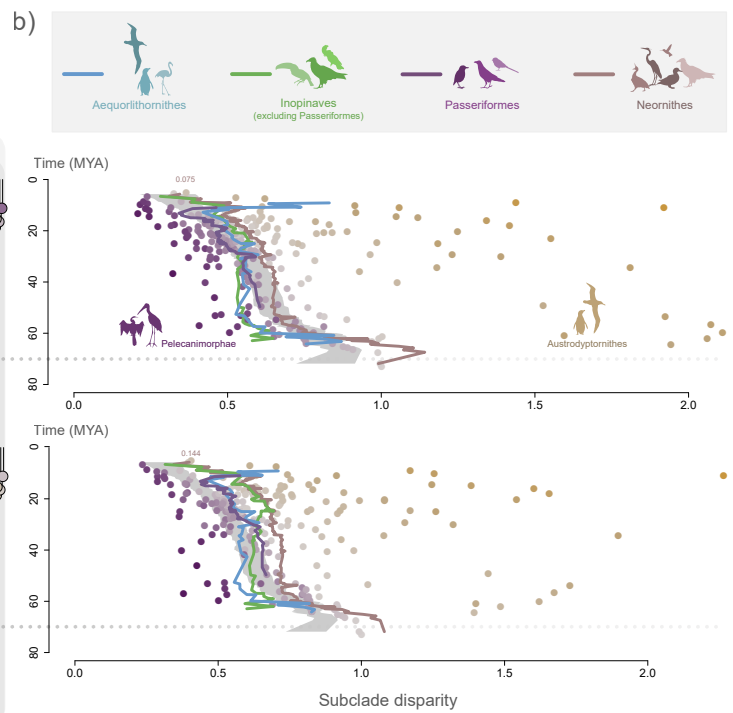
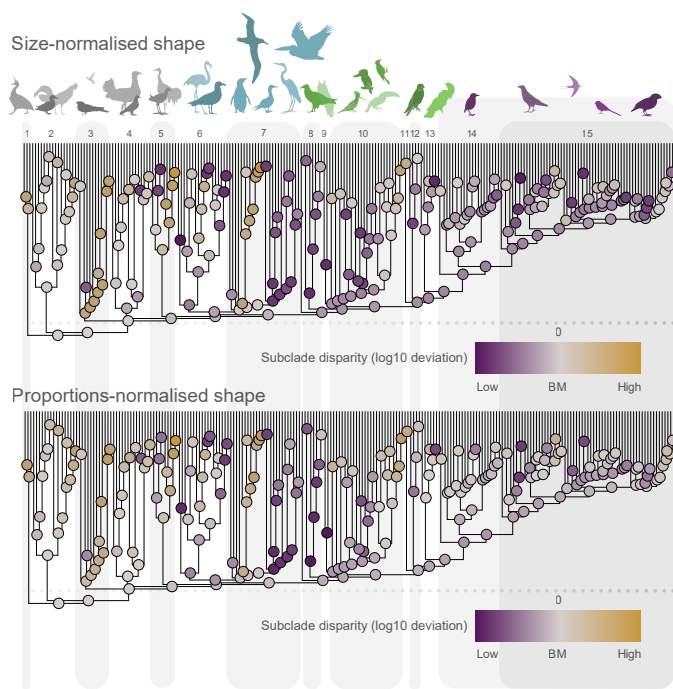


**Figure S27. Subclade disparity–age plotted across avian phylogeny and through time for ulna shape (size-normalised shape) and local shape (proportions-normalised shape).** Legend as in Figure S15 and Figure 1 in the main text.

a) Radius

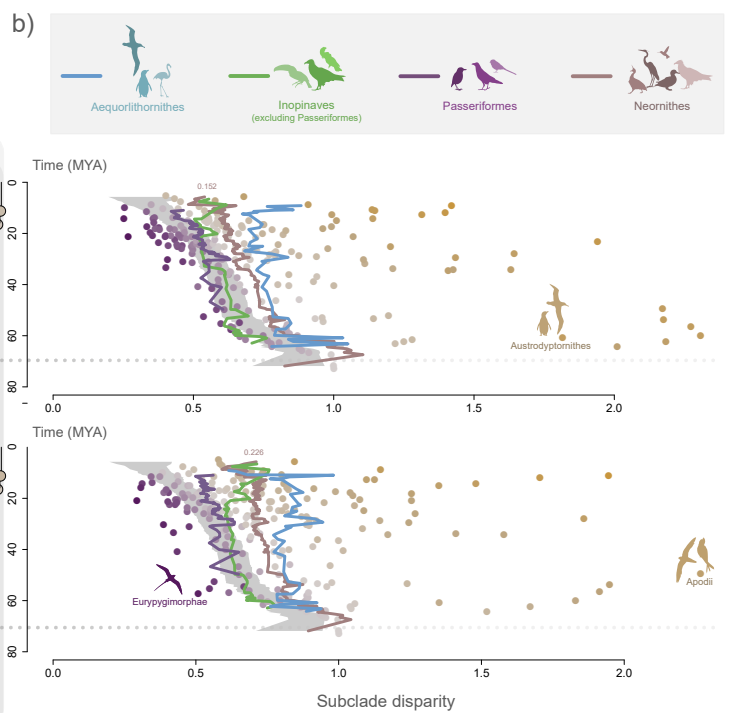
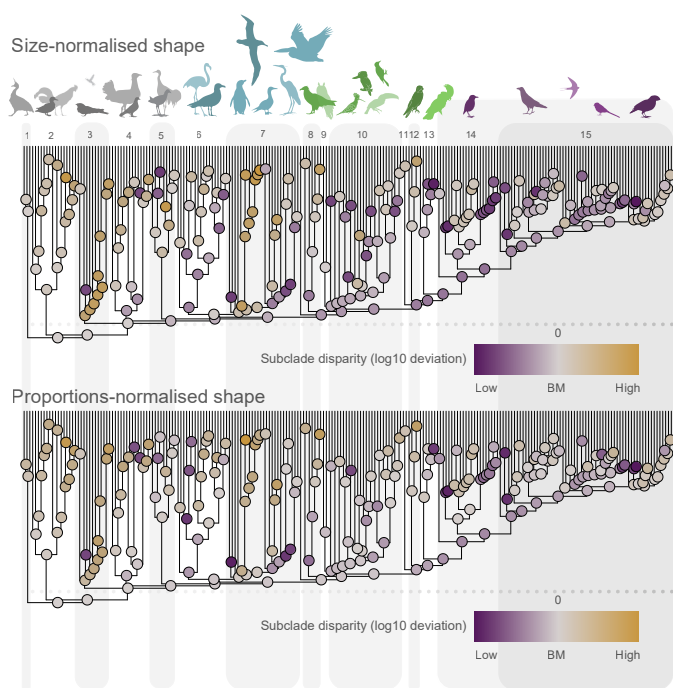


**Figure S28. Subclade disparity–age plotted across avian phylogeny and through time for radius shape (size-normalised shape) and local shape (proportions-normalised shape).** Legend as in Figure S15 and Figure 1 in the main text.

### a) Carpometacarpus

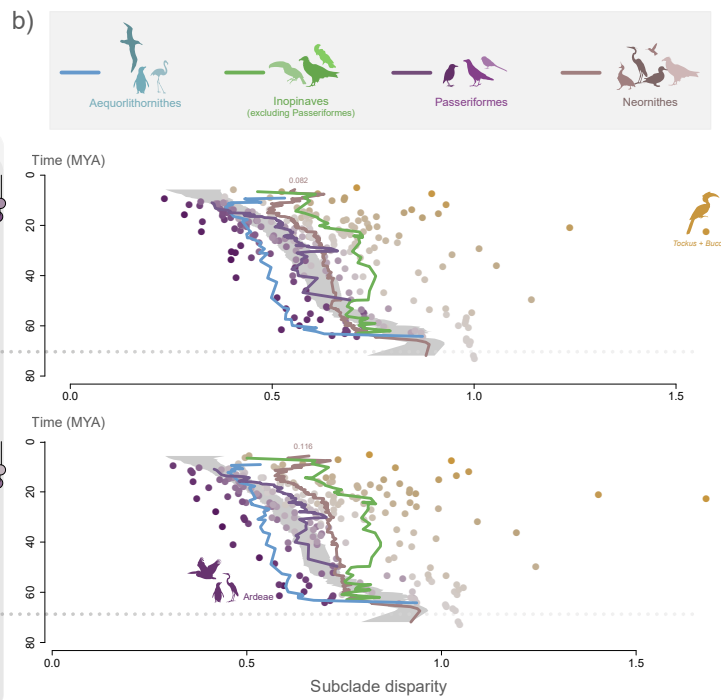
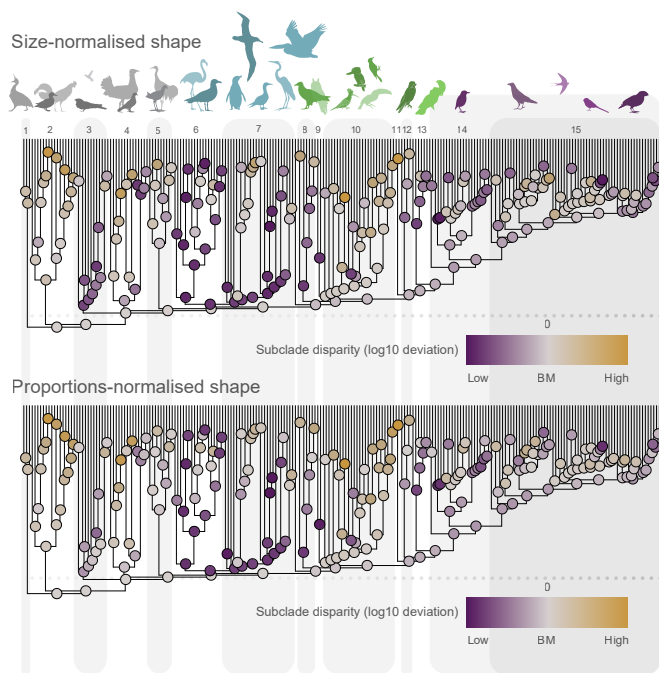


**Figure S29.** Subclade disparity–age plotted across avian phylogeny and through time for carpometacarpus shape (size-normalised shape) and local shape (proportions-normalised shape). Legend as in Figure S15 and Figure 1 in the main text.

### a) Symsacrum

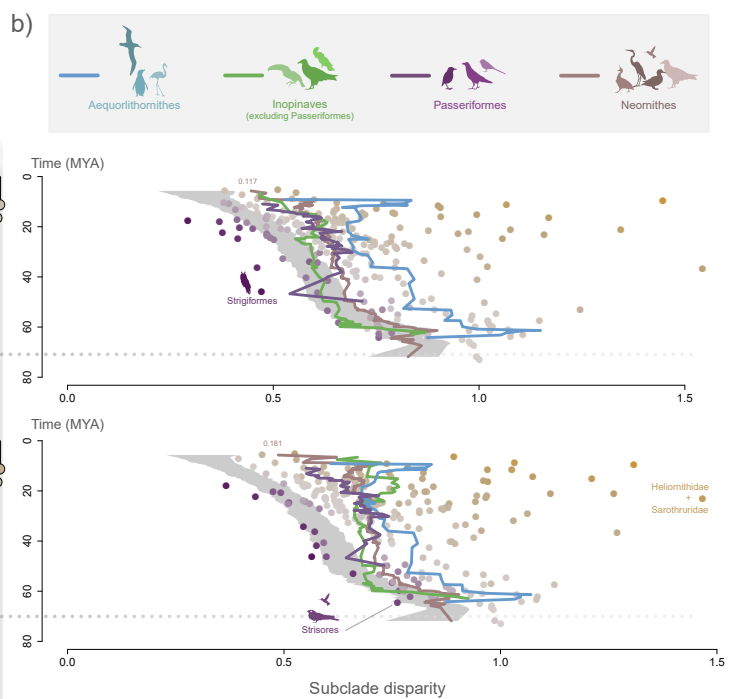
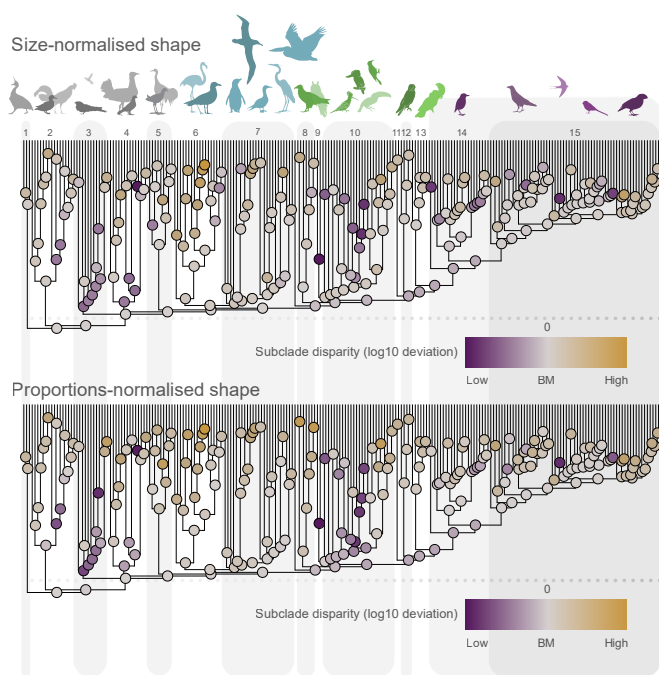


**Figure S30.** Subclade disparity–age plotted across avian phylogeny and through time for symsacrum shape (size-normalised shape) and local shape (proportions-normalised shape). Legend as in Figure S15 and Figure 1 in the main text.



a) Femur

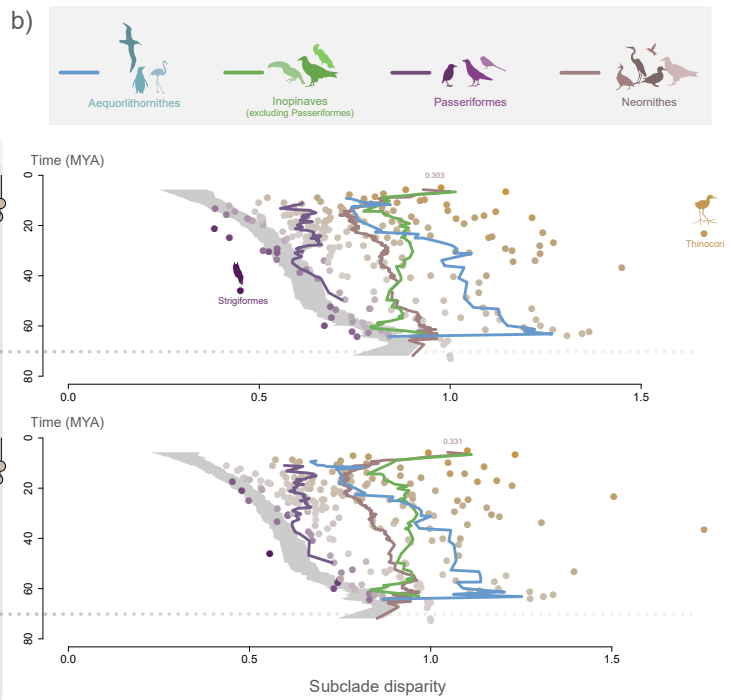
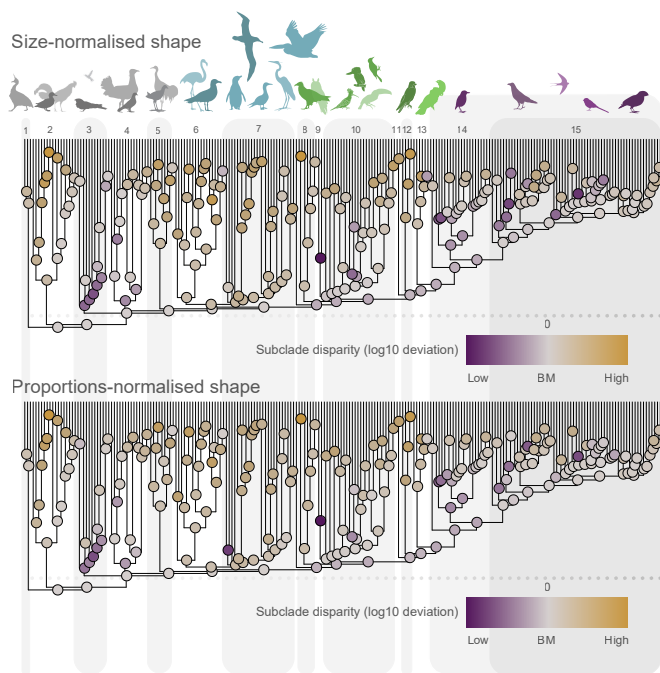


**Figure S31. Subclade disparity–age plotted across avian phylogeny and through time for femur shape (size-normalised shape) and local shape (proportions-normalised shape).** Legend as in Figure S15 and Figure 1 in the main text.

a) Tibiotarsus

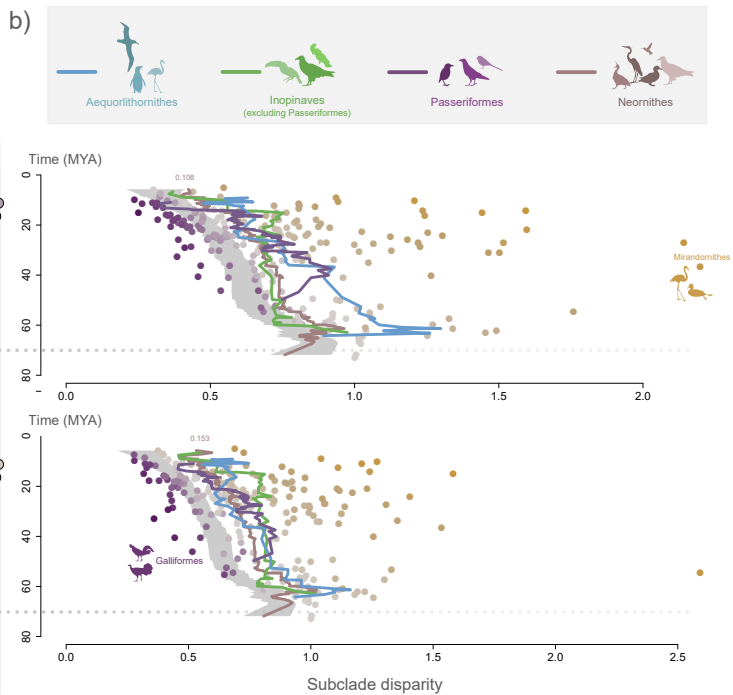
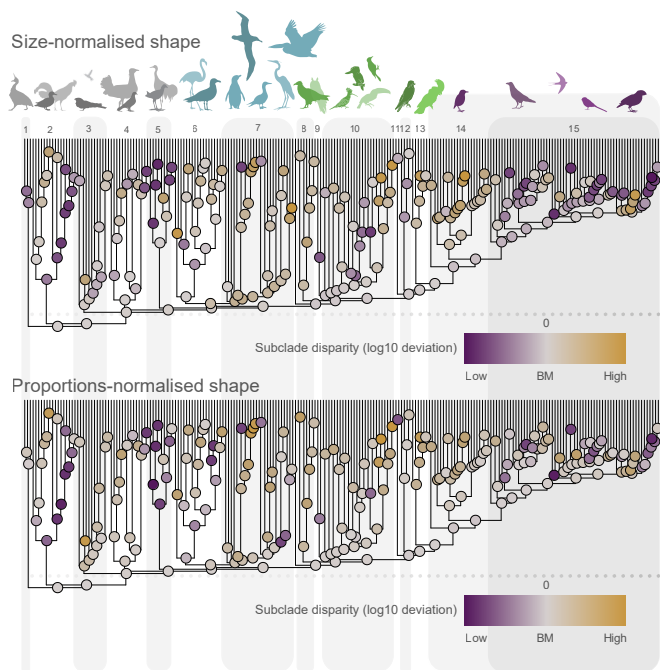


**Figure S32. Subclade disparity–age plotted across avian phylogeny and through time for tibiotarsus shape (size-normalised shape) and local shape (proportions-normalised shape).** Legend as in Figure S15 and Figure 1 in the main text.

a) Tarsometatarsus

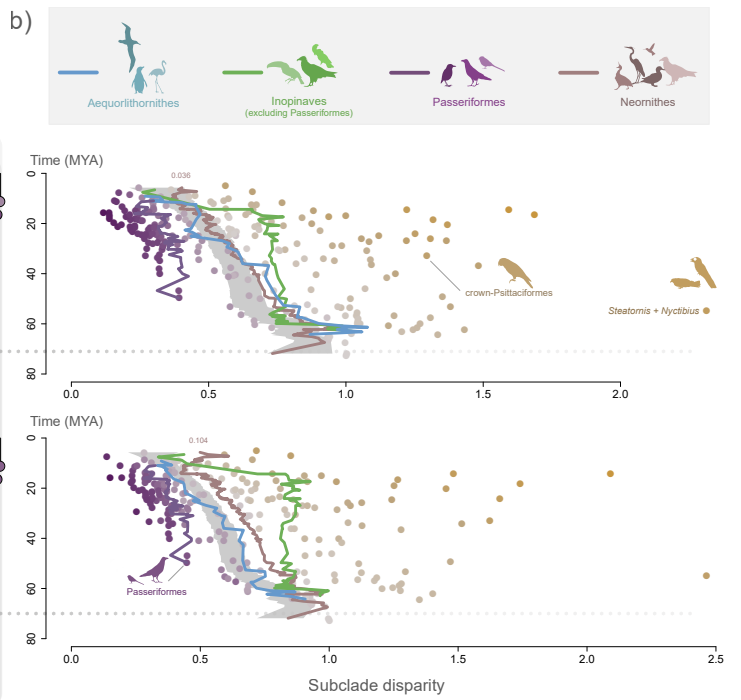
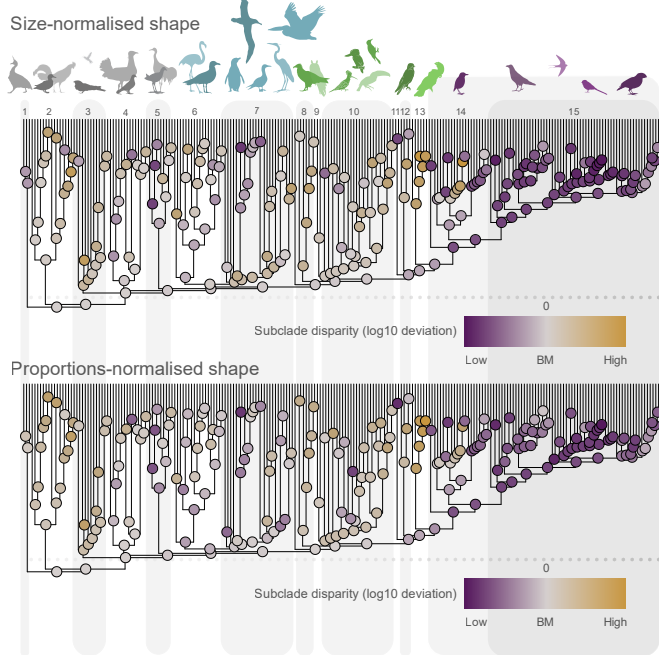


**Figure S33. Subclade disparity–age plotted across avian phylogeny and through time for tarsometatarsus shape (size-normalised shape) and local shape (proportions-normalised shape). Legend as in Figure S15 and Figure 1 in the main text.**

a) Whole skeleton

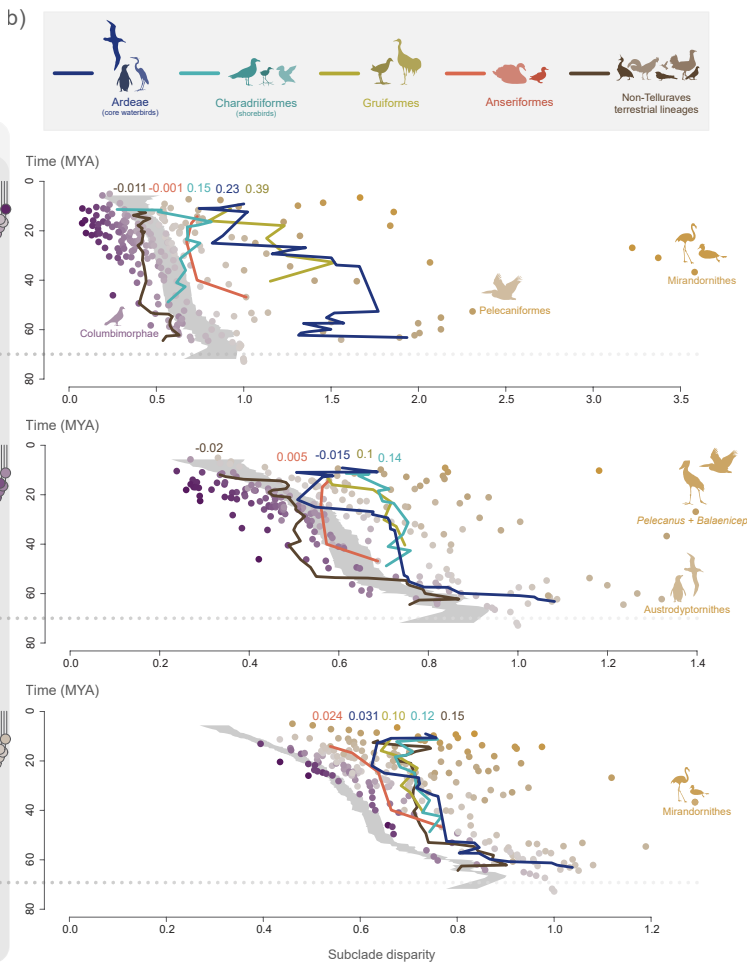
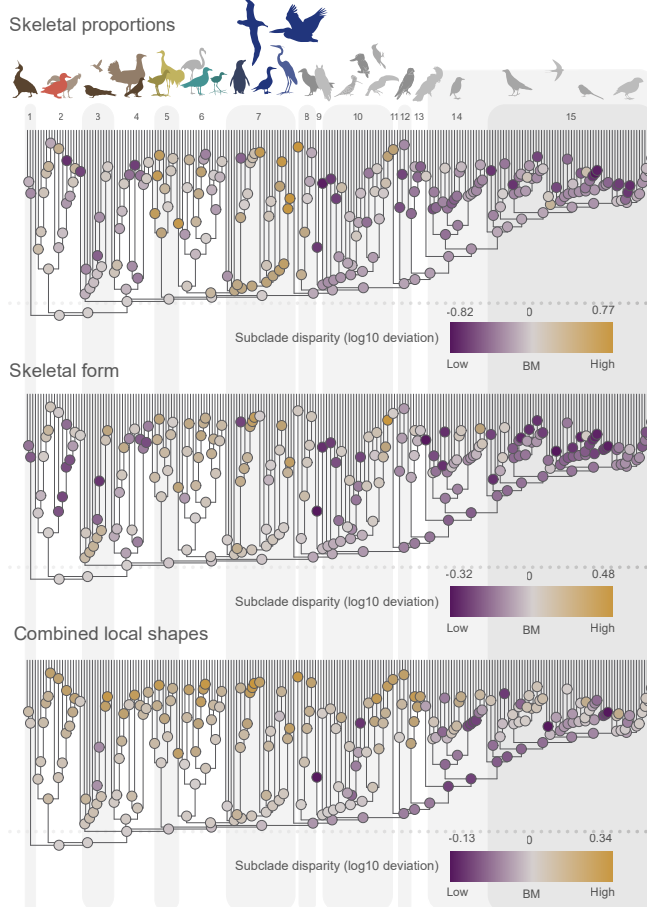


**Figure S34. Whole skeletal subclade disparity–age plotted across avian phylogeny and through time (additional water-linked and terrestrial groups).**



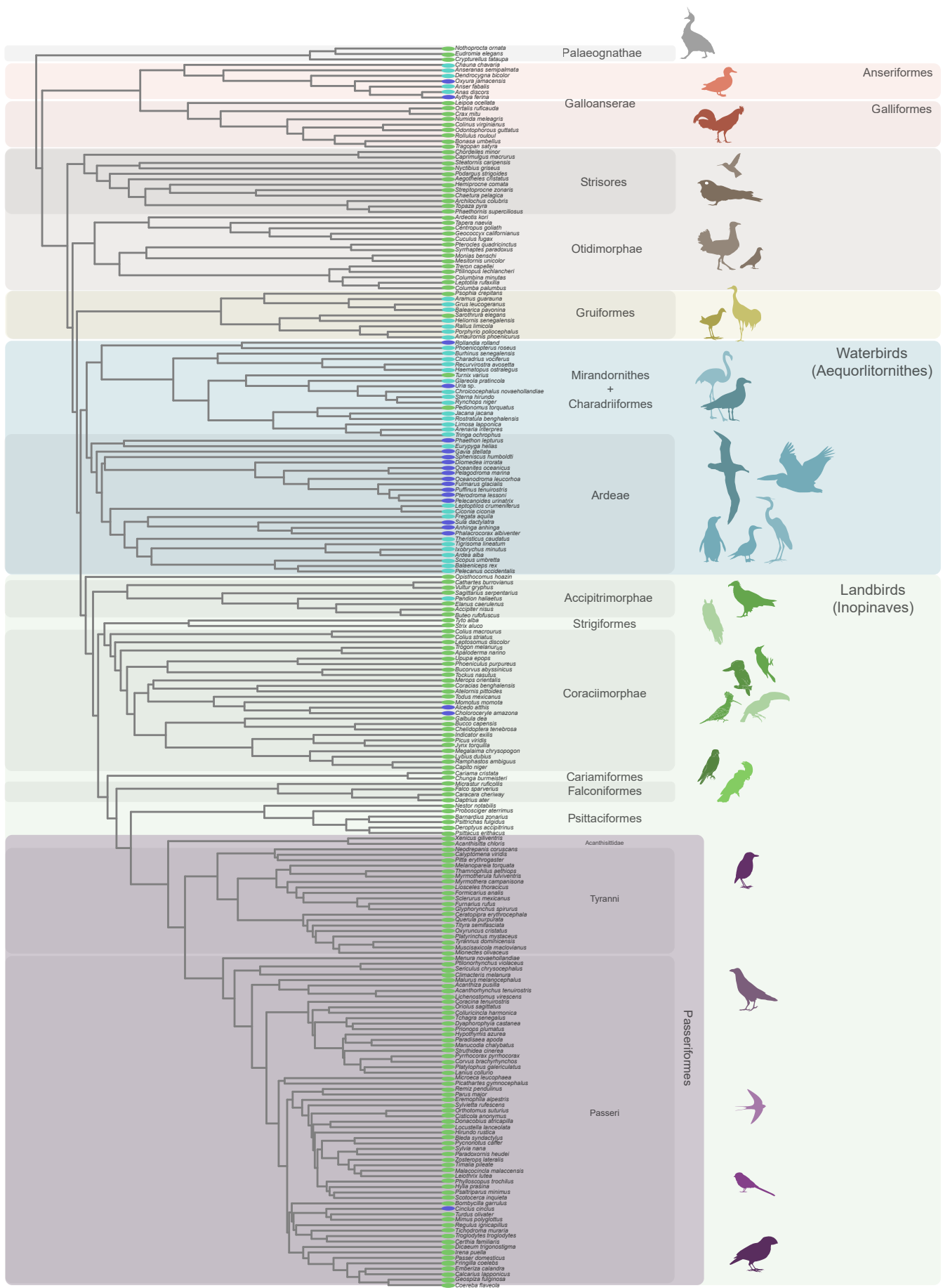


**Figure S36. Phylogeny of Neornithes and phylogenetic distribution of water versus non-water linked autecologies in neornithines (finer partitioning of water-linked ecologies).** Composite phylogenetic framework combining recent phylogenetic hypotheses for non-passerines<sup>1</sup> and passerines<sup>2</sup>. Subdivision among water-linked ecologies follows<sup>3</sup>.

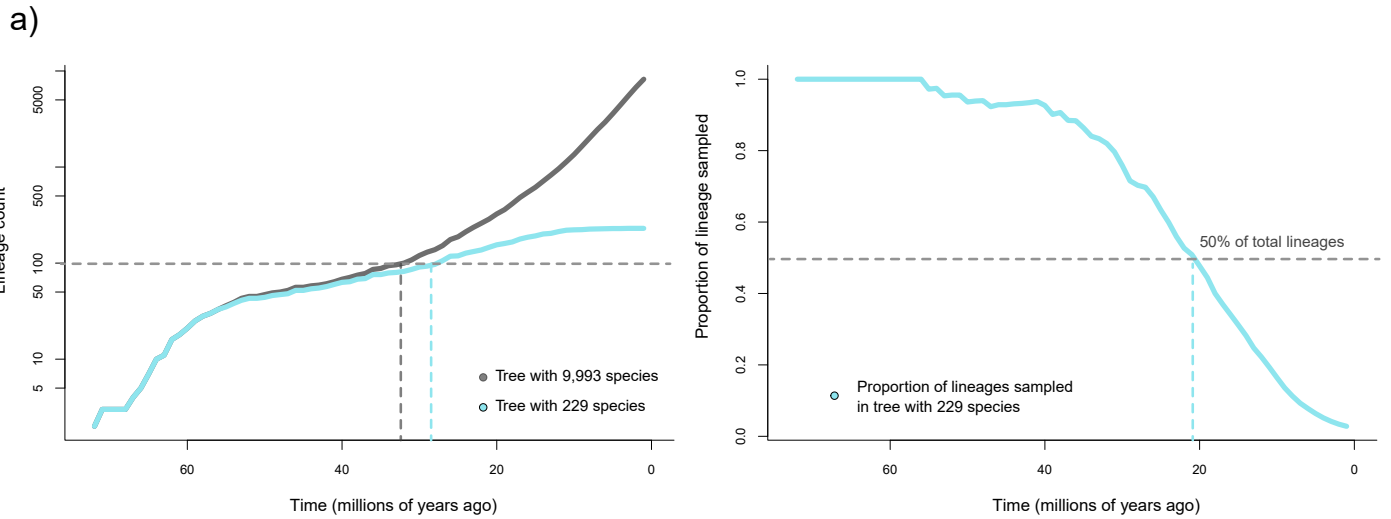


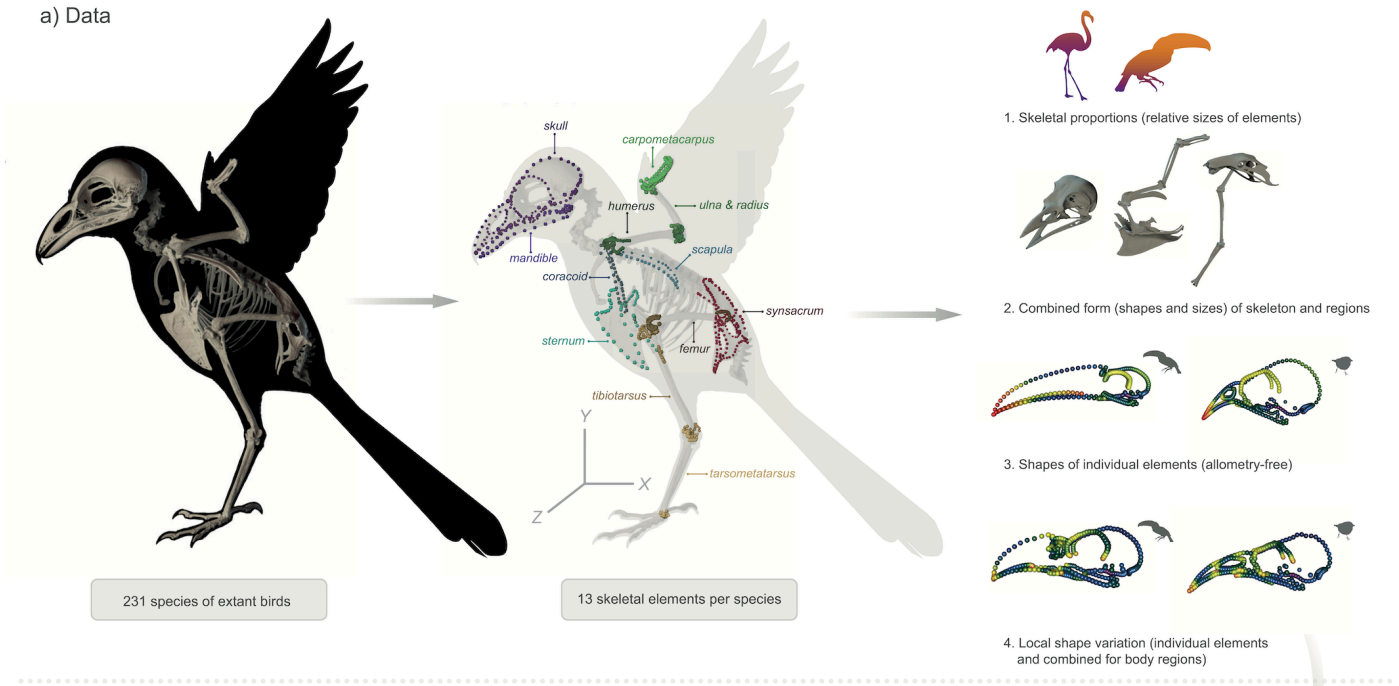
**Figure S37. Proportional sampling of lineages of the tree used in this study compared with the total living bird diversity across time.** Count of lineages through time for the total supertree from<sup>4</sup> with backbone from<sup>1</sup> (black line) as compared with the phylogenetic subset used in this study (blue line). Horizontal dashed line indicates 100 lineages, achieved at slightly different times for both subsets (vertical dashed lines). Proportion of total lineages sampled in the subset tree used in this study. The proportion drops below 50% only at around 20 million years while before 40 million years the proportion is higher than 80%. This indicates our phylogenetic subsample effectively captures most deep divergences in avian diversity.

## References

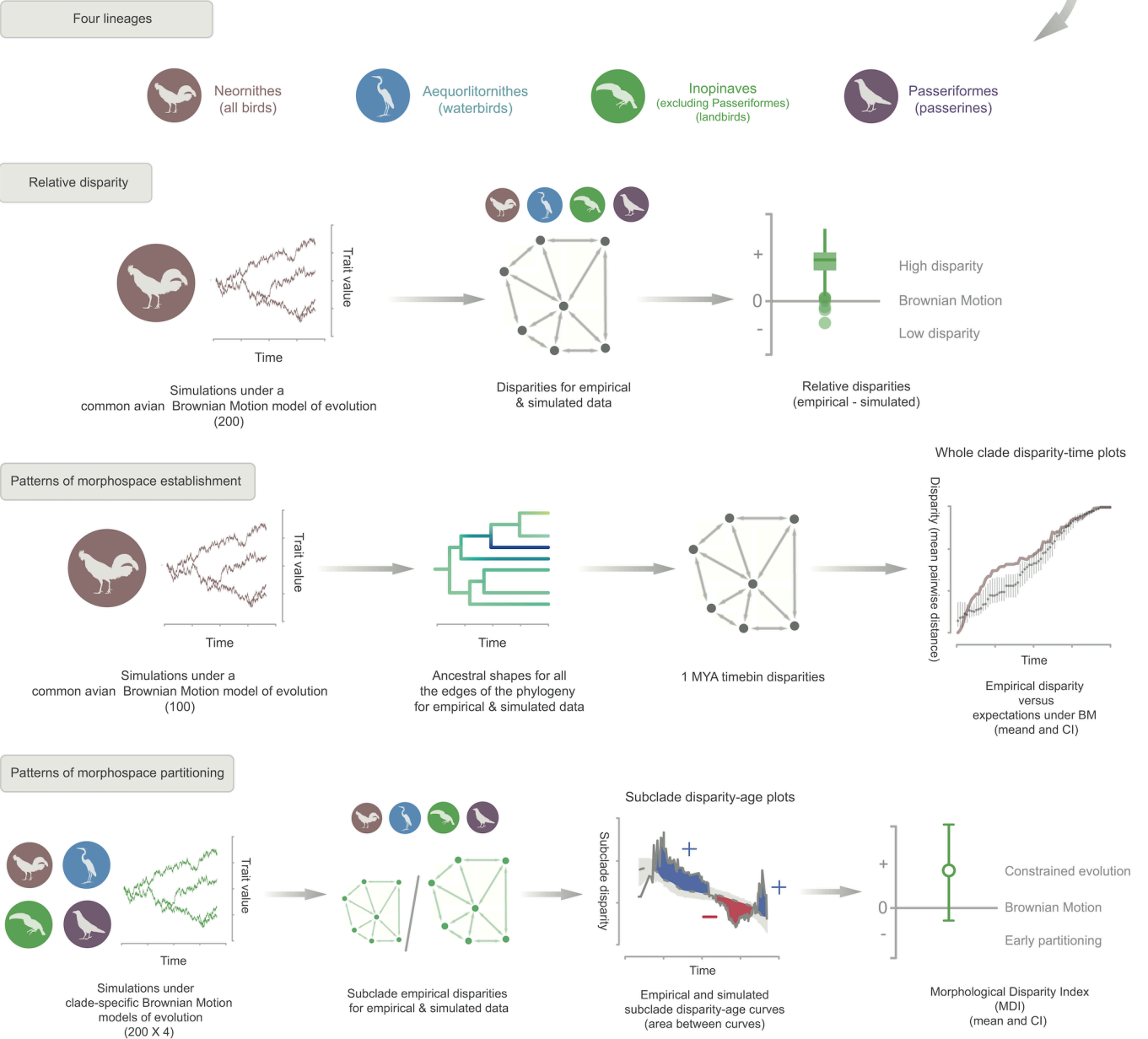
- 1 Prum, R. O. *et al.* A comprehensive phylogeny of birds (Aves) using targeted next-generation DNA sequencing. *Nature* (2015).
- 2 Oliveros, C. H. *et al.* Earth history and the passerine superradiation. *Proceedings of the National Academy of Sciences* **116**, 7916-7925 (2019).
- 3 Fabbri, M. *et al.* Subaqueous foraging among carnivorous dinosaurs. *Nature* **603**, 852-857 (2022).
- 4 Jetz, W., Thomas, G., Joy, J., Hartmann, K. & Mooers, A. The global diversity of birds in space and time. *Nature* **491**, 444-448 (2012).

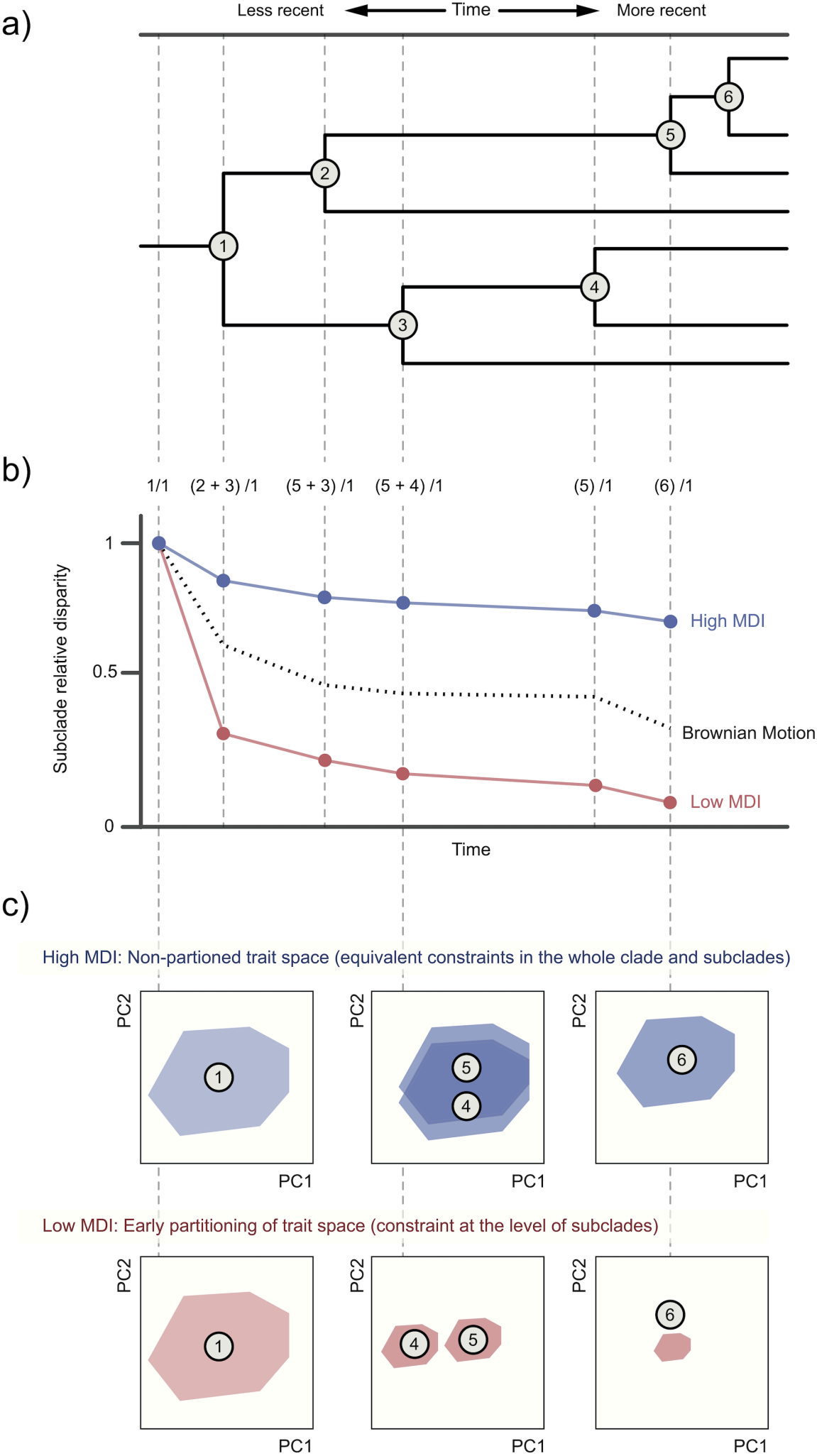
Extended Data 1

a) Data



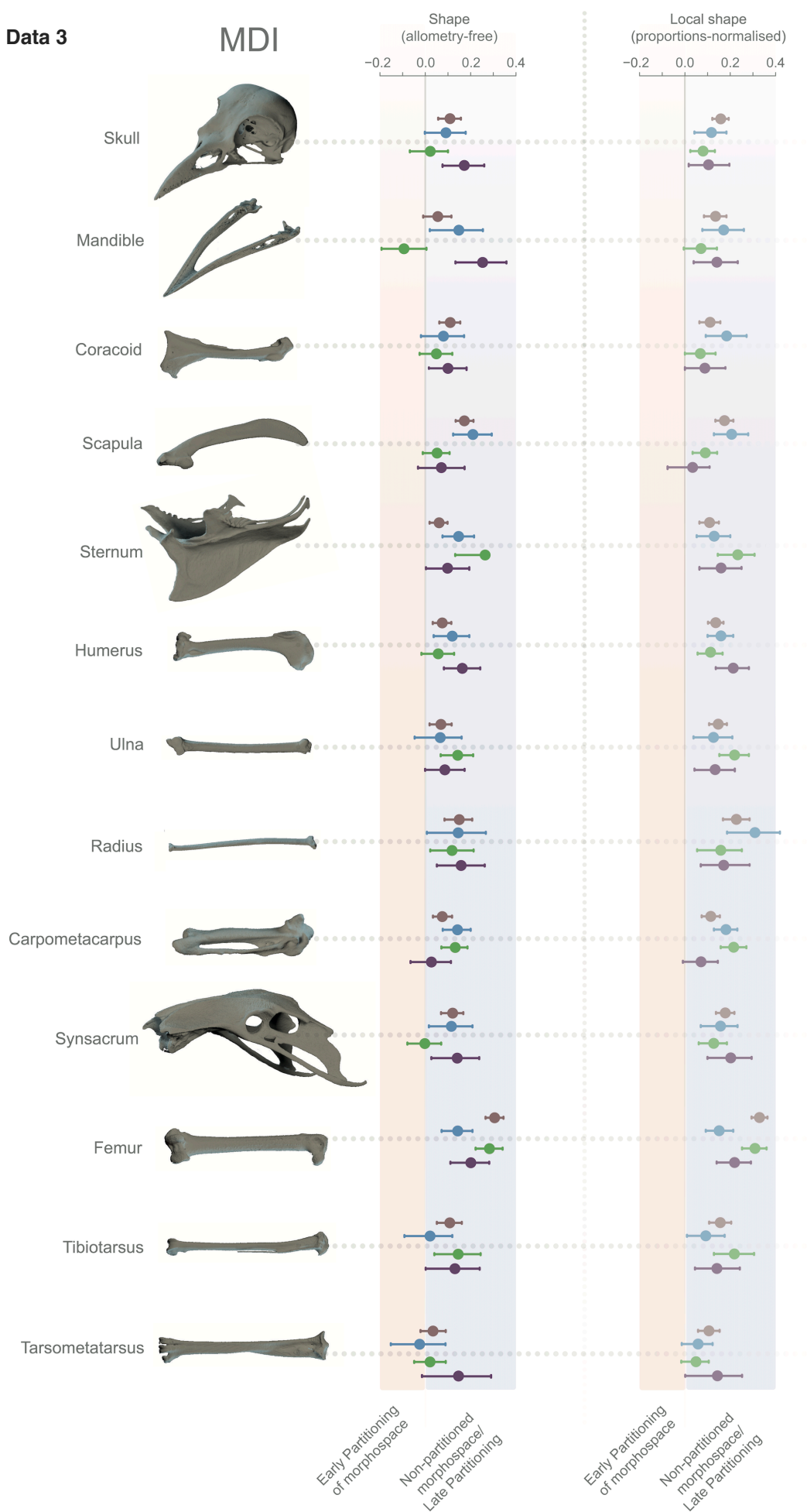
b) Methods







# Extended Data 3



Neornithes



Aequorlornithes



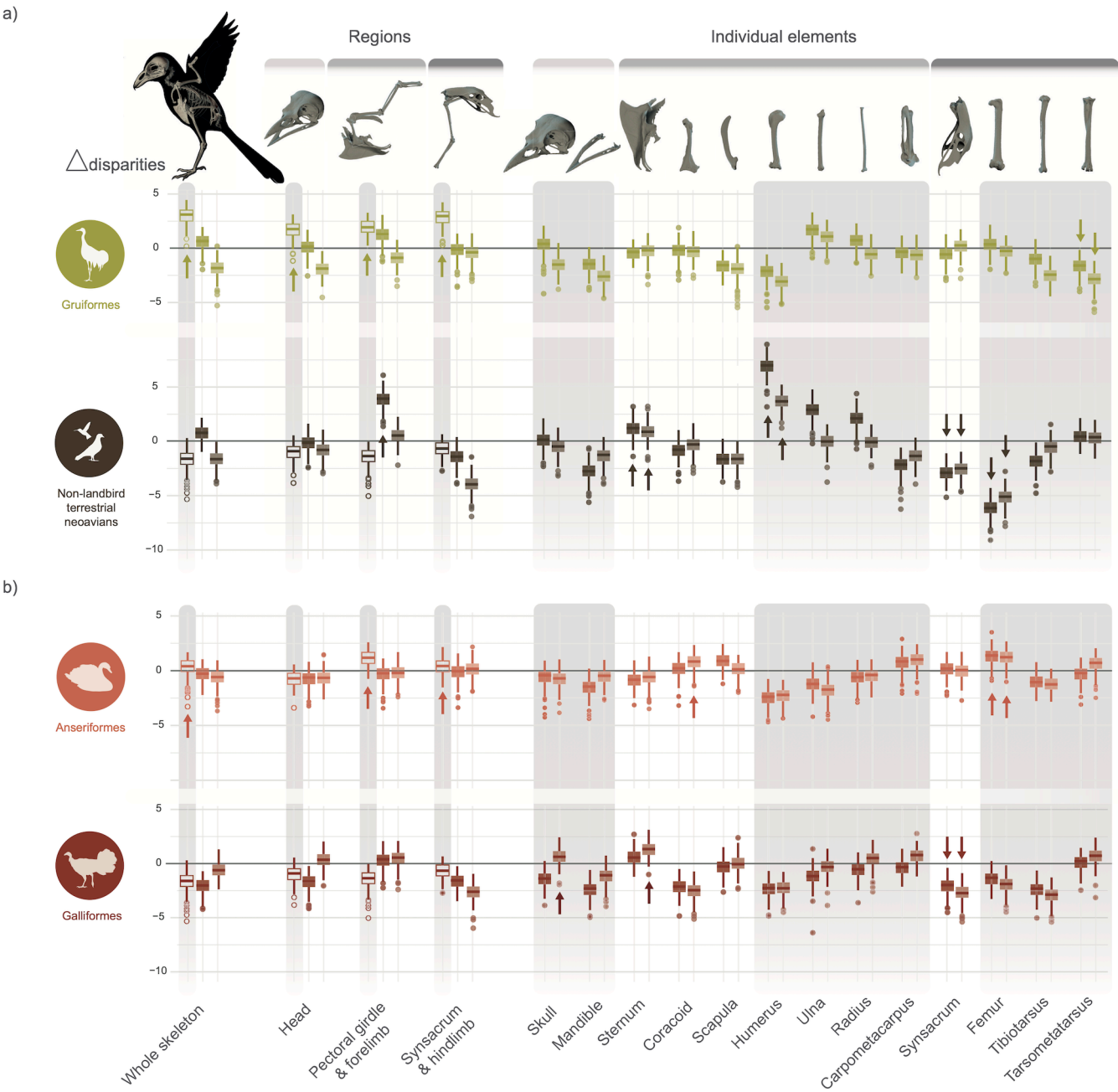
Inopinaves  
(excluding Passeriformes)



Passeriformes



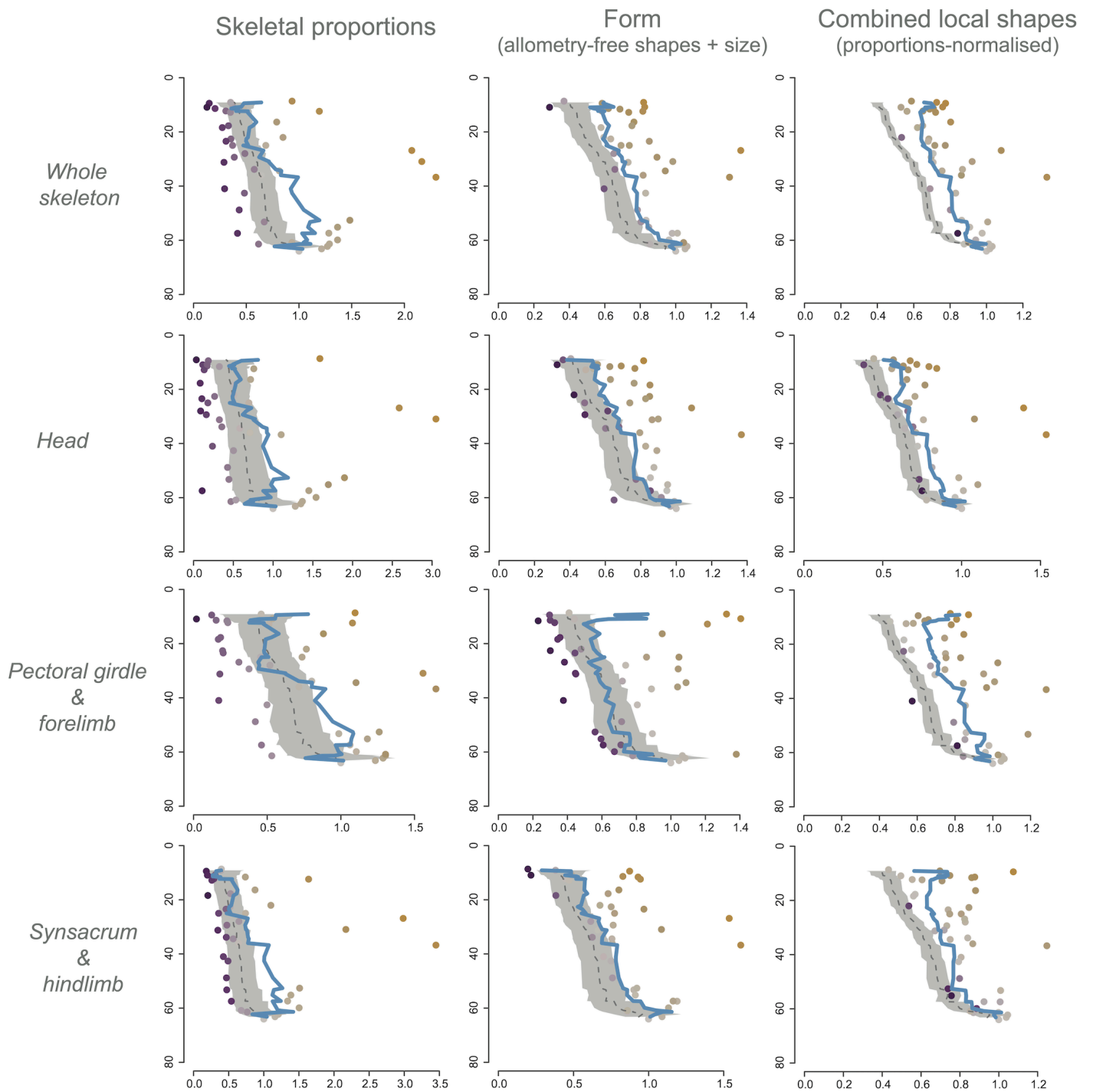
Extended Data 4



## Extended Data 5



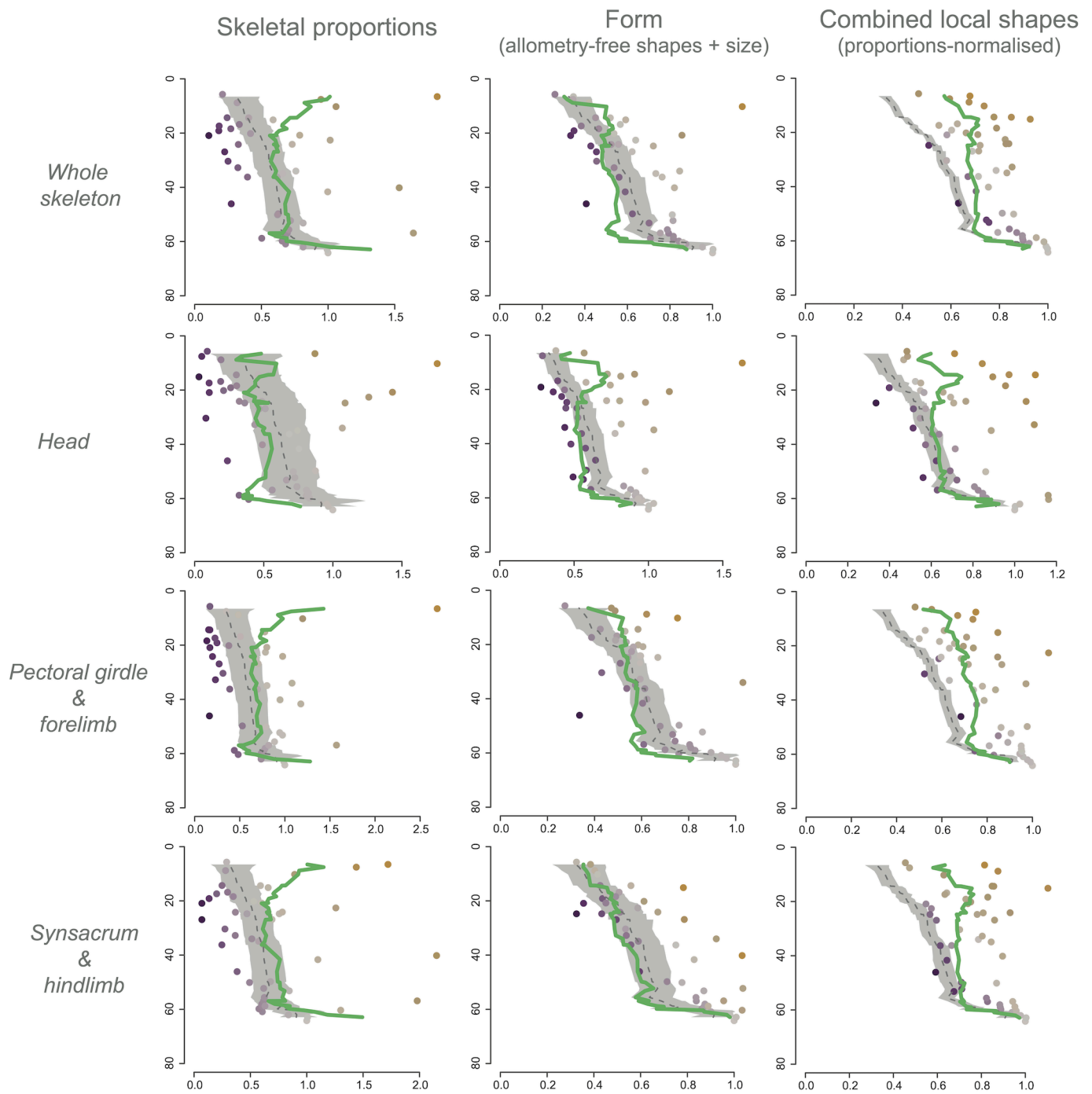
## Aequolitornithes (Regions)



## Extended Data 6

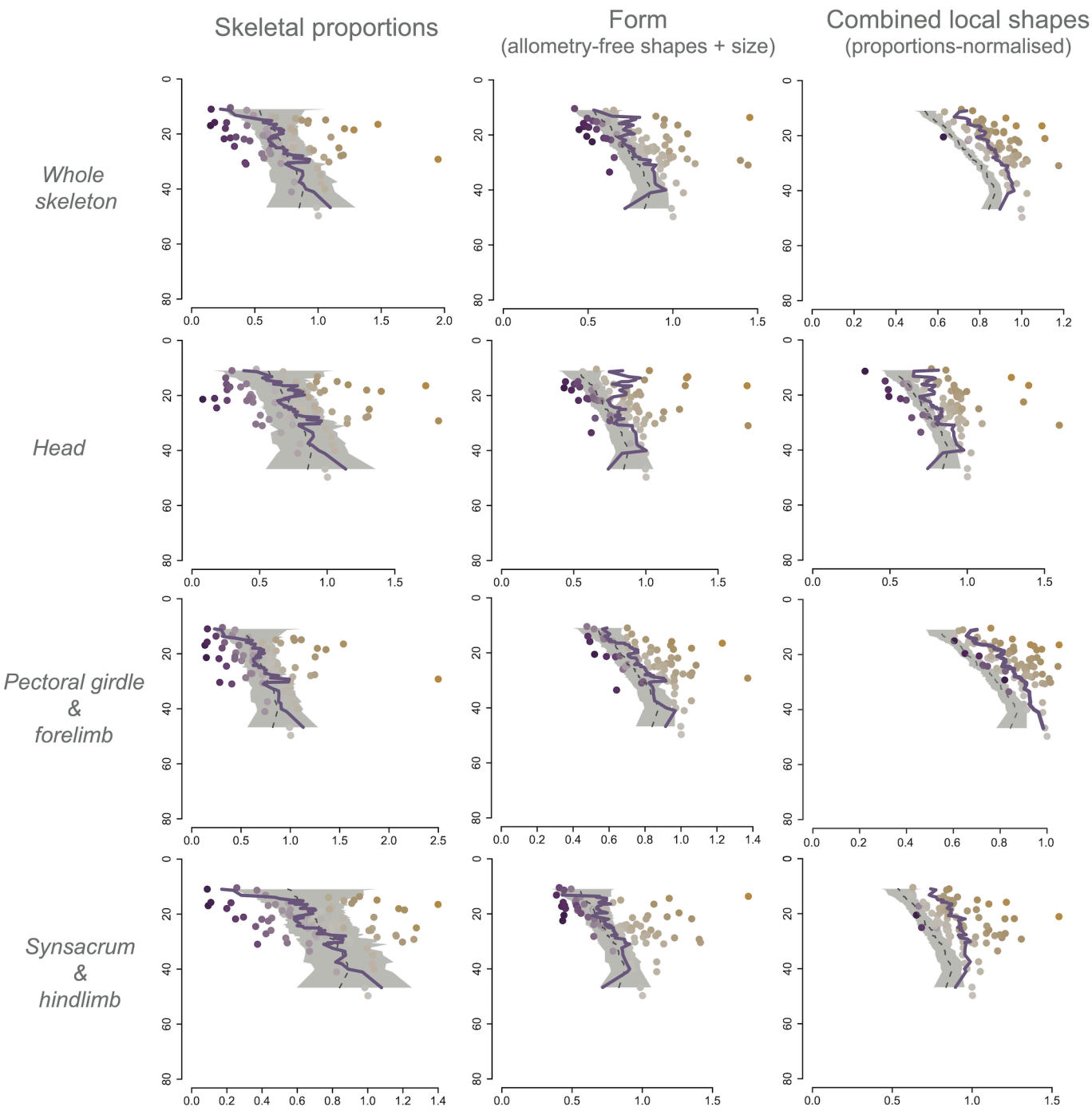


## Inopinaves (Regions)





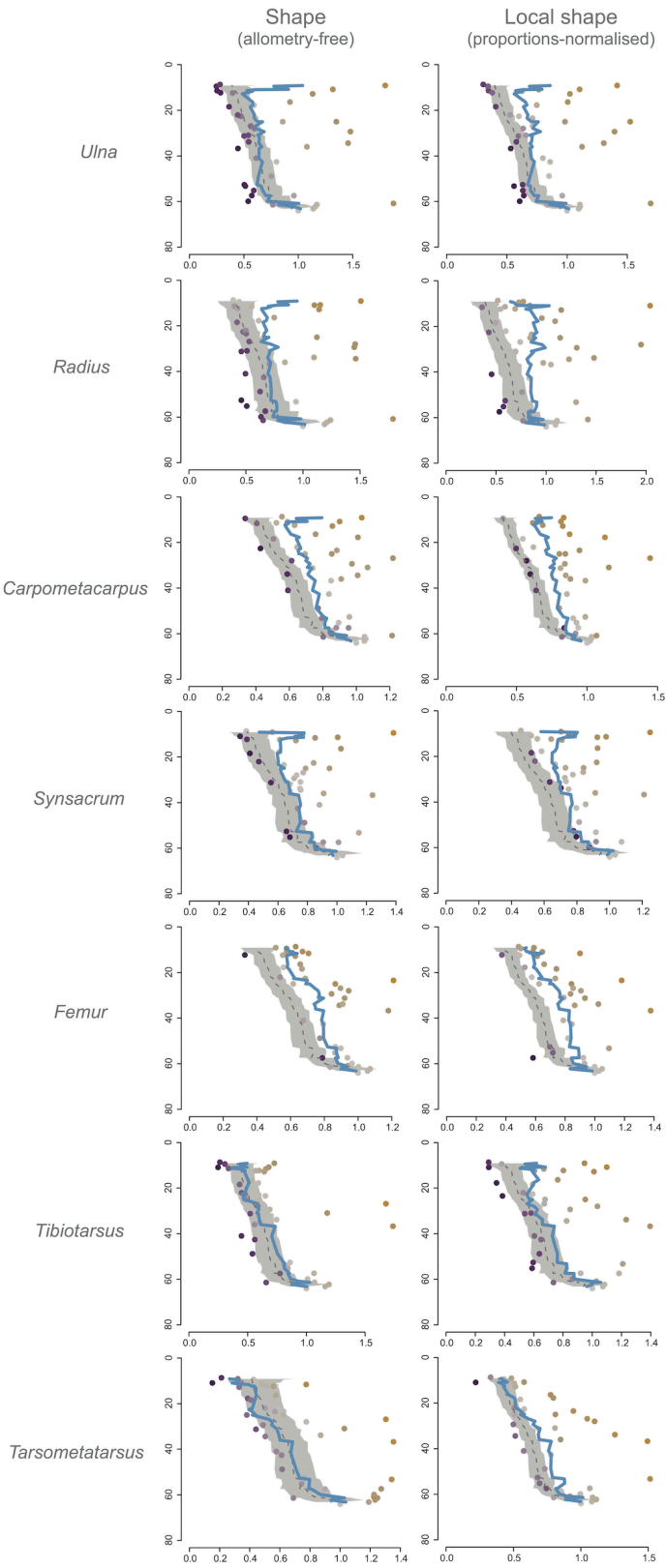
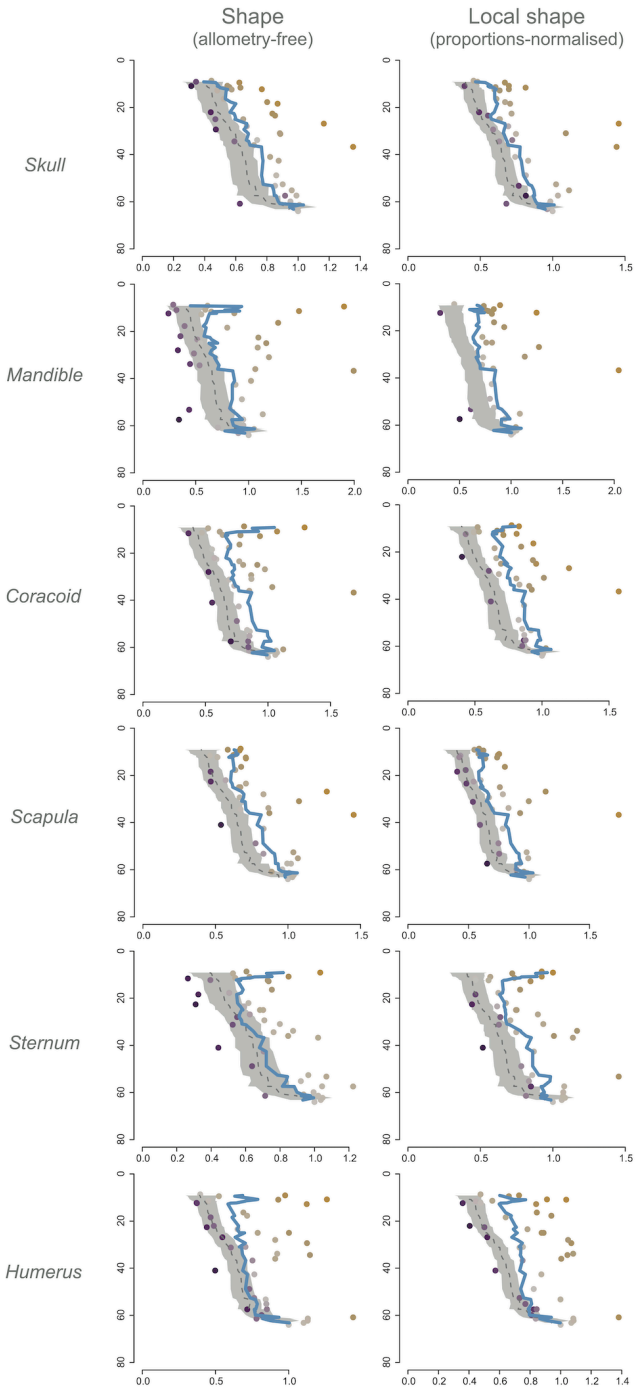
Passeriformes (Regions)



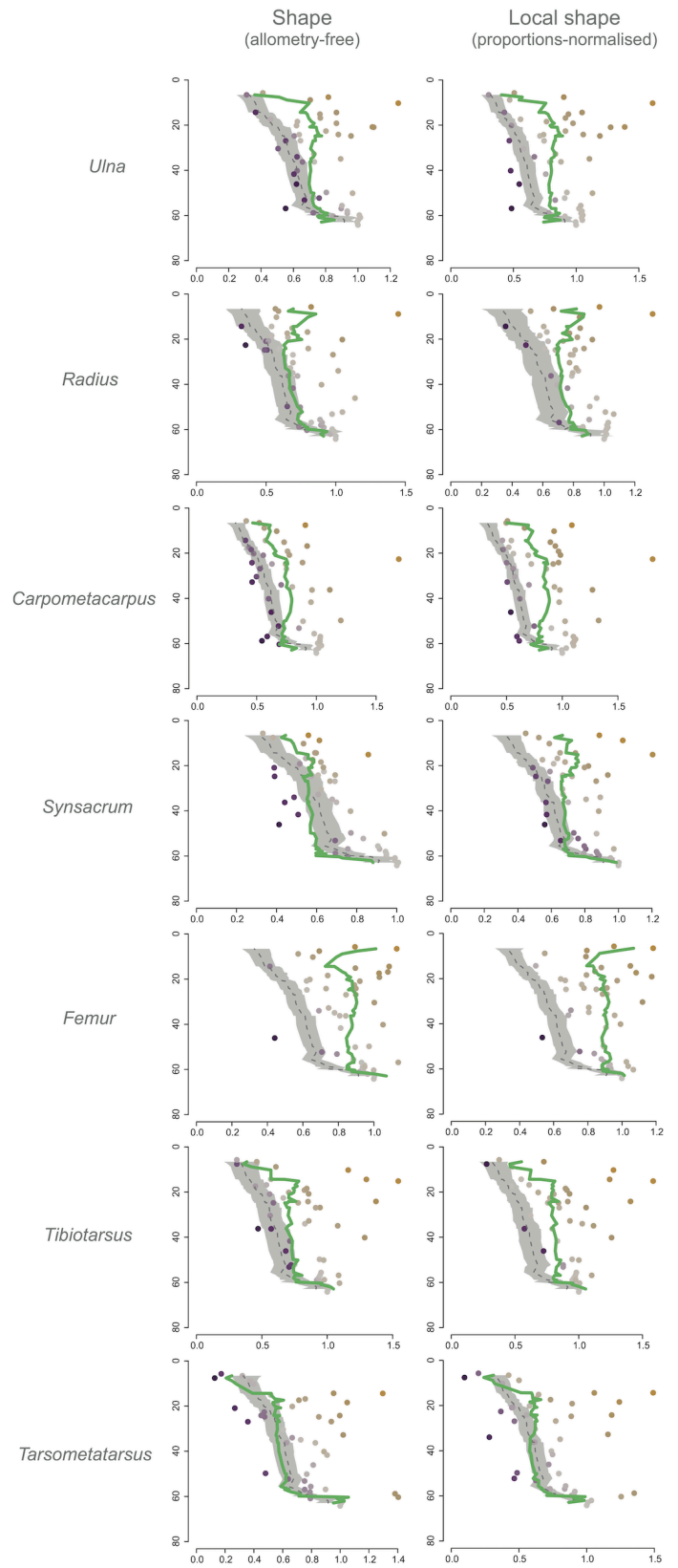
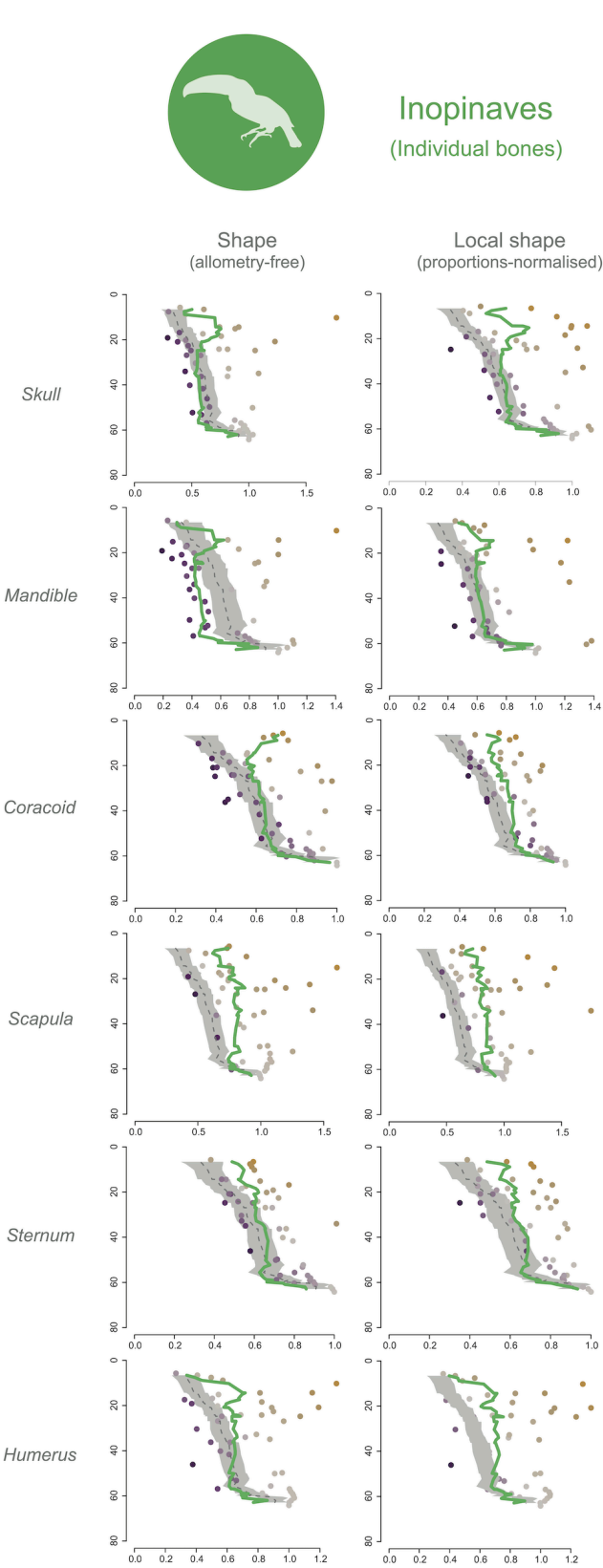
Extended Data 8



Aequolitorornithes  
(Individual bones)



Extended Data 9



Extended Data 10

